Development of an AFM-based nanomotion detection device for microbiological samples

Thèse N° 8898

Wojciech CHOMICKI

2019

ÉCOLE POLYTECHNIQUE
FÉDÉRALE DE LAUSANNE

In memory of Piotr

Acknowledgements

Firstly, I would like to express my sincere gratitude and appreciation to my thesis director and advisor Giovanni Dietler for the guidance, support and patience during my PhD. Often Giovanni engaged me with stimulating discussions and his vast knowledge helped to overcome research troubles.

I would like to thank Sandor, for sharing his ideas and discussing method development.

I thank Petar for daily research collaboration and teaching me the basics of the biological laboratory work and engaging in conversations both scientific and purely entertaining. His company is mostly appreciated.

I would like to thank also other members or former members of our Laboratory for research discussions, entertainment and company: Ula, Ewelina, Gianni, Sandro, Simone, Katya, Serguei, Anton S., Andrzej, Raphael, Zeno, Jingtao, Kamila, Anne-Celine, Leonardo and Anton M.; our students: David, Robert, Ingalena, Massimo, Neige, Raphael, Phillipe and Veronika; our collaborators: Onya, Allison, Zoe and Ines; and colleagues from another lab: Christian, Ambroise, Aster, Kyle, Dora, Anna and Timo.

I would like to express my gratitude towards Christine and Mireille, our Laboratory administrative staff and Michel, Florent and Aubry for the help with computers. Many thanks to Raymond and other people from the electronic workshop for the help with electronics and Florian, Alain and other members of the mechanical workshop for manufacturing and help. Thanks to Anh from the doctoral school. Thanks to Carine, Caroline and Helen for the help with biological preparation.

Again I would like to thanks again everyone I met at EPFL for their hospitality and kindness.

I would like to acknowledge late Piotr Pierański for his guidance prior to the start of my PhD and continuous support along.

I would like to thank my close ones.

Résumé

Les principaux buts de cette thèse sont de mettre au point un appareil capable de détecter la viabilité des micro-organismes via la mesure des oscillations à l'échelle nanométrique d'un levier transducteur microscopique, d'améliorer cet instrument et de tenter de décrire en termes physiques les causes sous-jacentes à l'effet observé.

La thèse commence par une brève introduction à la résistance aux antibiotiques, à la microscopie à force atomique et à l'application de la méthode de détection de viabilité présentée à des tests de susceptibilité antimicrobienne. Les techniques de test de référence (*gold standard*) et les techniques émergentes pour tester la susceptibilité microbienne sont ensuite décrites. L'accent est mis sur les techniques basées sur des leviers.

Par la suite, une tentative est faite de décrire théoriquement l'effet observé en évaluant les possibles phénomènes en cause. Ces phénomènes sont divisés en deux groupes: ceux contribuant de façon positive aux effets observés et ceux contrefaisant la signature de micro-organismes viables. Tous les phénomènes sont quantifiés par des calculs effectués sur la base de modèles et évalués par rapport à l'importance de leur contribution à l'effet total.

Le développement des appareils et des logiciels permettant de les contrôler est exposé au chapitre suivant. La construction de l'appareil est décrite en détail. Son fonctionnement et les procédures liées à son utilisation sont caractérisés. Le logiciel utilisé pour la préparation de la machine avant les expériences ainsi que pendant l'acquisition de données est présenté.

Les résultats expérimentaux sont donnés dans les chapitres suivants. Une première section est dédiée à la technique utilisée, aux procédures de base et à la méthodologie. Dans la deuxième section, la procédure de calibration de l'appareil est brièvement décrite. Un exemple d'application de la méthode à des bactéries à croissance lente est présentée dans la troisième section comme cas extrême de test rapide de la susceptibilité microbienne. Enfin, la quatrième section détaille l'utilisation de l'appareil pour l'analyse de l'activité métabolique de la mitochondrie.

La discussion des résultats est présentée dans l'avant-dernier chapitre.
Le dernier chapitre conclut la thèse.

Mots-clés: microscopie à force atomique, AFM, résistance aux antibiotiques, AMR, test de susceptibilité microbienne, AST, nanomotion.

Abstract

The main goals of this thesis pertain to the development of a device capable of detecting microorganism viability through monitoring the oscillations of a microscopic cantilever transducer, to improve the presently used device and to attempt to explain in physical terms the underlying cause of the observed effect.

The thesis begins with a brief introduction about the antimicrobial resistance, atomic force microscopy and application of the presented method in antimicrobial susceptibility testing. The state of the art for assessing antimicrobial susceptibility (so called gold standard) and the emerging methods in antimicrobial susceptibility testing follows. A special emphasis was given to cantilever – based techniques.

Afterwards a theoretical description of the observed effect is attempted by evaluating the possible contributing phenomena. Those phenomena are divided into two groups: ones that contribute to the effect positively and ones that are mimicking viable microorganisms. All the contributing phenomena are quantified using model calculations and evaluated based on the significance of the contribution to the total effect.

The development of the devices and controlling software is given in the subsequent chapter. The construction of the devices is described in detail. The operation and procedures regarding the utilization of the device are characterized. The software that manages the preparation of the device before the experiment and the data acquisition during the experiments is demonstrated.

Experimental results are reported in the following chapters. First section is devoted to introduce the technique, its basic procedures and methodology. The following section is briefly presenting the calibration procedure. Afterwards a section describes the application of the method to slow-growing bacteria as an extreme case of rapid antimicrobial susceptibility testing. Subsequent section elaborates on the utilization of the technique to assess the metabolic activity of mitochondria.

The discussion of the results and possible effects are presented in the penultimate chapter. The final chapter concludes the thesis.

Keywords: atomic force microscopy, AFM, antimicrobial resistance, AMR, antimicrobial susceptibility testing, AST, nanomotion,

Table of contents

List of figures

xiv

List of equations

List of tables

Chapter I

Introduction

1.1. Introduction

This thesis examines the problem of antimicrobial resistance (AMR) and sets out a novel approach to rapidly carry out an antibiotic sensitivity test. In doing so, it will seek to explain the underlying causes of the effect which is observed in the new method under discussion. The opening chapter is intended to outline the growing problem of antimicrobial resistance and explain how and why it is the motivation behind the work; in doing so it will describe the foundations of a method which has been developed utilizing the atomic force microscope (AFM). The second chapter is devoted to examining the current state of the art in the field of bacterial resistance detection, while the third chapter will provide a thorough theoretical description of the observed effect and tries to explain its working principle. The fourth chapter will describe the development of the device itself and the software involved in controlling it and analyzing the data being gathered. The fifth chapter presents the data which has been obtained as proof of both the principle and the application of the device, while the sixth chapter discusses the results which have been obtained. The seventh and final chapter will present a summary of and conclusion to the entire thesis.

1.2. Antimicrobial resistance

Antimicrobial resistance (AMR) is a public health problem in all parts of the world, and is likely to grow in terms of both scale and geographical scope in the immediate future [1–5]. According to the World Health Organization (WHO) the AMR is a threat to the effective prevention and treatment of infections induced by: bacteria, which becomes resistant to antibiotics and other antibacterial drugs; parasites, as in the case of resistance to anti-malaria medicines; viruses, as in the resistance to anti-HIV medicines, and fungi, exemplified by the resistance to medicines used to treat Candidiasis [3]. This is doubtless a serious threat which calls for a firm and decisive response across all echelons of society, including all parts of the private and public sectors. The WHO takes great care to present a powerful and persuasive argument, pointing out that the lack of effective antibiotics threatens to jeopardize the delivery of major surgery, such as organ transplants, caesarean sections or hip replacements, at the same time as compromising much needed medical interventions such as diabetes management and chemotherapy. In addition to the severe consequences to the health of individual patients, and thus wider society, there is an economic impact to be considered. This is driven by the fact that treating an AMR infection is much more expensive than possible alternatives, because the patient is highly likely to be hospitalized for a longer period, and will probably make use of a costly Intensive Care Unit (ICU). Other additional costs are driven by multiple additional tests, such as

an antimicrobial susceptibility test (AST), and the necessity of making use of more expensive, specialized drugs.

According to the estimates included in a 2014 WHO report [3], the AMR is responsible for 25 thousands deaths per year in the European Union [6,7], 38 thousands deaths per year in Thailand [8] and more than 23 thousands deaths per year in the USA [9]. Estimates for the future impact of the AMR state that by 2050 the number of global deaths it causes per year will be as high as 10 million [10,11]. According to the World Bank [12,13], the AMR will simultaneously have a devastating economic impact, particularly in developing countries. This will be driven by a reduction in consumer income, employment and savings and the need for additional national investment, particularly in the field of healthcare spending, and will create a projected drop in Gross Domestic Product (GDP) of 1.4% to 1.6%. As an illustration, in 2016, 490 000 people developed multi-drug resistant tuberculosis (TB) and drug resistance is starting to complicate the fight against HIV and malaria, as well [14].

Antimicrobial resistance refers to the acquired ability of a microorganism to become immune to drugs, agents or medications which have previously provided effective treatment. The spread of the AMR is driven by genetic mutation or the acquisition of genetic information from other microbes, and is a process which naturally occurs within microorganisms. The natural development and spread of the AMR is further accelerated by the misuse of antibiotics within health care systems. This misuse might include over prescription and overuse, patients not taking antibiotics as directed, or antibiotics being used without adequate professional oversight. Other contributory factors include the widespread use of antibiotics as growth promoters within the animal and fish farming sectors and poor standards of hygiene in less developed countries, while the global spread of the AMR is accelerated by shifting populations and the greater ease and widespread take-up of international travel. New forms and types of the AMR are developing constantly and spreading globally, and they undermine the ability to treat infectious diseases and carry out major surgery. The key to effectively treating infections caused by microorganisms lies in identifying the right drugs, and the AMR means this is increasingly difficult to do.

Bacteremia [15,16] occurs when live bacteria capable of replication are present in the blood, which is normally a sterile environment. There are several sets of circumstances which could conceivably lead to bacteremia: an infection not being treated properly which eventually allows bacteria to infiltrate the blood; infection acquired during surgery; infection brought about by catheters - arterial, venial or uretic - needles or dental intervention. Once present, bacteremia can lead to the infection of

4

other organs and conditions such as endocarditis, osteomyelitis and meningitis, or to sepsis.

Sepsis is the response of a patient's immune system to the presence of infection. It is technically defined as a state which satisfies the systematic inflammatory response syndrome (SIRS) criteria, which means demonstrating at least two of the following: abnormal body temperature, heart rate, respiratory rate, blood gas tension values and white blood cell count. Sepsis usually develops from bacteremia, although it can also be caused by fungal or viral infection. The risk of an affected patient dying is approximately 25% [17]. Severe sepsis is a negative progression of sepsis. It causes tissue hypoperfusion and organ dysfunction in the affected patient. Septic shock is a further negative progression of sepsis which, in addition to the previously documented symptoms of severe sepsis, causes persistent low blood pressure and may lead to multiple organ dysfunction syndrome and, ultimately, to the death of the patient.

1.3. Objectives of this thesis

The problem outlined above calls for development of methods that characterize rapidly, accurately and reproducibly microorganism response to antimicrobial agents.

The classical antibiotic sensitivity or antibiotic susceptibility test (AST) is an in vitro test that consists in growing the bacteria of interest in the presence of different antibiotics. It is important to emphasize that the test duration depends on bacterial replication time. Rapidly growing organisms requires 24h whereas slowly growing bacteria about one month. The test results in quantitative information indicating the bacteria susceptibility to the tested antibiotics. The data is usually presented as a chart showing the effect of the different antibiotics on the growth of the bacteria i.e. susceptible or resistant. It also indicates the minimum inhibitory concentration (MIC), which is the lowest concentration of the antibiotic that stops the microorganism growth as well the minimum bactericidal concentration (MBC) that corresponds to the lowest concentration of an antibiotic that induces bacterial death.

Quicker alternative methods also exist: some are based on the bacterial growth rate but are quicker than the one previously described due to their higher sensitivity (18–20). Other methods are based on the measurement of certain bacterial physical quantities such as mass fluctuations in time and that are independent from the microorganisms replication rate [21]. Finally some methods are based on the detection of specific molecules linked to microorganisms vitality or their susceptibility to specific drugs [22].

The method described in this thesis relies on commercial atomic force microscopy (AFM) as reported in [23]. It uses traditional AFM cantilevers onto which bacteria of interest are attached. As long the bacteria are alive, the cantilever oscillates whereas the oscillations stop as soon as the organisms die. Trying to explain the specific mechanism that drives the cantilever oscillations is one of the goals of this thesis. The other goal of this study is the development, optimization and implementation of the method and its dedicated apparatus in hospitals and research centers.

1.4. Atomic force microscopy

Atomic force microscope is an instrument that was designed to image, at the nanometric scale, the topography of conductive and non-conductive samples. Alternatively, the instrument can also record some additional physical (stiffness, adhesion) and chemical characteristics of the sample. The AFM is actually a modified version of the scanning tunneling microscope (STM) [24,25]. The working principle of the STM relies on a quantum phenomenon referred to as tunneling current. This current is exponentially dependent on the distance between the STM tip and the sample. The displacements of the STM tip (or the sample) are induced by exposing piezo electric crystals to a varying electrical potential. The vertical resolution of the instrument is about 20 pm whereas its lateral resolution reaches around 200 pm. The tunneling current dependence on the tip – sample distance is given by:

$$I = \frac{4\pi q_e}{\hbar} V e^{-2\frac{d}{\hbar}(2m_e \phi E)^{½}}$$

Eq. 1.1. Tunneling current.

Where I is the tunneling current, V is the bias voltage, d is distance between the sample and the tip, ϕ is the barrier height, $\hbar$ is the reduced Planck's constant, q_e is the electron charge and m_e is the electron mass.
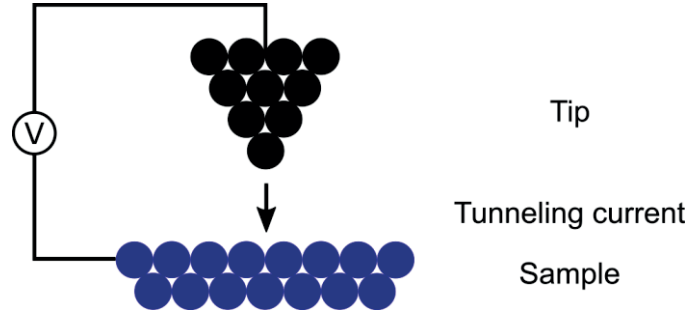
Fig. 1.1. Scanning tunneling microscope. The black dots represent the atoms of the conductive tip. The blue dots represent the atoms of the conductive sample. Arrow represents the tunneling current. The tip and the sample are in electrical contact.

To image a sample the STM tip scans its surface while a dedicated electronic circuit records the tunneling current intensity. A computer eventually displays the tunneling current as a function of the STM tip position as a map that corresponds to the electronic density of the atoms on the surface of the sample. One drawback of this method is that it only works with conductive samples.

To overcome this limitation a modified version of the scanning tunneling microscope called atomic force microscope was developed by Binnig, Quate and Rohrer [26]. The instrument consists in a tip that is anchored to the end of a soft cantilever that scans the surface of the sample. The interaction forces between the tip and the sample deflect the cantilever and this deformation is proportional to the interaction forces between the atoms of the tip and those of the sample. They consist in attractive long range (van der Waals force) and repulsive short range forces (Pauli repulsion of overlapping electron orbitals). The resultant interaction takes the form of Lennard-Jones potential, a formula which describes the interaction between two atoms. The Lennard-Jones potential formula is given below:

$$V_{LJ} = 4\,\varepsilon \left[\left(\frac{\sigma}{r}\right)^{12} - \left(\frac{\sigma}{r}\right)^{6} \right] = \varepsilon \left[\left(\frac{r_m}{r}\right)^{12} - 2\left(\frac{r_m}{r}\right)^{6} \right]$$

Eq. 1.2. Lennard-Jones potential.

Where r is the distance between the particles, ε is the depth of the potential well, σ is the distance at which the potential is equal to zero, r_m is the distance at which the potential function is equal to $-\varepsilon$.
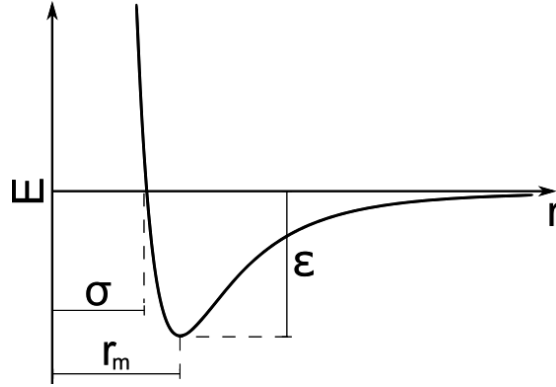
Fig. 1.2. The Lennard-Jones potential. This plot illustrates the potential - distance dependence, ε is the depth of the potential, σ is the distance at which the potential is equal to zero, r_m is the distance at which the potential function is equal to $-\varepsilon$.

The sample topography reconstruction is based on the cantilever deflection. Different methods exist to detect and quantify this deflection. The most widely used one relies on the deflection of a laser beam that is focused on the end of the cantilever. The reflected beam ends its path on a two or four segment photodiode. The photocurrent intensity difference induced in the segments of the photodiode is proportional to the cantilever deflection.

Other methods rely on the measurement of the electric properties (voltage, current, resistance, and capacitance) of an element that is subjected to a strain and that is embedded in or placed on the cantilever itself. Finally some other methods rely on variations on the distance between a fixed (or feedback loop controlled) element and the cantilever. In these cases, dedicated electronic devices monitor the changes in capacitance, tunneling current or laser beam interferences and infer the AFM cantilever deflections.

To date, the AFM has been utilized as a research tool within a broad range of scientific disciplines, including surface physics, solid state physics, condensed matter physics, molecular biology and microbiology.
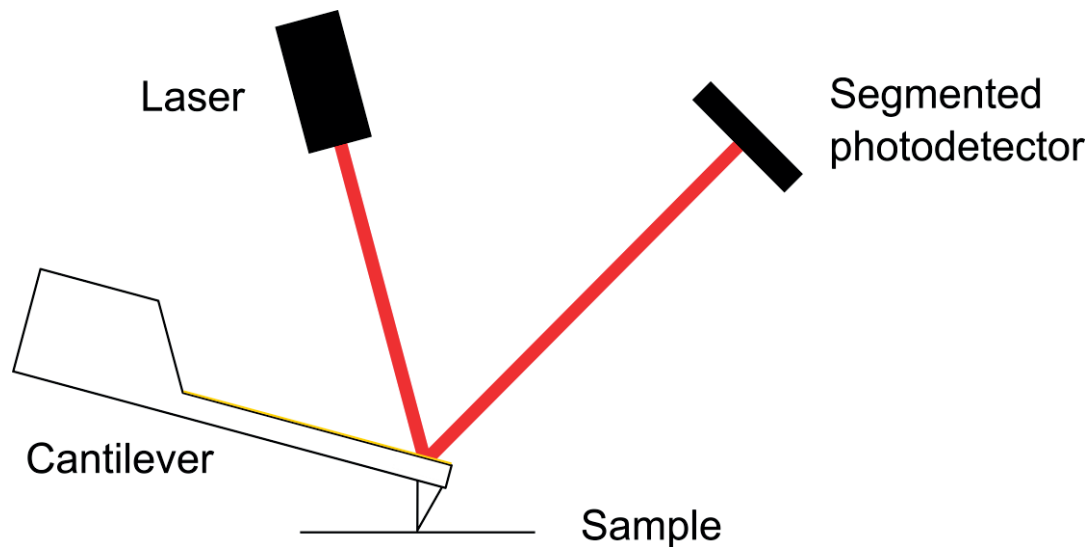
Fig. 1.3. Schematic of an atomic force microscope. The gold plated cantilever with a tip is near the sample surface. Usually the cantilever is capable to move in the vertical direction, while the scanner is moving the sample on the horizontal plane. The laser and the segmented photodetector are parts of the beam deflection detection system.

The AFM can operate in different imaging modes [27–30]. The contact mode is a mode within which the tip - sample interaction is in the repulsive regime of the Lennard - Jones potential curve. The interaction between the tip and the atoms of the sample surface is exerting a force on the cantilever sufficient to deform it. In this mode the cantilever deflection corresponds the topography directly (constant height mode). Alternatively a feedback controller maintains the force acting on the cantilever constant (constant force mode) and the topography mapping is achieved by recording the vertical (z) piezo voltage. The force acting between the cantilever tip and sample surface has to be kept below a certain level not to destroy the sample surface or the tip.

The non-contact mode is a mode within which the tip - sample interaction is in the attractive regime of the Lennnard - Jones potential curve. Since the tip is not in contact with the sample surface, there is no danger of damaging the sample or the tip. This mode is therefore preferable for imaging soft samples such as polymers, or fragile biological specimens. The cantilever is actively driven at or near its resonant frequency and hold at an optimal distance from the sample where attractive van der Waals interaction dominates. Different options exist to actively drive the cantilever. Some of them consist in embedding a piezo element in the cantilever holder, placing or embedding a piezo element in the cantilever itself, applying a pulsed laser at the base of the cantilever and deforming it by induced bimaterial thermal effect. Alternatively the cantilever can be driven to oscillate through an electromagnetic field. In this case, an external magnet and a coil are required. The interaction between the tip and the atoms of the sample surface exerts a force on the cantilever that changes either

its oscillation frequency or amplitude. Each of these two parameters can be monitored to reconstruct the sample's topography and reveal its mechanical properties (stiffness and adhesion).

Another imaging mode is the so-called intermittent contact mode. It is a mode in which the tip - sample interaction is alternately in the repulsive and attractive regime of the Lennard - Jones potential curve. The cantilever is forced to oscillate at or near its resonant frequency with a constant amplitude. The mode was developed to minimize the contact duration and reduce lateral forces.

In addition there are several other different modes available. One of those is the so-called force spectroscopy mode [31,32] that provides a force curve at every single pixel of the AFM image. Force curves are obtained by alternatively approaching and retracting the tip on and off the surface of the sample and by monitoring the cantilever deflection during the process. This mode permits to measure the sample's topography at zero force, as well as its stiffness and adhesion.

Chapter II

State of the art in bacterial sensitivity detection

2.1. State of the art in bacterial sensitivity detection

The growing spread of antimicrobial resistance has prompted the scientific community as a whole to focus on finding new techniques for characterizing the viability of bacteria. Being able to quickly assess the viability of different microorganisms is also hugely important in the field of targeted therapies, such as personalized medical treatment of cancer. There is also a purely scientific motivation behind the search for new techniques in this field, which are also likely to provide the answers to many of the basic questions around microbiology.

It should be noted that the relatively brief account contained in this chapter is not meant to represent an exhaustive review of currently developed methods to conduct AST and microbiological research, rather that the current state of the art will be used as a base line from which to investigate innovative approaches to the topic.

The second section describes the standard antibiotic susceptibility tests, the next section characterizes the flow cytometry based AST method, microcalorimetry is depicted in the following section, in the fifth section MALDI TOF MS based AST is considered, polymerase chain reaction based AST is portrayed in the subsequent section and finally the cantilever based ASTs are detailed in the seventh section. The last section concludes the chapter.

2.2. Standard antibiotic susceptibility tests

Currently antibiotic susceptibility testing (AST) methods are based on the optical or chemical detection of the bacteria growth in the presence of a specific concentration of a drug or a combination of drugs. The test starts by taking a urine, sputum or blood sample from the patient, the sample is eventually divided and incubated in different types of culturing media to accommodate the various types of bacteria that are possibly causing an infection. After a sufficient period has passed for the bacteria to divide multiple times and the sample to be marked as indicating the presence of infection, the bacteria are separated from their culture medium using a centrifuge. These separated bacteria are then placed in a Petri dish on top of a nutrition layer, usually comprised of agar, and small wafers containing antibiotics are placed on top of this layer. The Petri dish is then incubated and monitored for visible indications of bacteria growth; the presence of any such indications around the antibiotic wafer is taken to indicate resistance, while the absence demonstrates susceptibility. The method described above was developed by Bauer et al. [33–35]. It is usually referred to as the Kirby-Bauer antibiotic test and is a standard method used worldwide. There are alternative methods used to achieve the same goal such as a broth dilution,

an Etest and others. The Etest [36] uses a plastic strip that has an increasing concentration of the antimicrobial along its length, once placed in a Petri dish, the drug diffuses and if microorganisms are susceptible the zone of growth inhibition appears after incubation. The place where bacteria barely grow near the plastic strip determines the concentration of inhibition.
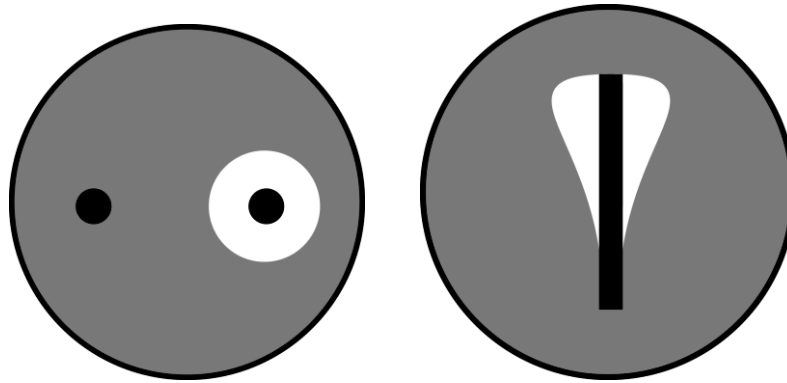
Fig. 2.1. Schematic of the Kirby-Bauer antibiotic test and Etest. The black spots on the left panel represent the antibiotic wafers, the grey color represents the bacteria coverage, the white spots represents the place where bacteria are not growing. This shows that the bacteria are resistant to the antibiotic from the right wafer and that the antibiotic wafer on the right was effective against the bacteria. The black strip on the right panel represents the antibiotic strip with gradient of antibiotic concentrations, rising from bottom to the top of the strip, the grey represents the bacteria growth, while the white one the place where bacteria are not growing. With increasing concentration at some point the bacteria are not growing, which is represented by the appearance of white area at some specific concentration that is an estimate of the MIC.

2.3. Flow cytometry AST

Cytometry measures properties of cells, and depending on the specific method being used it can include: cell count, cell size, cell morphology, cell cycle phase and presence of specific components like cellular machinery, proteins or DNA. Cytometry detection is performed with the use of an optical microscopy and staining methods to selectively label molecules or increase contrast, hence it is usually referred to as image cytometry. The process can be automated with a camera and software.

Flow cytometry [37–39] is an adaptation of image cytometry to increase yield and simplify the detection process. Flow cytometry is used for detecting, counting and/or sorting microbiological samples. This method work by suspending microorganisms in stream of liquid and performing detection through optical or electronic (measuring impedance, Coulter counter) means.

There are methods to perform AST [22,40,41] using flow cytometry. It requires incubating bacteria with nourishing medium, antibiotic and fluorescent markers for an hour. Bacteria are obtained from blood culture that was observed to multiply. Then the liquid is passed through the detection chamber that identifies, based on fluorescent markers, if bacteria are dead or alive, thus telling if the bacteria are susceptible or resistant to that antibiotic concentration.

2.4. Microcalorymetric AST

Isothermal microcalorimetry (IMC) is a method that measures amount of energy in time (power) exchanged between the sample and the external heatsink. This method is capable of monitoring produced or consumed heat energy in exothermal and endothermal processes respectively. The sample is sealed in a capsule and placed in the device. Detection of the heat flow is achieved through thermoelectric effect in a Peltier device. This method is capable of measuring microwatts of power being transferred to the heatsink. One side of Peltier element is in heat contact with heatsink kept at a constant temperature the other side is in heat contact with the sample. In heat conduction mode the difference in voltage is proportional to the difference in temperature which corresponds to heat energy. In power compensation mode the heat change of the sample is compensated so that the sample is kept at a constant temperature. The difference between those two modes is the time constant is lower for the power compensation mode, while the dynamic range is higher for the heat conduction mode. This method can utilize two capsules to measure differentially, one capsule for reference and the other one for the sample.

This method can be utilized for both the detection of microorganisms in the sample and for ASTs. Viable organisms produce heat as a side effect of their metabolism and the detection is possible when the heat produced by microorganisms exceeds the detection threshold of the device. AST is performed by monitoring the heat produced by bacteria after the introduction of an antibiotic. A single bacterium is capable of generating approximately 1 pW heat power depending on the bacterium type and growth conditions, although studies show high range of values for *E. coli* from 0.8 pW to as high as 7.8 pW [42–45]. IMC requires around 1 million bacteria for detection, and is also able to perform MIC and MBC measurements. Equilibration of the sample temperature in the device is a relatively slow process, which takes approximately 1 hour, and no data is collected during that time.

The calorimetric measurement can be performed using a bimaterial cantilever, taking the advantage of the different thermal expansion coefficient of the cantilever layers [46–48]. One study performed cantilever based experiments with brown fat cells (BFC) [46], being a thermogenic cell that is responsible for temperature regulation in

mammals. Norepinephrine stimulated the cells to convert fatty acids into heat, and the heat was detected by deflection of the cantilever which was either in contact with the cell or in close proximity to the cell. The authors claim to achieve resolution of 5.2 pJ in calorimetric measurements. The heat energy output of the BFC was measured at 560 pJ during a 20 minute experiment with norepinephrine stimulation.

Alternatively [43,49,50] chip-calorimetric devices based on complementary metal-oxide-semiconductor (CMOS) technology can be used to monitor biological samples heat energy production. These devices were shown to have a detection threshold of 20 nW, which equates to the energy released by twenty thousand viable bacteria.

2.5. MALDI TOF MS AST

Matrix assisted laser desorption/ionization time of flight mass spectroscopy (MALDI TOF MS) [51] is a combination of sample vaporization (MALDI) and a time of flight mass spectroscopy techniques (TOF MS). The sample to analyze is mixed with a matrix that absorbs the laser light. The absorbed energy is converted into heat, which causes the matrix to evaporate together with the sample that is ionized in the process. After the evaporation, the time of flight mass spectroscopy is used to ascertain the mass spectrum of the molecules contained in both the sample and the matrix. The identification is based on the difference in the time of flight of ions through a chamber exposed to an electric potential. This method is routinely used to identify microorganisms in patient's sample. This method is based on the detection of specific peptides and is possible only if the reference databases contains the specific peptide mass profile [52,53]. The presence of specific peptides is used to identify the bacterial species and eventually to prescribe its specific antibiotic.

2.6. Polymerase chain reaction AST

Polymerase chain reaction (PCR) [54] is a molecular biology method used to repeatedly replicate a specific segment of DNA into copies which are detectable by conventional means such as staining. It is most commonly used in DNA sequencing, genomics and the detection of specific DNA sequences. PCR involves repeatedly heating up and cooling down a sample containing target DNA, DNA primers, DNA polymerase, deoxynucleoside triphosphates (dNTPs), buffer solution and cations. The first step, known as the denaturation phase, involves heating to melt double-stranded DNA into two single-stranded DNA molecules. The next step, called annealing, is performed at a lower temperature, and is used to anneal primers to

18

3' ends of DNA molecules, usually involving one type of primer for each end. The next step, called elongation or extension phase is executed at an intermediate temperature, and involves attaching dNTPs with the help of DNA polymerase, starting from the primer attached to the single-stranded DNA, and then the process is moving in a 5'-to-3' direction of the replicating DNA. The time needed for the cycle is mainly dictated by the third step, which is dependent on the length of the DNA target, the properties of other reagents involved and the conditions under which these reagents can be used. Each cycle should double the number of DNA target molecules resulting in exponential multiplication. PCR is able to identify specific section of DNA, which is responsible for antimicrobial resistance [55]. However this method has a number of shortcomings: it offers extremely specific results and it cannot be used to obtain MIC and MBC values.

2.7. Cantilever based AST

Nanomotion

The Longo et al. [23] publication described in this section is at the basis for this thesis. It describes the use of an AFM to conduct experiments assessing the viability of bacteria by observing low frequency fluctuations of the cantilever with bacteria attached to it. The developed method permitted to highlight bacterial response to antibiotic exposure far more quickly than traditional ASTs. Using this method it was also possible to conduct measurements quantifying MIC and MBC by using increasing concentration of antibiotic in the media. Moreover it could also quantify the metabolism of bacteria by using different amounts of sugar in the media. The results were obtained by measuring the temporal oscillations of the cantilever and its modifications upon exposure to antibiotics. The variance of the data was used to quantify the effect of the antibiotic or the change of nourishing media. In this study the method was applied to two strains of *Escherichia coli* and one strain of *Staphylococcus aureus*. One of the *E. coli* strains was resistant to ampicillin, whereas the other one to kanamycin. Those bacteria were used since *E. coli* represents the gram-negative motile and *S. aureus* the gram-positive non-motile bacteria.

A cantilever not populated with bacteria and immersed in a buffer solution is a subject of thermal oscillations, and these fluctuations were treated as a baseline. The bacteria were attached onto the cantilever with (3-Aminopropyl)triethoxysilane (APTES). Liquids used in the experiments were the buffer, which was a phosphate-buffered saline (PBS) and nourishing media consisting of lysogeny broth (LB). The living bacteria attached to the cantilever were causing significative difference in both the amplitude and the variance of the observed oscillations.

In the experiments involving susceptible bacteria – of both the *E. coli* and the *S. aureus* strains – the introduction of the antibiotic ampicillin saw the variance value decrease, and eventually reached the value of the baseline. It was noticed that the non-motile *S. aureus* induced oscillations was a factor of two lower in the amplitude than those generated by the motile *E. coli*. Experiments intended to quantify the MIC and the MBC were conducted with *E. coli*. In these experiments the media was enriched with increasing concentrations of the antibiotic and induced a change in the variance of the signal. Eventually the value of the variance was plotted against the concentration and the data fitted with a sigmoid curve (*see Fig. 2.2. c*).
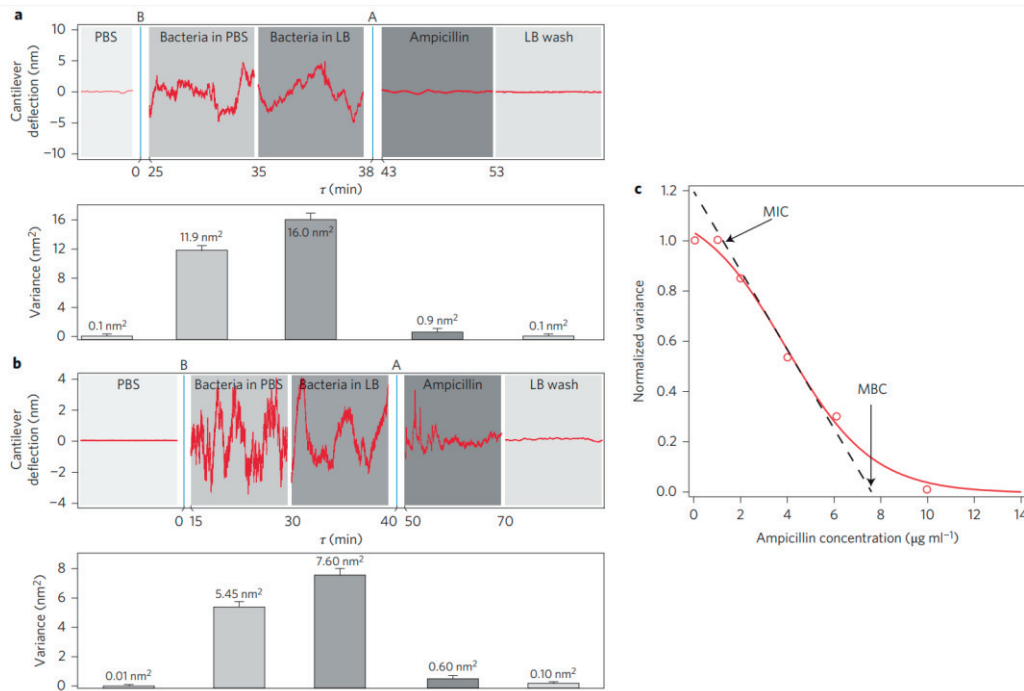
Fig. 2.2. Experiments involving E. coli and S. aureus bacteria susceptible to ampicillin. a) Deflection of the sensor (top) and corresponding variance (bottom) for the E. coli experiment. The traces represent 20 s of recording for 'PBS' and 30 s for the other media. The time axis indicates the minute (starting from bacterial injection at 'B') when each recording was started. The 'A' line indicates when ampicillin was injected. The error bars represent the variation of the variance values in measurements performed in similar conditions. b) Corresponding results for the S. aureus experiment. Each trace represents 30 s. c) Normalized variances obtained when exposing the susceptible E. coli to different ampicillin concentrations (open circles) and the corresponding fit using a sigmoid function (red curve). The MIC and MBC values were obtained by intercepting the tangent at the inflection point (dashed line) with the 1 and 0 horizontal lines. [23]

Experiments involving ampicillin resistant *E. coli* presented a drop in the variance immediately after the injection of the antibiotic but the variance increased again a dozen of minutes later (*see Fig. 2.3. a*).

20

In experiments with *E. coli* strain known to be resistant to kanamycin, the data indicated a decrease in variance in the presence of kanamycin. When the liquid was subsequently exchanged with a nourishing medium the signal recovered its initial value, indicating the resistance to kanamycin. Afterwards, ampicillin was introduced in the analysis chamber and the variance decreased. However when the liquid was subsequently exchanged with a nourishing medium, the bacteria did not recover indicating a susceptibility to ampicillin (*see Fig. 2.3. b*).

Additional experiments were carried on to address the metabolic activity of the bacteria. The study reported gradual increase in the variance of the cantilever oscillations with increasing glucose concentration (buffer solution, 2% glucose and 4% glucose) testifying a correlation between the signal variance and the metabolic activity.
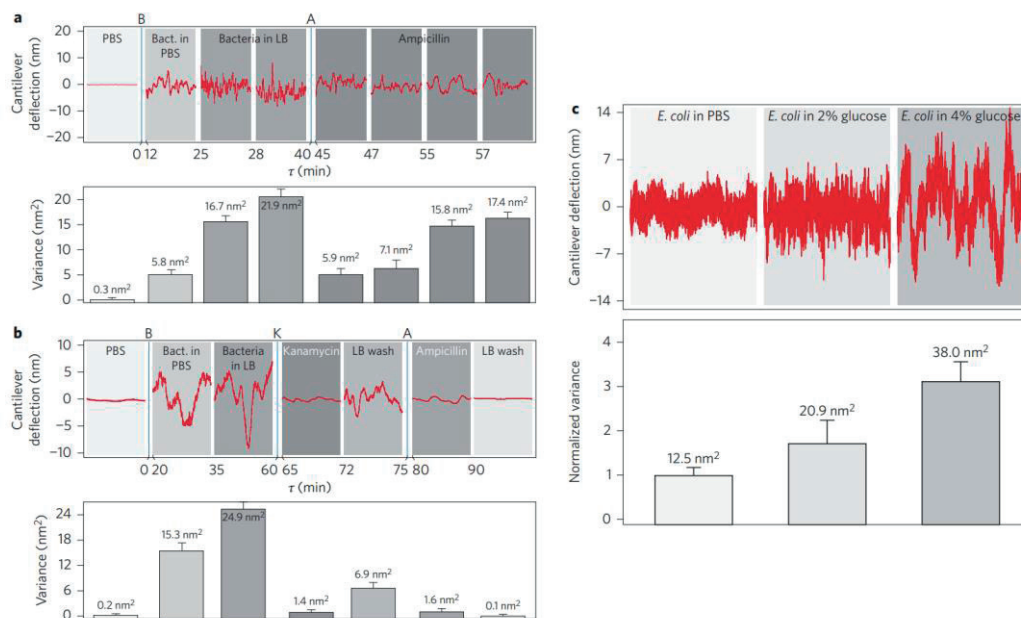
Fig. 2.3. Experiments describing the correlation between metabolism and fluctuations. a) Deflection of the sensor (top) and variance (bottom) for the ampicillin-resistant E. coli experiment. Each trace corresponds to 120 s. The time axis indicates the minute (starting from bacterial injection 'B') when each recording was started. The 'A' line indicates when ampicillin was injected. The error bars represent the variation of the variance values in measurements performed in similar conditions. b) Corresponding results from the experiment involving E. coli exposed to kanamycin and ampicillin. Each trace corresponds to 120 s. The lines indicate when kanamycin (K) and ampicillin (A) were injected. c) Deflection of the sensor (top) and variance (bottom) for the experiment involving E. coli exposed to glucose. Each trace represents 30 s. The measured variances are indicated over each corresponding column. The columns represent the variance normalized by the 'PBS' value. [23]

Longo et al. reports that the viable bacteria induced cantilever oscillations in the 0.1 - 200 Hz range. The main advantage gained from this method is that it is not dependent on the growth rate of bacteria, which is otherwise a limiting factor for the traditional methods due to the replication times involved. The method was proven to be viable when used with two highly distinct types of bacteria, and can also be used to perform multiple types of experiment resulting in not only standard AST, but also MIC and MBC. Authors discussed the fact that the energy needed to sustain the observed fluctuation of the cantilever is actually only a fraction of the energy used by the bacteria. The interpretation they provided for the observed effect was that small movements of the bacterial cell walls transduced to the cantilever, although the ionic pump, molecular motors and other metabolic activities were noted as a possible additional contributing factor in cantilever oscillation.

Nanomotion – 1/f noise analysis

Lissandrello et al. in their paper [56] replicated the method presented in [23] with addition of a different method to analyze the obtained data. The experiment is conducted as follows: cantilever is functionalized for 15 minutes with non-specific binding agent 1% (3-aminopropyl)triethoxysilane (APTES), afterwards genetically modified *E. coli* bacteria are introduced and then incubated for further 15 minutes. Cantilever oscillations are detected with an optical beam deflection technique. The measurement is conducted at 3125 Hz sampling frequency for 40 seconds for every phase of the experiment. The authors of this paper were using cantilevers with low spring constant of 0.03 N/m.

The experiment and the following data analysis shows differences in the 1/f noise amplitude in the range of frequencies from 1 to 80 Hz. This paper acknowledges the presence of the large-amplitude low-frequency oscillations originating from the viable bacteria attached as noticed before in [23]. This publication discusses the origin of the 1/f noise like oscillation caused by presence of viable bacteria attached to the cantilever.
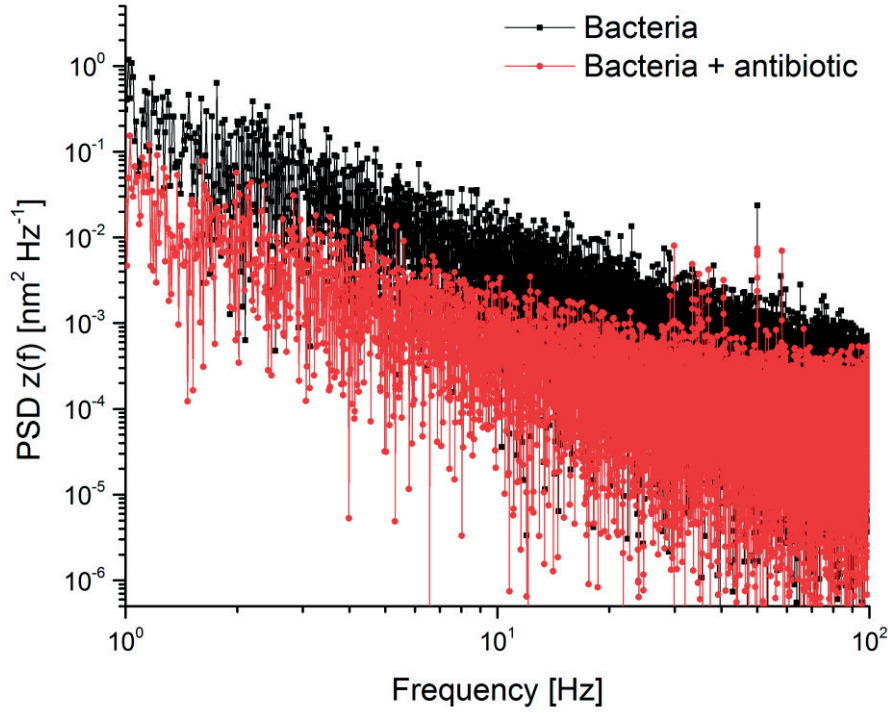
Fig. 2.4. Power spectrum density of cantilever deflection. The bacteria are shown in black and the bacteria with antibiotic added are shown in red. The difference is present in the low frequency region of the cantilever fluctuations, it vanishes above 100 Hz. Method from (56) was adopted to analyze data from one of our experiments.

Authors concluded that those results may help to understand the motion of microorganisms adhered to the surfaces and develop a micromechanical sensors for assessing bacteria viability.

The motion of the bacteria couples efficiently to the cantilever well below its resonance frequency, causing a measurable increase in the cantilever fluctuations. In the time domain, the fluctuations exhibit a large-amplitude low-frequency oscillations. In the corresponding frequency domain measurements, it is observed that the mechanical energy is focused at low frequencies with a 1/f type power law. A basic physical model is used for explaining the observed spectral distribution of the mechanical energy. These results lay the groundwork for understanding the motion of microorganisms adhered to surfaces and for developing micromechanical sensors for bacteria.

Cantilever weighting system in liquid environments

Martin-Martinez et al. developed a method to measure temporal mass changes of cells attached to a cantilever in a liquid environment and at the same time being able to use normal or fluorescent microscopy. Authors link those changes to metabolic activity of cells. This method could be used as another approach to characterize the viability of microorganism [21]. This method is capable of characterizing single cell mass at mass and time resolutions required to observe fast cellular dynamics. The cells used in the experiment were human cancer derived cell lines (HeLa) and mouse fibroblast cells. The cantilevers were functionalized with fibronectin for fibroblasts and with collagen type I for HeLa cells. The cells were picked up by the cantilever that lowered to contact the cell with a force in a range of 1 - 5 nN. Afterwards the cantilever was raised to about 150 um above the surface of the culture dish. The experiments were conducted in a controlled environment chamber with conditions proper for culture growth.
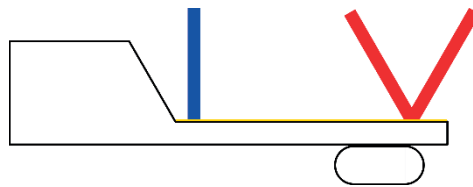
Fig. 2.5. Schematic of the cantilever weighting system. The blue laser is for driving the cantilever. The red laser is for detecting the deflection of the cantilever.

The cantilevers were actuated with a pulsed laser to gain higher quality factor of the resonant peak. The optical beam deflection detection method was used to detect the oscillations of the cantilever. By monitoring changes in the cantilever resonant frequency as a function of time, the detection of the cellular mass change was obtained. Authors claim to achieve picogram mass sensitivity. They observed fluctuations in mass from 1 to 4 percent on a timescale of seconds. A Coulter device was used to determine the volume of the cells. Analysis of the collected data has shown two components in the mass fluctuations: a slow and a fast one. This shows that this method has a great potential of being a great tool in basic research and is highly applicable in targeted therapies against diseases e.g. cancer.

Channeled cantilever weighting system

Burg et al. [57] report an alternative approach to weigh biological samples. The technique is based on the use of cantilevers that containing channels and in monitoring their quality factor. Weighing is achieved by monitoring the changes in the resonant frequency of the cantilever. Cantilevers were placed in a vacuum chamber to increase their quality factor, thus increasing their sensitivity. Authors claim to reach quality factor of 15000 that improved sensitivity by six orders of magnitude compared to commercial quartz crystal microbalance. With this method it is possible to conduct mass-based flow cytometry experiments, direct detection of pathogens and non-optical sizing and mass density measurements of colloidal particles. This method is highly sensitive to the presence of objects with density different than that of the solution. Surface adsorption for biomolecular mass sensing is feasible due to high surface to volume ratio. The cantilever is driven by an electrode placed underneath through electrostatic force. Cantilever deflection is detected optically. Authors suggest that the limit of mass detection could be improved, but it would require to use gold labelled secondary antibodies, thus losing the advantage of label free approach. The drawback of the system noted by the authors is low fluid volume processing capabilities due to high flow resistance of the channel, on the other hand this system requires little amount of sample to function properly. The cantilever in this method is reusable with a cleaning procedure involving acid combination.
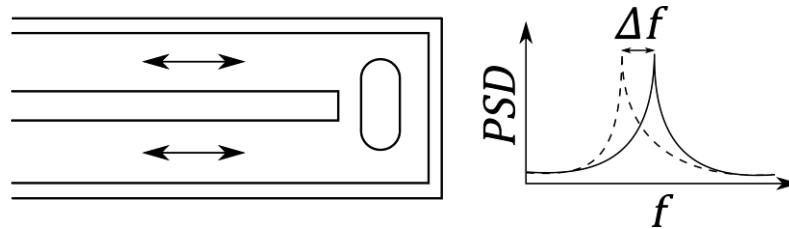
Fig. 2.6. Channeled cantilever weighting system. Left panel: schematic of channeled cantilever weighting system. Arrows indicate the fluid flow control that keeps the bacteria at the apex of the cantilever. Right panel: power spectrum density plot of a shift in resonant frequency due to mass change.

2.8. Conclusions

As have been shown in this chapter there exist many methods, both established gold standards such as Kirby-Bauer method and emerging innovative methods. Some of them are based on the growth of the bacteria while others are based on the detection of molecules associated with the microorganism's drug resistance. However the method that this thesis is based on are linked directly to the metabolic activity of the microorganism in question. This method provides the information about the resistance or lack thereof to tested drugs.

The second section described the well-established Kirby-Bauer method and its variations that are used throughout many laboratories around the world to find the MIC and MBC for infection treatment. Because these are microorganism growth-based methods, it takes a day or two for fast growing bacteria and even weeks for the slow growing ones to complete the test. Due to this time restriction these methods are not well-suited for the cases of sepsis or septic shock. In the case of the bacteremia the use of quicker methods would allow to reduce the patient's stay at the hospital.

The third section covered the flow cytometry method that is an improvement over the above mentioned standard growth methods. While this method require far less bacteria for the detection of the alive or dead bacteria, it still requires to incubate the microorganisms with fluorescent markers that are specific to the type of the bacteria. Due to the sensitivity improvement over the standard method it is better suited for the cases of bacteremia to shorten the patient's stay at the hospital, however it might not be enough for more severe cases.

The fourth section considered the microcalorimetry based AST, which requires at least one million bacteria for the detection threshold. That number involves prior phase of culturing the bacteria isolated from the sample. The thermal equilibration of the microcalorimeter and the sample is a slow process and usually takes around one hour, however the whole experiment is significantly faster than the standard AST.

MALDI TOF MS based AST discussed in the fifth section and the polymerase chain reaction based AST characterized in the sixth section both operate based on the detection of a specific molecule related to antimicrobial resistance. This relies on the prior experiments and data to compare with the detected molecular profile. In the quickly evolving and genetically diverse antimicrobial resistance environment this might not account for new types of resistance.

And finally the seventh section discussed the cantilever based ASTs. The first subsection described the nanomotion technique [23,58–64] developed in our group, the second section detailed the power spectrum density analysis of the 1/f noise of nanomotion technique results [56]. The last two sections concentrated on the cantilever based weighting systems [21,57]. The nanomotion technique has the advantage of being relatively quick and works irrespectively of the type of

microorganism. The method can provide accurate MIC and MBC, although the experimental procedure is rather complicated. The weighting techniques relies on the bacterial mass changes on the timescales short enough to account for metabolic activity. Cantilever based methods have the advantage of relying on the metabolic activity of the microorganisms and not requiring the growth, thus operating at timescale smaller than the standard methods. This advantage is crucial in the fight with sepsis. Another benefit of these methods is the non-specificity, the knowledge of the specific strain of the microorganism is irrelevant, because those methods work well regardless. Those two advantages are crucial for the improvement in the treatment of the dangerous infections and sepsis, and deem the cantilever based ASTs promising.

Chapter III

Theoretical study of the viable organisms induced cantilever oscillations

3.1. Introduction

Longo et al. [23] have discovered that bacteria attached to an AFM lever in a physiological solution provoke fluctuations of the lever's deflection which are larger than the thermal induced fluctuations. These additional fluctuations disappear rather quickly after an antibiotic is added to the solution. The underlying cause of the cantilever oscillations with living organisms attached to it has still not been explained [23,56,58–64].

This chapter is devoted to the evaluation of different possible physical, chemical or biological processes that could explain the observed effect. Moreover, their relative contribution to the phenomenon is numerically estimated if the case allows. In the last section of the chapter the false positives effects (effects mimicking viable bacteria) will be discussed. Understanding the phenomenon is mandatory for the improvement and further development of the method and could expand the tool to new biomedical applications.

In the attempt to describe the phenomenon here are some of the features that characterize the cantilever oscillations:

1) The deflection of the cantilever is approximately $10\ nm$.

2) It is possible that the bacteria also induce a torsion of the lever.

3) The deflection of the lever is measured as a function of time and its variance is calculated with a time window of 10 seconds: the variance of the signal is larger when the bacteria are alive.

4) It was observed that the variance of the signal is increasing in time after the start of the experiment indicating that the signal depends on the number of bacteria on the lever due to their multiplication.

5) The variance of the signal is a function of the metabolism of the microorganisms.

6) The increased fluctuations of the lever last at least for few hours.

7) The power spectrum of the lever's deflection shows an increase with respect to the one of a bare lever at frequencies below $100\ Hz$.

3.2. Description of the observed effect

We are discussing here the phenomenon that was first observed by Longo et al. in 2013 [23]. In these experiments, *E. coli* bacteria were attached to an AFM by treating the lever's surface with APTES in order to enhance the adhesion of the bacteria. Both sides were covered with approximately 500-1000 bacteria and the lever was freely fluctuating in a physiological nourishing solution. By means of the AFM optical detection system, the bending of the lever was recorded as a function of time. It was observed that the lever was fluctuating around its rest position and that these oscillations stopped when a chemical or a drug killed the bacteria and returned to the amplitude typical for thermally excited fluctuations. The results of these experiments were repeated by other laboratories [56] and also, we could confirm that this phenomenon is not limited to *E. coli*, but other bacteria, mobile or not mobile, slow growing bacteria, yeast, cells, etc. exhibit the same behavior [58–63].

The cantilever under these conditions is behaving as a damped and asymmetrically driven anharmonic low quality factor oscillator. The driving energy comprises of a component due to the thermal energy and a component given by the microorganisms attached on its surface. The damping is caused by the viscosity of the analysis medium and other friction terms that might exist. Independently of the microscopic phenomenon that causes the additional oscillations of the lever, we can already estimate the power required to induce and sustain these oscillations. According to point 7) above, we assume that the oscillations are in the low-frequency region of the spectrum and for the sake of simplicity we take a characteristic frequency of $100\ Hz$.

The power $p_{dissipated}$ dissipated by the harmonic oscillator of spring constant $k = 0.12\ N/m$ and having a quality factor of 1 and an oscillating frequency of $100\ Hz$ with amplitude of $\bar{x} = \sqrt{\langle x^2 \rangle} = 10\ nm$ (point 1) above) is given by:

$$p_{dissipated} = 100 \cdot \frac{1}{2}k\bar{x}^2 = 6 \cdot 10^{-16}\frac{J}{s} = 0.6\ fW = 600\ aW \approx 1\ fW$$

Eg. 3.1. Power dissipated by harmonic oscillator.

In comparison the thermal power dissipated by 100 bacteria it is estimated to be $9 \cdot 10^{-7}W$ [42–45] which is largely greater than the power needed to drive the lever's fluctuations. We assume therefore that the bacteria have enough power to drive the lever. We can also make a crude estimation of the power stored in the lever by using its power spectrum [56]. The spectrum extends from 1 Hz to 100 Hz with a frequency dependence $\propto \frac{1}{f^3}$, before it runs into the electronic noise. The power

spectrum at $1\,Hz$ has a value of $0.5\,nm^2/Hz$ [56] that we multiply by $100\,Hz$ bandwidth (here is the crude approximation by assuming a constant dependence of the power spectrum on frequency, thus forgetting the $\frac{1}{f^3}$ frequency dependence), giving an average lever's displacement of $\langle x^2 \rangle = 50\,nm^2 = 5 \cdot 10^{-17} m^2$. Using again *Equation 3.1* and assuming that the quality factor is equal to 1, we obtain a dissipated power of $P = 100\,Hz\,\frac{1}{2}k\langle x^2 \rangle = 7.5 \cdot 10^{-17}\,W \approx 75\,aW$ (the spring constant in this case is $k = 0.03\,N/m$). The baseline of the power spectrum density is dominated by the electronic noise of the detection system with a contribution of the thermal oscillations of the cantilever itself. We can therefore estimate from our measurements (point 1) above) and from [56] that the power dissipated in the lever's oscillations is approximately in the range $0.075 - 1\,fW$. The power dissipated by 1000 bacteria $10^{-9}\,W$ [42–45] is largely above these values and therefore we can safely assume that the additional oscillations observed when bacteria are attached to the AFM lever are originated by the bacteria.

3.3. Possible positive contributions to the observed effect

In this section different phenomena that could contribute to the observed effect are investigated and their contribution is evaluated using estimations and data about *E. coli* in order to reach some conclusions about the dominant effects. To this end we need always to use some kind of a model and take into account the constraints of our experimental system (*E. coli*) and setup.

3.3.1. Flagellar contribution

This section will focus on the flagellum equipping the *Escherichia coli* bacteria and we want to investigate the contribution of this motor system to the fluctuations of the lever to which the bacteria are attached. The flagella allow the bacteria to move in liquids or on moist surfaces. The flagellum can also have sensory functions since it can detect certain chemicals and/or changes in temperature. The Escherichia coli thrust system consists of a rotary motor with a hook like shaft to which filaments are attached. This motor can rotate clockwise and counter-clockwise. When turning counter-clockwise, the flagellum's filaments bundle under the influence of hydrodynamic forces to form a screw like structure that propels the bacteria. When the motor turns clockwise, the filaments are unbundled and cause the tumbling of the bacteria, thus changing its orientation. The rotation of the flagellum causes the counter rotation of the cell consistent with the conservation of angular momentum.

The rotation of the motor is powered by a positive (proton or sodium ion in some cases) ion current through the MotA and MotB proteins to the M-ring of the motor that form the stator and rotor of the motor, respectively. The ionic current is a result of a net diffusion due to the electrochemical gradient across the bacterium's membrane. The ion density gradient is sustained by the bacteria pumping the protons by means of ionic pumps. The change in the rotation direction is caused by the conformal change in M-ring generated by the switch protein complex which is activated by the chemotaxis signaling system.

In the case of eukaryotic cells, the propulsion system is different than the one of bacteria and is based on bending movement (lashing and undulatory movements) rather than rotation. Some bacteria have only one flagellum (*monotrichous*) and use it to move in one direction or to randomly change the direction. Some other bacteria have two flagella on each end of their body (*amphitrichous*) that permits them to move in two directions, whereas some other possess multiple flagella on one end (*lophotrichous*). Other bacteria have multiple flagella distributed on the whole cell that are projecting into all directions (*peritrichous*).

Escherichia coli can reach speeds up to 36 micrometers per second at a flagellar rotation rate up to 16 rotations per second. The rotation speed of the motor's shaft without flagellum can reach up to 270 rotations per second.
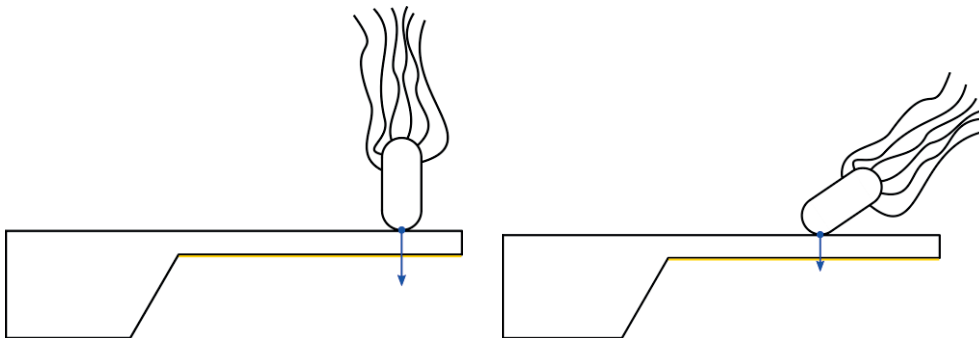
Fig. 3.1. Flagellar contribution model. Left panel: schematic of simple model of bacteria attached to the surface of the cantilever with active flagella pointing away and exerting a force on the cantilever. Right panel: more realistic model of bacteria pointing in a random direction thus exerting smaller force in the deflection direction of the cantilever.

In [65] it is described that 1040 protons are needed for one rotation of the motor. For the reasoning concerning the potential effect that the flagella have on the oscillation of the cantilever certain assumptions are needed. The most extreme case will be shown and discussed. On average an E. coli possess 6 flagella that rotates at 16 Hz. Thus an *E. coli* requires 1040*16*6=99'840 protons per second to drive its flagella where each proton has motive force of 150 mV. Thus, the energy delivered by a proton is

equal to $E = 1.6 \, 10^{-19} \, C \cdot 0.15 \, V = 2.4 \cdot 10^{-20} J$. This amounts to a total power delivered by the protons:

$$p_{protons} \approx 99840 \frac{1}{s} \cdot 2.4 \cdot 10^{-20} \, J \approx 2.4 \cdot 10^{-15} \, W = 2.4 \, fW$$

Eq. 3.2. Power delivered by the protons.

This power is comparable to the power needed to sustain the observed oscillations of the AFM lever. On the other hand, we can estimate the power that has to be delivered by the flagella for the motion of *E. coli*. We assume a maximum speed of $v = 32 \, \mu m/s$ and that we are in the low Reynolds regime for the motion of the bacteria. The hydrodynamic friction force is then given by the Stokes law $F_{Stokes} = 6\pi\eta R v$ where $\eta = 0.001 \, Pa \cdot s$ is the viscosity of water, $R \approx 5 \cdot 10^{-6} \, m$ the hydrodynamic radius of *E. coli*, and $v = 3.2 \cdot 10^{-5} \, m/s$ the speed. The power dissipated will be:

$$p_{Stokes} = F_{Stokes} \cdot v = 6\pi\eta R v^2 = 9.6 \cdot 10^{-17} \, W \approx 0.1 \, fW$$

Eq. 3.3. Power dissipated due to hydrodynamic friction.

This dissipated power is approximately one order of magnitude lower than the power delivered by the flagella's motors, thus it is a reasonable value assuming that we have not taken into account the efficiency of the motor-flagellum system. The efficiency of a flagellum is in the range from 0.1 to 1 % [67,68]. If we further assume that the number of bacteria attached on the lever is in the range 100-1000, this leads to a total power estimated from the hydrodynamic friction of 10-100 fW, and from the electromotive force of the proton of 240-2400 fW.

Another point of view on the action of the bacteria on the cantilever is if we considered that the bacteria could act on the lever by pushing with its flagella. Again, by taking the Stokes force as a measure of the force produced by the flagella, we obtain:

$$F_{Stokes} = 6\pi\eta R v = 3 \cdot 10^{-12} \, N = 3 \, pN$$

Eq. 3.4. Stokes force as a measure of the force produced by a flagellum.

This force can bend the lever to an amount of $x = \frac{F_{Stokes}}{k} = 2.5 \cdot 10^{-11} \, m$. If the action of the bacteria would be synchronized and the force perpendicular to the lever's surface, then the total deflection of the lever with 100-1000 bacteria on its surface can have a maximum value in the range $2.5 - 25 \cdot 10^{-9} \, m = 2.5 - 25 \, nm$. We found again that the bacteria can cause the observed deflections of the lever. Experimentally we have tested the effect of the flagella by doing measurement of

the oscillations under conditions of very high glucose concentrations: high concentration of glucose inhibit the function of flagella. We have observed a significant drop in the amplitude of the oscillations and a corresponding reduction of the variance of the signal.

3.3.2. Surface stress contribution

The surface stress is defined as a work per unit area that induces an elastic stretch of a surface. In other words, the surface stress is equal to the surface energy in units of J/m^2 or else N/m. In our case, when the bacteria are attached to the surface, the surface energy of the interface bacteria – lever has to be considered. Therefore, attaching molecules to the surface of the cantilever causes either an increase or a decrease of the interface energy. In order to cause a static deflection of the lever, the surface energy change should affect only one side of the lever. Thus, the bacteria should be attached to one side of the lever only. However, in our experiments bacteria are actually attached to both sides of the lever, so we have to assume that the observed oscillations of the lever are induced by random fluctuations of the surface energy in time affecting both sides of the lever. These fluctuations are caused by a small number of bacteria (100-1000 bacteria in total are attached to the lever) and do not average out causing the observed oscillations of the lever.
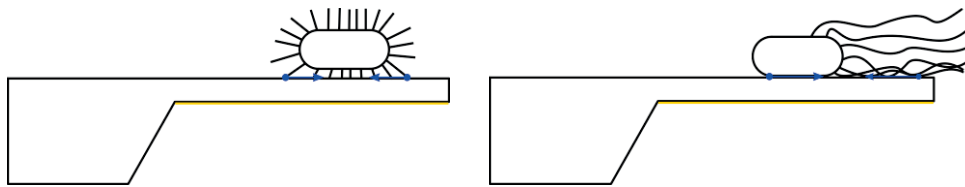
Fig. 3.2. Schematic of simple model of a bacterium attached to the surface of the cantilever with pili or flagella. Bacteria are exerting forces on the surface, thus inducing a surface stress causing deflection of the cantilever.

Microorganisms can attach to surfaces by the means of the cellular surface proteins (see *Fig. 3.2*), cellular appendages (pilus, fimbria or flagellum) forming sometimes even biofilms. After the initial adhesion, the pili may retract allowing other parts of the cell to bind to the surface. Thus, microorganisms have many ways to induce a surface stress to the surface of the cantilever through adhesins and the cell's body itself.

Using the Stoney's formula that was further developed by Jaccodine and Schliegel the surface stress σ needed to obtain a deflection Δz of the lever is given by:

$$\sigma = \frac{\Delta z \, E \, t^2}{3(1-\nu)L^2}$$

Eq. 3.5. Surface stress necessary for the observed deflection.

Where E is the Young's modulus, ν the Poisson ratio, t the thickness of the lever and L its lengths. In our experiments with silicon nitride lever, $\Delta z = 10 \, nm$, $E \approx 3.1 \cdot 10^{11} \, Pa$, $\nu = 0.27$, $t = 550 \pm 30 \, nm$ and $L = 200 \, \mu m$, the surface stress difference between the two sides of the lever is then approximately $\sigma \approx 10^{-2} \, N/m$ corresponding to a force of $100 \, pN$.

If we assume that the forces at the surface of the lever are generated by the molecules at the surface of the bacteria, we can estimate the magnitude of these generated forces and compare them to the forces needed to bend the lever. The outer surface of the bacteria's membrane is covered with peptidoglycan molecules and their elastic modulus is approximately $3 \, MPa$ [66] and they also estimated the ultimate force that a bacterium can withstand to be $F \approx 12 \, nN$, well above the force needed to bent the lever. Bacteria are also covered by fimbriae, thin filaments of few nanometers in diameter and few micrometers long that are responsible for the attachment of bacteria to surfaces. Fimbriae can withstand forces in the range of 7.5 to 30 pN [67] and since bacteria can have up to 1000 of fimbriae, the total force can be estimated to be in the nN range, again enough to bent a lever. Similarly, biofilms formed by bacteria have tensile strengths in the range of 500 to 1000 Pa [68], 780 - 4550 Pa [69], and 395 - 416800 Pa [70]: a very wide range of values, but we can still assume that also biofilms can produce forces needed for the bending of the lever.

If we are considering a eukaryotic cell attached to the lever, we have observed the exact same behavior: viable cells induce oscillations of the lever with large amplitude and when the cells are killed these oscillations disappear. In this case, one of the cell's structure that can produce forces needed to bend the lever is the cytoskeleton, made up of tubulin, actin and other intracellular filaments. There is a wealth of measurements on the forces that cells can make on substrates and the deformation induced on the substrates: typical range of values for the traction stress are between 10^{-3} and $1 \, N/m$. Again, these are the values that are compatible with the bending of the lever that we observe in our experiments.

3.3.3. Bacterial vertical movement component

Bacteria or cells attached immobilized on the surface due to internal processes can move its center of mass in the direction perpendicular to the surface of the cantilever.

The scale of this movement can be approximated by the observed motion of the bacterial surface.
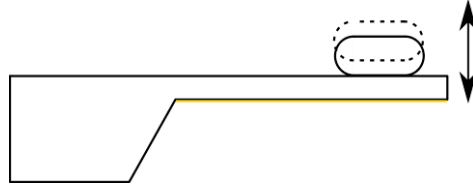
Fig. 3.3. Schematic of simple model of bacteria moving vertically.

If we admit that the bacteria "dance" on the top of the lever with a sinusoidal movement of the type $x(t) = A \sin(\omega t)$ with an amplitude $A = 1\ \mu m$ and an angular speed $\omega = 2\pi \cdot 100\ Hz = 6.28 \cdot 10^2\ \frac{rad}{s}$, then the reaction force acting on the lever is given by:

$$F(t) = m_{tot} \cdot A\omega^2 \sin(\omega t)$$

Eq. 3.6. Reaction force of the sinusoidal movement.

Where m_{tot} is the total mass of the "dancing" bacteria. The maximum force amplitude will be in the case of 1000 bacteria

$$F^{max} = m_{tot} \cdot A\omega^2 \approx 4 \cdot 10^{-13} N$$

Eq. 3.7. Maximal exerted force.

The maximal exerted force possible is largely insufficient to bend the lever by 10 nm.

3.3.4. Bacterial horizontal movement contribution

A microorganism attached to the cantilever can crawl on its surface by the means of sequentially breaking former bonds and forming new ones. The resultant change of the center of mass position of uniformly distributed bacteria can provide an additional force.
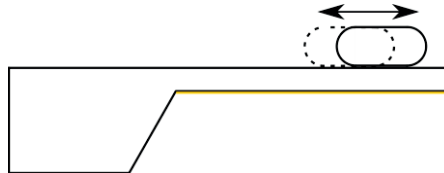
Fig. 3.4. Schematic of simple model of bacteria moving horizontally.

In our case the experiments are done in liquid and the "weight" of the bacteria on the lever is almost compensated by the Archimedes buoyancy force, we do not expect effect from the shift in position of the bacteria on the lever.

3.3.5. Mass fluctuation contribution

Viable bacteria due to their metabolic activity constantly exchange particles with the environment and therefore the mass of the attached bacteria might fluctuate. Again, as in the previous section, buoyancy forces almost exactly compensate the weight of the bacteria and we do not expect bending under the weight of the attached bacteria.
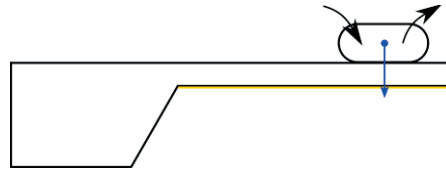
Fig. 3.5. Schematic of a simple model of a bacterium gaining or losing mass.

3.3.6. Ion channels thrust contribution

Cells and bacteria possess numerous ion channels in the membrane that transfer ions through it. Among others, there are sodium and potassium channels. It is estimated that there are around $n_{channels} = 10^3$ ion channels on the surface of a bacterium [71]. One of the hypotheses of the origin of the oscillations of the cantilever is that the ion channels, by emitting ions at a certain speed can, by reaction, exert a force on the lever.
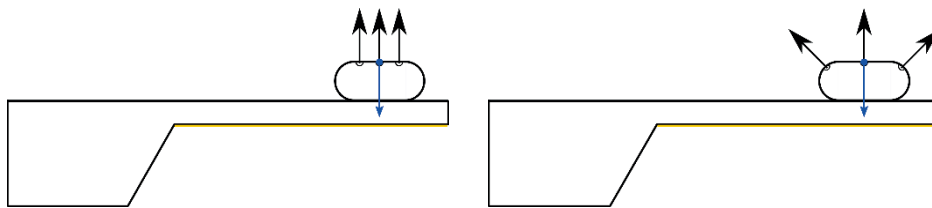
Fig. 3.6. Schematic of a simple model of bacterial ion channel thrust, the left panel represents extreme case of perfect alignment of ion channels and the right panel represents more realistic case with random orientation of the ion channels.

Each ion channel can expel particles at a rate of up to $\varphi_{ions} = 10^7 \frac{ions}{s}$ [71], corresponding to a current of $1\,pA$. To this end we apply Newton's second law of motion in the form $F = \frac{dp}{dt}$, where dp is the moment carried away by the ions in the time interval dt. The momentum dp_{ion} of one ion is given by:

$$dp_{ion} = m_{ion} \cdot v_{ion}$$

Eq. 3.8. Momentum of a single ion.

Now we have to estimate the ion's velocity v_{ion}. Here we assume that the ions move through the ion channel under the influence of the electric field $E = \frac{\Delta V}{d}$, where $\Delta V = 0.15\,Volts$ is the membrane potential and $d = 7 \cdot 10^{-9}\,m$ the thickness of the membrane. Thus, $E = 2 \cdot 10^7\,V/m$. Further we approximate the motion through the ion channel as a motion in a viscous fluid and we can then write the equation for the balance between the force exerted by the electric field and the Stokes friction force:

$$qE = 6\pi\eta R_{ion} v_{ion}$$

Eq. 3.9. Electric field force and Stokes friction force equated.

Where q is the charge of the ion, $\eta = 10^{-3}\,Pa \cdot s$ is the viscosity of water and $R_{ion} \approx R_{Na} \approx R_K \approx 10^{-10}m$ the radius of the ion considered. The velocity is then given by:

$$v_{ion} = \frac{qE}{6\pi\eta R_{ion}} \approx 2\,m/s$$

Eq. 3.10. Ion velocity moving through an ion channel caused by the electric field.

This is the maximal speed of the ions in water under the action of the electric field E. We can now proceed in calculating the momentum carried by the ions, we take the case of a sodium ion:

$$dp_{ion} = m_{ion} \cdot v_{ion} = \frac{M_{Na}}{N_A} \cdot \frac{qE}{6\pi\eta R_{Na}}$$

Eq. 3.11. Momentum carried by a single ion.

The force is then given:

$$F = \frac{M_{Na}}{N_A} \cdot \frac{qE}{6\pi\eta R_{ion}} \cdot \varphi_{ions} \cdot n_{channels} \cdot n_{bacteria} = 0.78 \cdot 10^{-12}\,N \approx 1\,pN$$

Eq. 3.12. Maximum force exerted by the ion channels.

We can conclude that in the very unlikely situation that each ion channel of each bacterium on the lever ejects ions in the same instant and perpendicular to the cantilever, the reaction force on the lever is of the order of $1\ pN$. This force can therefore induce a bending of the lever of the order of $10^{-11}\ m$ in the case of a cantilever with a spring constant $k = 0.12\ N/m$. We have checked the assumptions made above for this calculation and by using a physiological concentration of ions and reasonable ion channel dimensions, we obtain an ionic current of $1\ pA$ which is in the correct range of values, thus confirming the correctness of our order of magnitude estimation. Of course, ion channels are not all directed perpendicularly to the lever, not all ion channels have burst of current at the same instant, etc. We conclude that ions emission are not contributing significantly to the observed fluctuations of the lever.

3.3.7. Contribution of pH changes in the vicinity of the cantilever

As presented in [72] changes in pH cause a static deflection of the gold coated cantilevers. In a later study, triangular cantilever made out of gold coated silicon nitride (similar to the one used in our experiments) have been characterized and their bending under the influence of pH has been measured in the range from 3.2 to 12 pH. The resulting cantilever deflection vs. pH curve shows a high rate of change in deflection for both low and high pH, and a flatter linear dependence in the range between pH 5.6 and pH 8.6. The deflections corresponding to those values of pH are +40 nm and -20 nm respectively. The average rate of deflection is 20 nm per 1 pH. The equilibrium position was registered at pH 7. The deflection is caused by the surface stress attributed to the interactions of the ions with the silicon nitride surface [72].

$$SiNH_2 + H^+ \leftrightarrow SiNH_3$$

$$SiO^- + H^+ \leftrightarrow SiOH$$

$$SiOH + H^+ \leftrightarrow SiOH_2{}^+$$
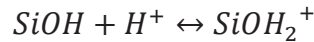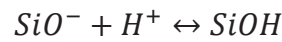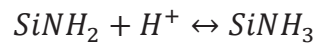
Experiments conducted in our laboratory with NP-O cantilevers from Bruker covered with glutaraldehyde showed similar rate of deflection on the order of 20 nm per 1 pH. Lysogeny broth used to culture bacteria and as a medium for experiments has a pH of approximately 7. Therefore, dynamic changes in the local pH in the range of $\Delta pH = 0.5$ resulting from bacteria metabolism can cause the observed oscillations of an amplitude $\Delta x \approx 10\ nm$.
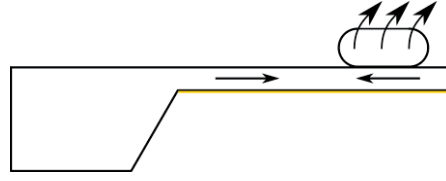
Fig. 3.7. Schematic of a simple model of bacteria changing the local pH and thus inducing surface stress into the cantilever through substrate interactions with hydrogen ions.

To estimate the effect, we make the following model: we assume that the *pH* at the surface of the cantilever has to fluctuate between *pH* 7 and *pH* 6.5 in order to induce oscillations of 10 nm in the bending of the lever. These oscillations have a time scale from very low frequency up to 100 Hz (see point 7) in the introduction). Therefore, a certain number of H^+ ions has to be produced on the time scale of the phenomena by the bacteria and the same amount has to leave the lever's surface again on the same time scale in order to approximately induce the expected *pH* fluctuations.
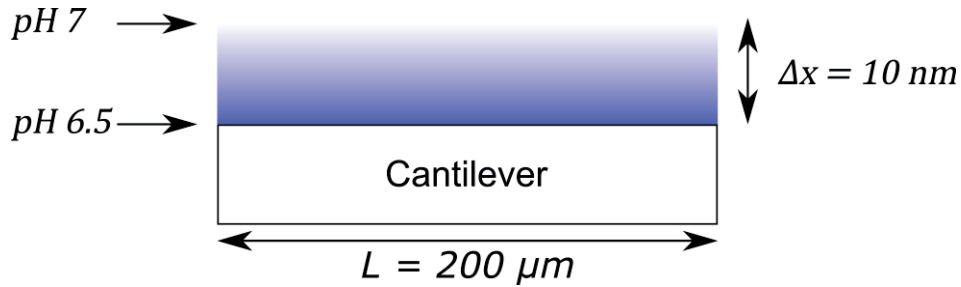
Fig. 3.8. Schematic depicting pH change in the vicinity of the cantilever. At the surface of the cantilever the pH is 6.5 due to the bacteria metabolism, at the distance of the oscillation amplitude it is assumed that the pH is 7, that is because the fluid cell volume is many orders of magnitude more volume then the considered immediate vicinity of the cantilever.

First, we calculate the flux of the H+ ions leaving the immediate vicinity of the cantilever. Moreover, since the lever is oscillating with an amplitude of $\Delta x = 10 \, nm$, we consider a slab of fluid of the volume drawn by the motion of the cantilever: $V = L \cdot W \cdot \Delta x = 200 \, \mu m \cdot 80 \, \mu m \cdot 10nm$, where L is the length and *W* is the width of the cantilever. We then assume a linear gradient of *pH* between the surface of the lever at *pH* 6.5 and the surface at 10 nm distance from the lever at *pH* 7. The concentration of H+ ions per m³ is related to the pH by:

$$c = 10^{-pH} \frac{moles}{liter} \cdot 1000 \frac{liter}{m^3} \cdot N_A$$

Eq. 3.13. Hydrogen ions concentration.

Where $N_A = 6 \cdot 10^{23} \frac{ions}{mole}$ is the Avogadro's number. The gradient in the ion concentration can be approximated by a linear relationship being $\Delta x = 10^{-8}\ m$:

$$\frac{\Delta c}{\Delta x} = \frac{(10^{-6.5} - 10^{-7}) \cdot 1000 \cdot 6 \cdot 10^{23}}{10^{-8}} = 1.3 \cdot 10^{28} \frac{ions}{m^4}$$

Eq. 3.14. Gradient of hydrogen ions in the vicinity of the cantilever.

According to the first Fick's law, the flux of ions is then:

$$j = -D \frac{dc}{dx} \cong -D \frac{\Delta c}{\Delta x} = 7.62 \cdot 10^{-9} \frac{m^2}{s} \cdot 1.3 \cdot 10^{28} \frac{ions}{m^4} = 9.88 \cdot 10^{19} \frac{ions}{m^2 \cdot s}$$

Eq. 3.15. First Fick's law.

where $D = 7.62 \cdot 10^{-9}\ m^2/s$ is the diffusion coefficient of H^+ ions in water at 25°C [73]. The ion current J is therefore:

$$J = j \cdot L \cdot W = 9.88 \cdot 10^{19} \frac{ions}{m^2 \cdot s}\ 200\ \mu m \cdot 80\ \mu m = 1.58 \cdot 10^{12} \frac{ions}{s}$$

Eq. 3.16. The ion current in the vicinity of the cantilever.

On the time scale of one oscillation at $100\ Hz$ we obtain the number of ions that can leave the immediate vicinity of the surface and diffuse into the fluid:

$$n_{leave} = J \cdot 0.01\ s = 3.16 \cdot 10^{10}\ ions$$

Eq. 3.17. Number of ions leaving the vicinity of the cantilever.

As presented in [74–76] it was measured that a single *E. coli* bacterium at a similar division time of 40 minutes requires $12 - 20 \cdot 10^9\ ATPs$ to double. This means that bacterium on average requires $5 - 8 \cdot 10^6\ \frac{ATPs}{s}$. Each ATP results in a release of 3 CO_2 to the outside of the bacterial cell. In water it forms carbonic acid H_2CO_3 and dissolves to HCO_3^- and CO_3^{2-}, releasing two H^+. The resulting rate of H^+ production is equal to $3 - 4.8 \cdot 10^7 \frac{ions}{s}$. For 1000 bacteria attached to the cantilever the resulting number of H^+ production on the time scale of one oscillation is equal to:

$$n_{production} = 3 - 4.8 \cdot 10^8\ ions$$

Eq. 3.18. Number of ions produced by the bacterial metabolism.

The comparison of n_{leave} and $n_{production}$ shows that the average number of produced ions in the vicinity of the cantilever is approximately 100 times lower than those that are capable of leaving under the given assumption. However, we calculate the number of ions required for the difference in pH in the vicinity of the cantilever for the effect to occur, we consider the same slab of liquid:

$$n_{required} = \Delta c \cdot \frac{moles}{liter} \cdot 1000 \frac{liter}{m^3} \cdot N_A \cdot L \cdot W \cdot \Delta x =$$

$$= (10^{-6.5} - 10^{-7}) \cdot 6 \cdot 10^{26} \frac{ions}{m^3} \cdot 200 \; \mu m \cdot 80 \; \mu m \cdot 10 \; nm = 2.08 \cdot 10^3 \; ions$$

Eq. 3.19. Number of ions in the vicinity of the cantilever required to bend the cantilever.

The number of ions required is miniscule in comparison to the number of ions produced and leaving. Experiment that could help understand the contribution of this effect would require a cantilever approaching viable bacteria attached to another surface and measure the oscillations of the cantilever. For this effect to be significant contributor the amplitude of fluctuations should be comparable and the power spectrum density of the deflection signal should take a 1/f noise form.

3.3.8. Contribution of bi-material effect

The AFM lever that we are using in our experiments are made out of silicon nitride with a thin gold layer on the top that reflects the laser beam used to measure the bending of the lever. One of the idea of the origin of the oscillations of the lever is that microorganism attached to the lever, due to their metabolic activity, expel heat and cause a locally fluctuating temperature of the lever and in turn, because of the bi-material effect, induce bending of the lever. We further assume that the whole heat produced by the bacteria is transferred to the cantilever (42–45). The schematic of a simple model of this effect is presented on *Fig. 3.8.*
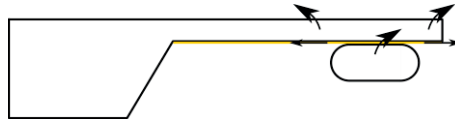
Fig. 3.9. Schematic of a simple model of bi-material effect induced by transfer of heat originating from bacterial metabolism. This model assumes that all the energy expelled by the bacteria is transferred to the cantilever. The cantilever consist of two layers: silicon nitride and gold that have different expansion coefficients resulting in bending due to temperature change.

Cantilevers can bend due to changes in temperature thanks to two mechanisms, a change in the Young modulus and the bi-material effect. Young modulus change is a less significant effect than the bi-material one. There are 1000 bacteria attached that can provide up to 2 nW of thermal power. Deflection due to the bi-material effect is given by [77]:

$$\Delta z = \frac{5}{4}\left(\alpha_{Au} - \alpha_{Si_3N_4}\right)\left(\frac{t_{Au} + t_{Si_3N_4}}{t_{Si_3N_4}{}^2 \kappa}\right)\frac{l^3 \, P}{\left(\lambda_{Au} t_{Au} - \lambda_{Si_3N_4} t_{Si_3N_4}\right) w}$$

Eq. 3.20. Deflection of the cantilever due to the bi-material effect.

Where length $l = 200 \, \mu m$, width $w = 80 \, \mu m$, silicon nitride thickness $t_{Si_3N_4} = 0.55 \mu m$, gold layer thickness $t_{Au} = 0.05 \, \mu m$, silicon nitride thermal conductivity $\lambda_{Si_3N_4} = 30 \, \frac{W}{m \cdot K}$, gold thermal conductivity $\lambda_{Au} = 310 \frac{W}{m \cdot K}$, silicon nitride thermal expansion coefficient $\alpha_{Si_3N_4} = 3.3 \cdot 10^{-6} \, \frac{1}{K}$, gold thermal expansion coefficient $\alpha_{Au} = 14.2 \cdot 10^{-6} \, \frac{1}{K}$, and κ is:

$$\kappa = 4 + 6\left(\frac{t_{Au}}{t_{Si_3N_4}}\right) + 4\left(\frac{t_{Au}}{t_{Si_3N_4}}\right)^2 + \left(\frac{E_{Au}}{E_{Si_3N_4}}\right)\left(\frac{t_{Au}}{t_{Si_3N_4}}\right)^3 + \left(\frac{E_{Si_3N_4}}{E_{Au}}\right)\left(\frac{t_{Si_3N_4}}{t_{Au}}\right)$$

Eq. 3.21. Equation for the constant κ.

Where Young's modulus of silicon nitride $E_{Si_3N_4} = 271 \, GPa$ and Young's modulus of gold $E_{Au} = 78 \, GPa$. The thermal power that the bacteria can provide, assuming perfect heat transfer efficiency, amounts only to $126 \, pm$ deflection. This effect is therefore not significant.

3.4. False-positive effects

This section contains the probable contributing factors that could mimic the viable bacteria hence causing occurrence of false positives. Each subsection contains a short description of the phenomena and procedures to minimize its effects.

3.4.1. Antenna effect

This effect is observed when viable or non-viable bacteria or clumps of bacteria are attached at the edge of the cantilever. This causes high amplitude random deflections of the cantilever by a yet unknown physical mechanism. The way to control it is to optically monitor the cantilever and detect the bacteria at the edge. If bacteria are present there they can be removed by repeatedly submerging and retracting from

liquid (crossing the liquid-air interface) or by flushing the fluid cell. However that can results in a failure of the whole experiment due to the removal of significant number of the bacteria from the surface of the cantilever that are contributing to the positive effect.

Fig. 3.10. Schematic of a simple model of bacteria attached at the edge of the cantilever. This effect contributes to the observed signal if present.

3.4.2. Contribution of freely swimming bacteria collisions

This effect is based on the momentum transfer of bacteria swimming freely in the vicinity of the cantilever and colliding with the cantilever. The bacteria momentum at velocity $v = 36 \ \mu m/s$ with mass $m = 10^{-15} \ kg$ is $p = 3.6 \cdot 10^{-20} \ kg \ m/s$ that can be compared to the previously estimated cantilever momentum of $p = 2.9 \cdot 10^{-17} \ kg \ m/s$. It would require around 800 bacteria transferring its momentum to the cantilever each second to have an effect. This effect has no significant impact on the motion of the cantilever in normally conducted experiments. However if the medium used in the fluid cell contained viable or non-viable bacteria regardless the observed oscillations exceed $100 \ nm$. To mitigate this effect, we have flushed the measurment chamber with filtered buffer solution or nourishing solution during each experiment, we therefore expect that there is a little number of bacteria that are free swimming in around the lever.
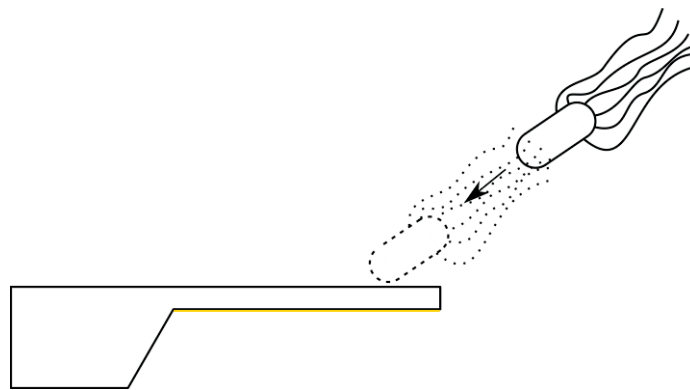
Fig. 3.11. Schematic of a simple model of bacteria swimming, striking the cantilever and transferring its whole momentum to the motion of the cantilever.

3.4.3. Optical effect

There was a suspicion that the observed cantilever oscillations could actually not be an effect of the lever motion but originate from the bacteria deviating the laser beam and changing its intensity through dispersion, reflection, diffraction, change of the refractive index or surface plasmon resonance [78]. However, this effect was excluded by experiments as presented in the dissertation of Petar Stupar [79]. If bacteria present on the cantilever disturb the path of the beam, the effect should still be present on rigid surface or when the cantilever is not able to oscillate (see *Fig. 3.12* right panel, cantilever pushed into contact with a significant force, that is higher than the assumed bacteria induced force). The experiments were conducted as follows: bacteria attached to either the rigid surface (silicon chip with a golden layer on the top to mimic the cantilever composition) or cantilever was placed in a nourishing medium, afterwards the laser was aligned as in a normal measurement, in the case of the cantilever, it was brought into contact with a rigid surface with a force higher than that required to produce the observed effect. This effect was proved to be insignificant.
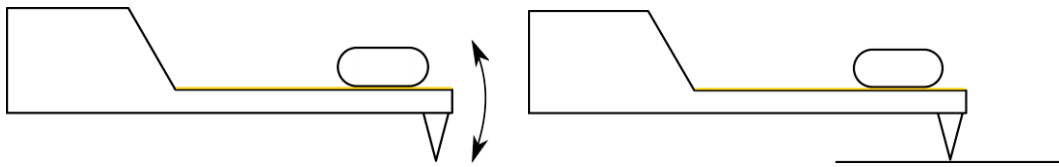
Fig. 3.12. Schematic of two experimental situations, the left panel shows that the nanomotion is present when the viable bacteria are attached and the tip of the cantilever is not in contact with any surface, the right panel shows that the nanomotion is ceased when the tip of the cantilever is in contact with a surface. The optical effect is eliminated as a possible explanation of the observed effect with such an experiment.

We also have carried out experiment in which the bacteria were attached on the chip holding the lever and reflecting the laser beam from this static surface: no fluctuations of the signal were observed, again showing that the effect in not an optical effect (see *Fig. 3.12* right panel).
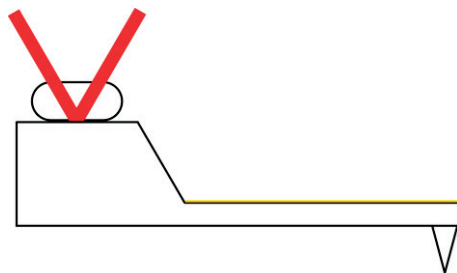
Fig. 3.13. Schematics of the experiment performed to test the optical effect with the bacteria attached to the cantilever chip.

3.4.4. Contribution of bacterial detachment and attachment

It was suspected that the cantilever can oscillate due to the force exerted by the bacteria leaving the surface, attaching to the surface, dividing or undergoing bacteriolysis. However as previously discussed in section 3.2.5. this mass-change effect cannot have significant impact on the motion of the cantilever other than changing the impact of the underlying effect due to a decrease or an increase in the number of bacteria attached or changing the surface stress due to detaching or attaching bacteria.
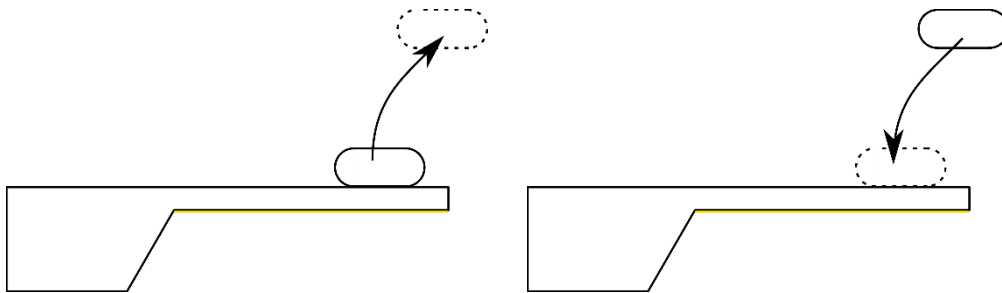
Fig. 3.14. Schematic of a simple model of bacteria detaching and attaching to the surface of the cantilever. The contribution through added mass is insignificant, however the process of attachment may induce surface stress.

3.5. Conclusion

This chapter was supposed to explain the possible causes of the observed effect. This analysis cannot present one certain explanation. However it can discard some of them for certain. It also gives few hints how to avoid and control for false-positives. This chapter gives few proposed experiments for further tests.

Of all the possible positive contributions to the observed effect considered/presented in this chapter, namely: flagellar drive, surface stress, bacterial vertical and horizontal movements, mass fluctuations, ion channels thrust, pH fluctuations induced deflection and the bi-material effect.

Discarded positive effects.

With physical reasoning and calculations given in this chapter we can exclude some of them. Bacterial vertical and horizontal movements contribution is excluded based on that the forces produced by those movements are insignificant in comparison with the force calculated based on the measured deflection and spring constant. The mass

fluctuations of the bacteria that could contribute to the force exerted by the bacteria upon the cantilever is also excluded based on the calculations of the forces induced by the attached mass fluctuations. Although the quantitative analysis of the contribution of the ion channel thrust concluded that the resulting forces are of sufficient magnitude. However the model considered was very simplistic and idealistic which turned out to be inaccurate and after taking into account more accurate assumptions caused rejection of this factor as a contributor explaining the observed effect. The contribution given by the bi-material effect was calculated to be inadequate to explain the greater part of the effect.

Included positive effects.

The other proposed solutions of the observed effect origins with the help were presumed worth considering. The contribution of the pH changes with the help of a simple model estimations and physical reasoning was shown to be a factor worth of further examination and we could not provide any definitive arguments against this idea. We did not make any experiments confirming nor denying the validity of this idea, however we proposed an experiment that could help resolve this issue. Another possible factor considered was the contribution of the flagella. This was proven a definitively contributing factor with a series of experiments that used the same strain of bacteria, one with flagella present and active and the other one with bacteria grown in a way that did not promote the occurrence of the flagella. The difference between those experiments was significant and the presence of active flagella increased the variance of the cantilever deflection by a factor of two. However the physical mechanism is not yet differentiated, it can be flagella providing force due to normal motion or flagella attaching to the surface of the cantilever and providing additional surface strain. It is worth noting that without the active flagella the effect is still present, thus the flagellar factor cannot be considered the sole explanation. The last aspect considered to contribute positively to the observed effect was the surface stress induced by the cellular appendages, such as pili and fimbriae, or by the adhesion of surface proteins to the cantilever. This effect was estimated to provide enough force to the motion of the cantilever to sustain it. The surface stress factor works well as an explanation of the effect for all the successfully conducted experiments that observed nanomotion from protein, through mitochondria, different types of bacteria to fungal and mammalian cells.

False-positive effects.

In the case of the false-positive effects the evaluation was similar to the positive ones. Some of the effects can be discarded right away due to the calculations and physical reasoning, however some of them have to be taken into account as factors that have to be controlled for during the experiment. The first example of the factor to consider with each experiment is the antenna effect, which does not have a solid explanation on its own, however it is always present when the bacteria are attached at the edge of the cantilever and the experiment cannot be continued unless the bacteria are removed from the edge, however that can remove the bacteria from the surface of the cantilever. The second aspect that has to be controlled for are the bacteria freely swimming in the volume of the fluid cell. The presence of the bacteria can influence the fluctuation of the cantilever by simply hitting the cantilever and transferring the momentum of bacteria to the cantilever. Our experiments have shown that even the presence of dead bacteria in the fluid can mimic the nanomotion on an empty cantilever. The other effects considered have been demonstrated to be insignificant. The optical effect was proven experimentally that it has no effect on the nanomotion. The attachment and detachment of the bacteria as a mass changing measure was discarded on the same basis as the change of the bacterial mass due to metabolic activity. However the attachment and detachment can have an effect through applying or removing the surface strain and as such has to be controlled for with the help of optical inspection.

Chapter IV

Device and software development

4.1. Introduction

This chapter details the current status of the development of the prototype device and its controlling software, as well as setting out the ongoing plans for the design, and features to be implemented in the future.

In our Laboratory, the idea of observing the deflection of the cantilever with attached bacteria was first implemented with a commercial Atomic Force Microscope (DI Nanoscope IV Picoforce) and it was soon observed that the presence of bacteria on the lever induced the oscillations of the lever. The injection of an antibiotic to the measurment chamber stopped almost immediately the oscillations (23). It was therefore soon imagined that the method could be used to assess the response of bacteria to antibiotics [80].

Since the experiments consists in measuring the lever bending in a solution and no other features of the conventional AFM are needed like the imaging of samples on surfaces, a prototype device was devised with reduced capabilities. Three main features were essential: a) the lever has to be in a liquid chamber, b) the possibility to exchange the liquid in order to introduce for example an antibiotic and c) the measurement of the lever deflection as a function of time. A simplified prototype was developed and constructed: its main characteristics was that the operation was completely manual with a rudimentary data acquisition software.

In the present thesis, the primary goals were to improve the current prototype design in order to permit motorization of the instrument adjustment and its automatization through software. These were the points deemed to be important if the prototype has to be operated by laboratory technicians not formed to use the complex commercial AFMs. Moreover, the motorization offered the possibility to remotely control the prototype, a feature that could come at hand if the prototype would be placed in a high security laboratory like the ones used for *tuberculosis* research or other dangerous pathogens. The motorization would also allow to adjust the setup and align the laser beam without touching the instrument, thus permitting a more precise alignment. A more precise control allows to achieve higher reproducibility of the results than aligning it manually. The overall goal of the automation is to simplify the otherwise laborious process of alignment.

The second section of this chapter will set out the features of the prototype and their development, at the same time as describing the manual version of the prototype and the process of the motorization. The third section will describe the development of the software and the features which enable automation of the device. The penultimate section will focus on proposals for a future design which draw heavily from

the previous versions of the device developed within the laboratory. The final section concludes the chapter with a summary of its contents.

4.2. Device

The device geometry is similar to the one of an Atomic Force Microscopy and the basic components are: a) a fluid cell to accommodate a tip-less cantilever secured in its holder, b) a laser source coupled to an optical fiber for light transfer and the focusing optical system, c) a detection system that consists of a 4-quadrants photodetector with the amplifying electronics, d) an aluminum frame that holds the parts together, e) variety of linear power supplies, f) a magnifying camera to observe the cantilever, and g) motorized linear and angular stages permitting to adjust the different optical and mechanical parts for an optimized alignment.
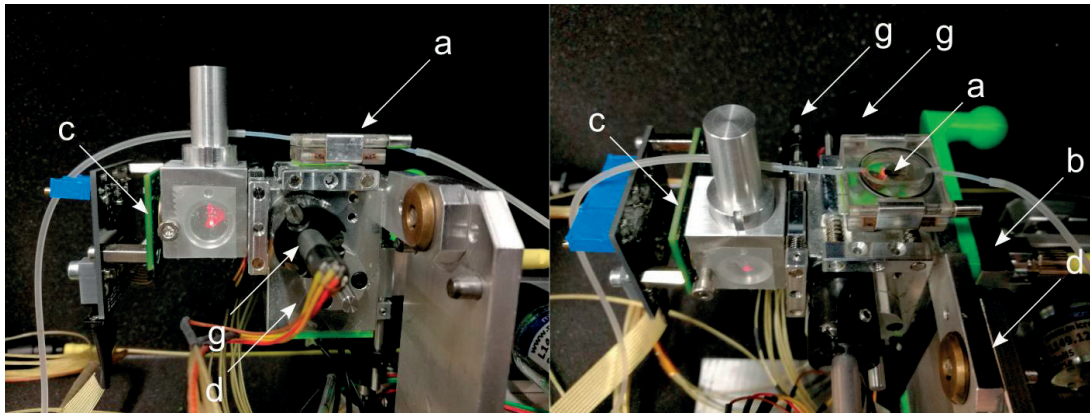
Fig. 4.1. Photos of the device. The visible components are: a) a fluid cell, b) a laser fiber and collimator housing, c) a 4-quadrants photodiode, d) an aluminum frame and g) stepper motors, its holders, linear and angular stages.

4.2.1. Components

For most of the experiments, the triangular, tip-less and low spring constant cantilevers were used. The two main cantilever types used differ in the reflective coating, one has a golden layer on the whole upper side of the cantilever (NP-O from Bruker), and the second one has a golden layer only at the apex of the cantilever (qp-BioT from Nanosensors).

The dimensions of the NP-O cantilever are $200 \ \mu m \ \cdot 40 \ \mu m \ \cdot 0.6 \ \mu m$ (length x width x thickness). The width represents width of one leg and the spring constant of the cantilever is equal to $k_{NP-O} = 0.12 \ N/m$ (with a rather large range of values for different wafers $0.06 - 0.24 \ N/m$). The dimensions of the qp-BioT cantilever are $200 \ \mu m \ \cdot 28 \ \mu m \ \cdot 0.9 \ \mu m$, the width represents the width of one leg and the spring constant of the cantilever is $k_{qp-BioT} = 0.08 \ N/m$ (range of values from different wafers of $0.06 - 0.12 \ N/m$).

The fluid cell is composed of a transparent Plexiglas or polycarbonate material incorporating a glass window through which the cantilever is observed with the help of the magnifying camera, the laser beam enters and leaves the cell through the fluid cell's body material. A kinematic position system consisting of three spheres for the precise alignment of the lever's holder was placed in the cell with a magnet to secure the cantilever holder in place. The closing mechanism clamps the lid and the bottom part of the cell with an O-ring in between providing a tight seal. The fluid cell is equipped with tubes that permit fluid exchange.

The lever holder was manufactured by our mechanical workshop from soft steel in order to be secured by the magnet to the kinematic position system. The lever holder is equipped with a spring that clamps the cantilever to secure it in place. To properly introduce the cantilever in its holder, a purpose designed tool is used to open the spring and then introduce the lever. This device consists of a custom made aluminum block with a pin and a lid with a screw used to clamp the holder in a way that a pin pushes away the holder's spring permitting the insertion of the lever.

The prototype is equipped with a camera (MU9PC-MH from Ximea) with a lens (TRH064-010-A from Thorlabs or Steinheil Triplet Achromatic Lens #47-673 from Edmund Optics) mounted in a holder (S-Mount Achromat/Thick Lens Mount #63-949 and S-Mount Extension Tubes #63-955 from Edmund Optics) that magnifies the cantilever to enable the observation of the cantilever and the alignment of the laser on the cantilever. In some experiments, the camera magnification was increased to allow to observe the bacteria on the cantilever.

The detection system consists of a photodetector (QP50-6SD2 from First Sensor) with current converters and a custom made electronic signal amplification board (with differential amplifiers OPA4131NA from Texas Instruments) and a 16-bits analog-to-digital converter and a data acquisition board (USB-6212 from National Instruments). In order to detect the lever deflection by the laser beam, the 4-quadrants photodetector electronics has to provide bottom minus top difference (B-T), left minus right difference (L-R), total laser intensity on the photodetector (SUM) and the bottom

minus top divided by the sum ((B-T)/SUM) signals (see *Fig. 4.2*). The signals are voltages proportional to the light intensity. The gain of the built-in amplifiers is 10^4.

The whole detection electronics has a bandwidth of up to $100\ kHz$ and we usually use a sampling frequency of $20\ kHz$ with the purpose to include the resonance frequency of the lever in liquid that is approximately $4\ kHz$. The actual useful signal bandwidth was evaluated in different experiments and limited to the range $0 - 100\ Hz$. This allowed us to increase the signal to noise figure by introducing before the analog-to-digital conversion a hardware Butterworth/Bessel low-pass filter (Model 3988 from Krohn-Hite) with a cut-off frequency is set to $100\ Hz$, therefore preserving the relevant biological signal. This filter is configured in an AC-coupled mode.

The laser system consists of a laser diode (LP635-SF8 from Thorlabs) pigtailed to an optical fiber connect to an adjustable collimator (CFC-5X-A from Thorlabs). The collimator allows to control the focus distance of the laser on the lever. The laser control and power supply is provided by a suitable controller (LDC201CU from Thorlabs) that allows for precise control in both constant power and constant current mode. The controller can be remotely driven through USB-6212's three channels: one digital input that can turn on and off the laser, one analog input that controls the laser diode current through the applied voltage and one analog output that provides a feedback voltage that is proportional to the current on the laser diode.

The motorized linear and angular stages system are driven by the stepper motors (F0620-V3-15 C90.003A from Faulhaber) with 256x or 1024x planetary gearheads (061K256:1 and 061K1024:1 from Faulhaber) attached, the electronic drivers (H-bridges DRV8833 from Texas Instruments premounted on PCB from Pololu) are mounted on a custom made PCB controlling board and the currents through the motors' windings are driven by the digital channels of the USB-6212 National Instruments board. The linear and angular stages were manufactured by our mechanical workshop.

There are three DC motors (L149.12.90 from Micro Motors) driving a coarse XY linear stage (M-460A-XY, 2x SM-13 from Newport) coupled with rubber belt and custom made belt wheels connected to the actuator (SM-13) that allow to control the position of the whole prototype in two axes (XY) and the third motor drives the cogwheel system that moves the camera in the vertical direction changing its focal point position for the imaging of the lever.

There is an additional software control of the LED based illumination of the fluid cell to provide the light for the observation of the cantilever through a magnifying camera.

To power the whole electronics, there are two low noise linear power supplies, one feeding the motor drivers (EPS12 500C from VxI) with +12 V and another one feeding the detection system (EPSD15 200C from VxI) with ±15 V. The first power supply is connected through voltage regulator (LM317T from STMicroelectronics) that reduces the voltage to 2.97 V.

The mechanical parts needed for this prototype were machined from aluminum by the mechanical workshop of our Institute. These parts consist of a base plate, a main block, a photodiode block, and a laser collimator block, the elements needed for the linear stages, the elements of the angular stage and other frame elements.

4.2.2. General principles of the functioning of the prototype

The light exiting the fiber passes through a collimator that is moved by a linear positioning stage with respect to the cantilever in the vertical axis allowing for the alignment of the laser beam onto the apex of the cantilever. A second linear positioning stage moves the lever in the perpendicular direction with respect to the previous stage, so that the final positioning of the laser beam on the lever's tip is possible. These two stages are motorized by two stepper motors (see *Fig. 4.1*).

The beam reflected off of the lever reaches the 4-quadrants photodiode through a mirror placed between the lever and the photodiode. The reflected beam is precisely placed in the center of the photodiode by a vertical displacement provided by the rotation of the mirror and by the lateral displacement of the whole photodiode. Both movements are performed by the stepper motors (see *Fig. 4.1* and *Fig. 4.2*).
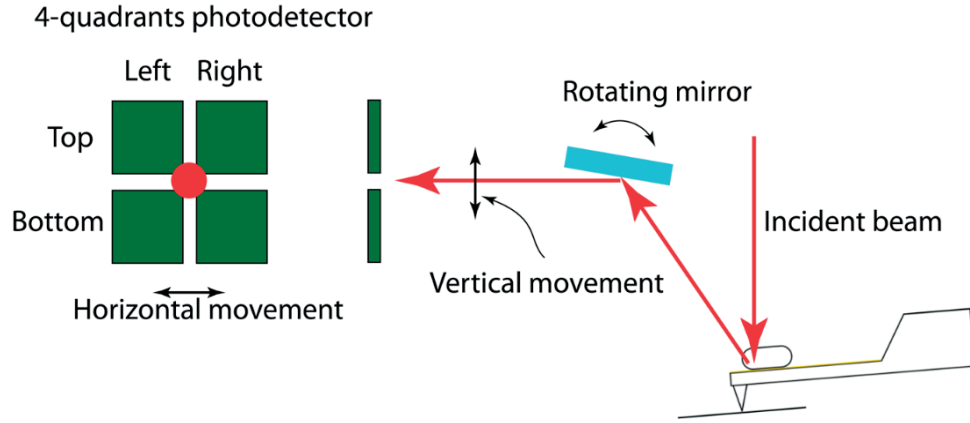
Fig. 4.2. Schematics of the basic principles of the optical beam deflection method for assessing the lever's bending.

Beam deflection method detects the deflection of the cantilever through the current generated by the laser beam incident on the semiconductor 4-quadrants detector through the photoelectric effect. The photocurrent is converted by a current-to-voltage amplifier and subject to mathematical operations (sum and difference, see section 4.2.1) and one-time amplification by 10^4 of the sum and difference signals. The difference signal corresponds to the deflection of the cantilever and can be divided by the sum signal to compensate for fluctuations of the laser light intensity. We record two deflection signals, one unfiltered and one filtered by the hardware Butterworth low-pass filter. The difference signal is acquired by a 16-bits analog-to-digital converter with the USB-6212 NI card. The whole acquisition is controlled by a LabView program and the data are saved for the later analysis. The LabVIEW program is also used to control the optical adjustments and beam alignment of the prototype.

4.3. Nanomotion control program

We call Nanomotion device 2 (NMD2) the new fully motorized and automated prototype. The device's control program is a program that a) controls the alignment of the laser onto the cantilever (first stage alignment) and the centering of the reflected beam onto the photodiode (second stage alignment) before the beginning of the measurement, b) allows for the data acquisition and the inline data analysis. Both stages of the alignment can be performed in a manual, semi-automated and an automated manner. The program also allows to manually control the position and the focus of the magnifying camera.

4.3.1. Graphical user interface of the program

The graphical user interface of the program features the data acquisition control, manual and automatic alignment controls, laser control, camera control and preview, data display and the settings.
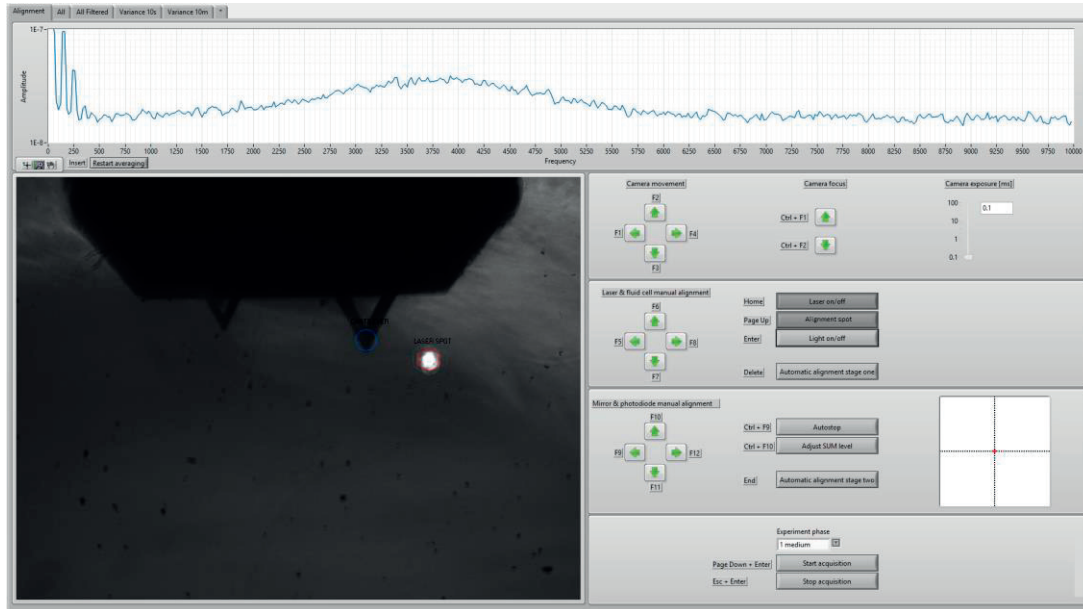
Fig. 4.3. The graphical user interface of the program. On the top left tab selection allows to switch between different spaces: alignment, all signals, all signals filtered, inline calculated variance in 10 seconds chunks and averaged for 10 minutes and the settings. On the top there is a power spectrum density plot with broadened resonant frequency peak that is decaying after the laser was moved from the cantilever and its power was reduced. On the bottom left is a camera preview with overlays showing the cantilever tip and the laser found with pattern recognition. On the bottom right there are 4 steps of alignment procedure in vertical order.

The graphical user interface was designed to present the experiment preparation procedure in four steps:

- 3-axes positioning of the camera to find the cantilever in the camera preview,
- the laser spot alignment on the cantilever,
- the reflected beam alignment on the photodetector,
- the data acquisition.

4.3.2. Control of the alignment and its automation

The alignment control is a part of the program that enables the control of the alignment process of the laser, cantilever and the photodiode. This part of the program also controls 3-axis motorized linear translation, exposure, gain of the camera and shows the fluid cell camera preview. The program enables to turn on and off light emitting diode (LED) mounted on the device to enable the fluid cell illumination.

The program enables to control the laser: turning it on and off, controlling its intensity and measuring the laser diode current. There is an option for a pre-set value of the laser intensity called 'alignment spot' which is a low intensity laser spot that appears as a well-defined, small spot in the camera view (see *Fig. 4.3*).

The program enables to automatically adjust the laser intensity based on the SUM voltage value through a loop that compares the actual SUM value with a previously set one and then increases or decreases the laser diode current by a set value based on the actual and set SUM values, this process is repeated until the SUM value is in a preset range close to the set value.

There are two stages of the alignment and three modes to conduct those: the manual, semi-automated and the automated. Regardless of the chosen mode, when an operation of the stepper motor is required the control program starts at the last step, uses an index to go through the array holding the Boolean values representing the coil energization sequence and the desired direction of rotation controls the addition to or the subtraction from the index. The stepper motor operation mode is chosen by selecting from specifically prepared arrays. Controlling the speed of the stepping is achieved by controlling the time for each iteration of the control loop. In the manual mode depending on the chosen direction the value of the index changes by one with each iteration of the control loop, it is a "switch until released" type of action when using a pointer or a "toggle" type of action when using keyboard. In both semi-automated and automated mode the control is done fully by the program.

The first stage alignment.

The alignment of the laser spot on the cantilever inserted into the fluid cell is realized by the laser linear stage and the fluid cell linear stage driven by geared stepper motors. This is the first alignment stage.
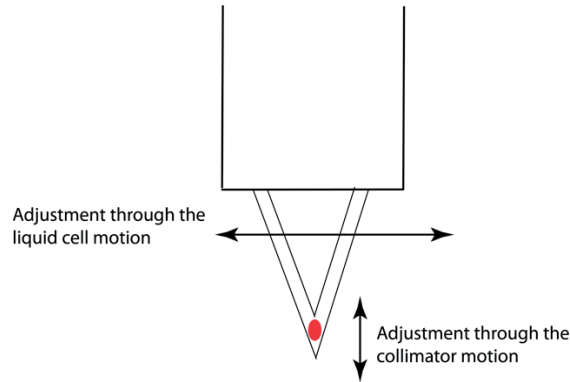
Fig. 4.4. The alignment of the laser spot on the cantilever apex. The cantilever can move horizontally due to the linear stage moving the fluid cell, the laser spot can move vertically due to the linear stage moving the housing of the collimator.

First method: This alignment can be realized with the manual control.

Second method: Another way to align the laser spot on the cantilever is to use a semi-automated option and manually select the laser spot and the cantilever with a pointer in the camera preview and then let the program calculate the number of steps needed in each axis and drive the stepper motors to align the spot on the lever automatically.

Third method: Another way to align the laser spot on the cantilever is to use an automated approach which uses a LabVIEW built-in pattern recognition for set laser spot pattern and cantilever pattern (see *Fig. 4.3*).

In the camera preview, the top part corresponds to the chip side of the cantilever, and the bottom part corresponds to the tip side of the lever. The first stage allows the laser carriage to move vertically along the z axis of the prototype which corresponds to the vertical (along the y axis) movement of the laser spot in the camera preview and also allows the fluid cell carriage to move horizontally along the y axis of the prototype which corresponds to the horizontal (along the x axis) movement of the cantilever in the camera preview.

The second stage alignment.

The second alignment stage is the alignment of the laser beam reflected off of the cantilever on the center of the photodiode is realized by the mirror angular stage and the photodiode linear stage driven by geared stepper motors (see *Fig. 4.2*).

a) This alignment can be realized with the manual control of the stepper motors. There is an additional feature helpful for the manual operation called "autostop" which will stop the control input when crossing the zero value of the signal for both the bottom minus top (B-T) signal and the left minus right (L-R) signal.

b) Another way to align the reflected laser beam in the center of the photodiode is to use the automatic option that controls the rotation direction of the stepper motors in response to the value of the bottom minus top (B-T) signal and the left minus right (L-R) signal. After the signal values has reached the set value range, the alignment is stopped and the control is released.

After manually performing the second stage it is possible to manually use the software to adjust the SUM value. Alternatively, after the second stage of the alignment in automated mode is complete the program also adjusts the laser power to reach set value of the SUM. The SUM set value comes from experience and it is optimized to have the best signal to noise ratio.

Stepper motor operation modes.

The program allows to select stepper motor operation mode. There are three operation modes available: the normal mode utilizing one coil of a stepper motor at a time, the high torque mode utilizing two coils of a stepper motor at a time, and the high-resolution mode utilizing one and two coils alternately.

The stepper motor control is based on the digital output channels that sends control signals to one of the H-bridges. The H-bridge sequentially energizes the stepper motor coils with current allowing it to rotate and in a reversed sequence allowing it to counter-rotate. In terms of the software it is based on reading arrays filled with TRUE and FALSE Boolean values, one array for each channel corresponds to a coil. For different operation modes the arrays are filled in different ways. Each enabled iteration of the motor controlling loop increases (moving one way) or decreases (moving the other way) the step count. The step count is divided by 8 (8 substeps in the high resolution mode, 2x4 substeps in the normal and the high torque). The division remainder is used as the index of the array to obtain certain Boolean value for each digital channel.

The tables below present the state of the coils with each substep, where the value 1 (TRUE) means that the coil is energized and 0 (FALSE) that it is not.

Tab. 4.1. The normal mode - one coil is energized at a time.

Substep	1	2	3	4	1	2	3	4
Coil A1	1	0	0	0	1	0	0	0
Coil B2	0	1	0	0	0	1	0	0
Coil A2	0	0	1	0	0	0	1	0
Coil B1	0	0	0	1	0	0	0	1

Tab. 4.2. The high torque mode - two coils are energized at a time.

Substep	1	2	3	4	1	2	3	4
Coil A1	1	0	0	1	1	0	0	1
Coil B2	1	1	0	0	1	1	0	0
Coil A2	0	1	1	0	0	1	1	0
Coil B1	0	0	1	1	0	0	1	1

Tab. 4.3. The high resolution mode - one and two coils are energized alternately.

Substep	1	2	3	4	5	6	7	8
Coil A1	1	1	0	0	0	0	0	1
Coil B2	0	1	1	1	0	0	0	0
Coil A2	0	0	0	1	1	1	0	0
Coil B1	0	0	0	0	0	1	1	1

The H-bridges enable the sleep mode, which allows motors that are not supposed to be used not to energize the coils at the current substep to prevent the motors from heating up.

A holding torque is an option for the mirror stepper motor to energize the coil corresponding to that of the last step to prevent the rotor from moving due to the backlash, it also prevents the sleep mode so in consequence may lead to overheating.

Pattern recognition.

The pattern recognition in the automated alignment mode uses an algorithm to recognize the cantilever shape and the laser spot. Then it takes their coordinates to calculate the number of steps needed to cover the distance between the laser spot and the lever. The pattern recognition uses the grayscale value pyramid algorithm [81,82]. The LabVIEW's additional NI Vision Development Module provides two components:

- IMAQ Learn Pattern 4 to read the previously prepared simplified high-contrast template images of the cantilever and the laser spot (see *Fig. 4.5*),
- IMAQ Match Pattern 4 to look for the templates in the camera feed.

Fig. 4.5. The high-contrast template images of the cantilever and the laser spot for the pattern recognition algorithm (IMAQ Learn Pattern 4 and IMAQ Match Pattern 4).

For either selected or recognized positions of the program, it calculates the distance between the cantilever's mass center and the laser spot in pixels, corrects for the position of the cantilever's apex and converts that to the number of steps for each axis. The program compares the coordinates to deduce the direction of motion. The number of steps is set as the beginning count of another loop, once initialized it counts down the steps to zero with each substep, when reaches zero the stepper motors are stopped and then releases the automatic alignment option.

Autocorrection feature.

In the experiments a drift of the B-T signal was observed that might be originating from four sources: temperature drift, relaxation of the cantilever deflection after the liquid introduction, backlash of the planetary gear of the mirror stepper motor or laser optical fiber relaxation after rotating the device. The prototype is rotated after the cantilever holder with a cantilever is placed in the fluid cell and the latter is closed, then the whole prototype is swiveled around the axis attaching two parts of the frame (see *Fig. 4.1* right panel 'd' mark). In the latter experiments the rotation was completely avoided by reversing the orientation of the prototype permanently (compare *Fig 4.1* and *Fig 5.2.1* panel B). The autocorrection is a feature that allows to correct the position of the beam on the photodetector as it drifts away from the set value range. When B-T difference signal drifts out of a preset range, the program stops the data acquisition and aligns the mirror so that B-T is in the set range close to 0 and also moves the photodiode so that L-R is in the set range close to 0. After those two set points are reached, the program starts acquiring the data again.

Data display.

The data is displayed in the form of graphs. There are quadruple stacked plots of B-T, L-R, SUM and (B-T)/SUM signals in the form of both directly acquired and processed by a software low-pass filter. There is a plot of calculated power spectrum density of the B-T signal. There is a plot of calculated variance in a 10 seconds window and a plot of 10 minutes average variance. All these channels are also saved in LabVIEW measurement (.lvm) file format.

Settings.

The settings is the part of the program that controls which device is used, which analog and digital channels are used, the data acquisition rate (and data buffer size), low-pass filter frequency, pixel to steps conversion rate for both the point select and the automatic alignment, the holding torque for the stepper motors and the autocorrection.

4.3.3. Data acquisition

The acquisition control is a part of the program that controls saving of the data to files and adds a prefix to the name of the file saved indicating the phase of the experiment.

In the settings tab there are more advanced controls allowing to change acquisition rate and duration of the measurement. The program allows to save data from three physical channels B-T, L-R, SUM directly and filtered channels with a software low-pass filter, and calculates and saves (B-T)/SUM directly and filtered with a software low-pass filter. Additionally, another B-T channel filtered with a hardware low-pass filter is saved. The program displays B-T, L-R, SUM and (B-T)/SUM channels stacked together in two tabs: direct and filtered. During the acquisition, the program calculates and displays the variance in 10 seconds window and averaged variance for 1 or 10 minutes. The variance of the deflection signal is a measure which in our case quantifies the nanomotion induced by the bacteria upon the cantilever. The program also calculates the power spectral density (PSD) of the BT/SUM signal: this is especially important when the noise or other signal disturbs the measurements. It also permits to determine the thermally induced resonance frequency of the lever, a quantity that tells us if the laser beam is correctly aligned on the lever and if the lever is damaged or not. The power spectrum data is also saved.

4.4. Future designs

The future designs will draw heavily from the previous and the current generations of the nanomotion detection devices.

Previous designs

There was the first generation of the prototype that was operated manually, usually referred to as NMD1 (nanomotion device version 1). It was based directly on the design of a commercial AFM. It was a platform to experiment on the beam light source for the beam deflection method, photodetectors, amplifiers, fluid cells, power supplies, manual linear stages, manual angular stages and other mechanical elements.

Current designs

After choosing the components, that version (NMD1) was equipped with motors that permitted to control linear and angular stages. At that time the decision was made to manufacture more devices, six in total. Simultaneously the development of the control program was progressing. Those devices are usually referred to as NMD2.

There were some inherent drawbacks associated with the NMD1/NMD2 design. Those devices were not robust enough to be put into hospital laboratory or field conditions. Hence the development of the NMD3 device that was built specifically as a nanomotion detection device with the experience from the previous prototypes.

Future designs

The future designs will combine the advantages of both NMD2 and NMD3. The immediate future apparatus is referred to as NMD4. This device will take clues from robust design of the NMD3, discarding the complexity of the mirrors and angle of the cantilever holder positioning. That device will also be equipped with a magnet system enabling a quick exchange of the fluid cells. For the hospital laboratory use it is a necessity to use sterile and disposable parts that are in contact with the sample for the purity of the measurement, the safety of the operator, rapidity and ease-of-use. This design might also enable the use of heated fluid cell for the scientific purposes. This device enables the illumination of the fluid cell from the opposite side of the microscope. The fluid cell used is the same design as in the NMD1/NMD2 that uses an O-ring and a metal rod to seal the fluid cell. Holders for linear stages are enabling the use of motors to align. The alignment chip will not be used in this design, it will be replaced with a custom made cantilever chip glued to cantilever holder by the manufacturer with cantilevers functionalized with the ink jet method. The amplification process, number of amplification stages and the data acquisition are being tested at the moment of writing to decide on the future designs.

4.5. Conclusion

The automated nanomotion detection device offers a number of advantages over the previous manually operated device. It provides better precision for the alignment of the laser beam on the cantilever and the reflected beam on the photodiode. The addition of the automation through the software enables easier alignment process. Moreover, the software enables the live data display.

The future design will take the best features of all the previous and current developments. This device has a chance to be implemented in the hospital laboratory environment and other scientific, microbiology and pharmacology laboratories for research.

Chapter V

Experimental results

5.1. Introduction

The devices presented in the previous chapter were used to conduct several types of experiments, some of those are presented in following sections. This chapter presents typical course of an experiment, the ecalibration of the cantilever, and the use of a low-pass filter, the data analysis and few of the many possible applications of this method.

The following section presents a typical experiment and preparation procedures using manual NMD1. Moreover, it contains the data processing and that is further expanded in the PhD dissertation of Petar Stupar [79]. That section is being prepared to be published as a *practical guide to reliable AFM-based nanomotion detection*.

The subsequent section describes the calibration of the cantilever and the low-pass filter application.

The following section contains a publication titled *Nanomotion detection method for testing antibiotic resistance and susceptibility of slow-growing bacteria* in *Small Journal* that shows the use of the nanomotion detection method applied to slow-growing bacteria, which relates to the problem of applying the right drug in diseases caused by difficult to culture microorganisms, especially lung infections such as *Bordetella pertussis* or *Mycobacterium tuberculosis*. *Bordetella pertussis* is the subject of that work.

The subsequent section contains a publication titled *Mitochondrial activity detected by cantilever based sensor* in *Mechanical Sciences* that presents the use of the nanomotion detection method applied to mitochondria, it compares the metabolism through the oscillations of the active and inhibited specimens.

The last section concludes the chapter.

5.2. Experimental methodology

This section is being prepared to be published.

Petar Stupar, Wojciech Chomicki, Maria Ines Villalba, Aleksandar Kalauzi, Ksenija Radotic, Massimiliano Bertacchi, Simone Dinarelli, Marco Girasole, Milica Pesic, Jasna Bankovic, Maria Elena Vela, Osvaldo Yantorno, Ronnie Willaert, Giovanni Dietler, Giovanni Longo, Sandor Kasas. **A practical guide to reliable AFM-based nanomotion detection**.

5.2.1. Introduction

The atomic force microscope (AFM) is a versatile tool consisting in a micro-fabricated tip, fixed at the end of a small cantilever. The tip is placed in contact or near vicinity of a sample, and a laser beam is focused onto the cantilever's apex to track its deflection as the tip scans the sample. Initially, the AFM was employed to produce high-resolution topographic images of its surface, with resolutions in the order of 0.1 Å [83]. Over the last 20 years, the range of information obtainable with the AFM has evolved to include the characterization of the nanomechanical properties of the sample [59,84–89] or the localization of the effect of drugs on biological specimens [90].

Very soon after its development, it has been shown that cantilevers can serve as very sensitive sensors [91]. For instance, they can be used as micro-balances, to measure extremely small masses directly deposited on their surface. In other applications, it was shown that if one side of a cantilever is coated with a molecular layer, it will undergo a static bending that depends on the abundance, interaction and type of molecules. These measurements can monitor with high sensitivity the binding of targeted molecules to biomolecular receptors [92–95].

Recently, we demonstrated that cantilevers can characterize the nanometer scale fluctuations produced by movements of living organisms [80]. The principles of this detection method are presented in *Figure 5.2.1, panel A*. Living specimens attached to such a sensor induce fluctuations and such measurable movements are correlated to their metabolic activity. We employed such nanomotion sensor to study various biological systems, such as bacteria, yeasts, mitochondria, plant and mammalian cells [23,58,60,96]. In all cases, as long as the attached sample was metabolically active, the cantilever oscillated, but as soon as the viability was lost, the oscillations stopped. In fact, we demonstrated a direct correlation between energy consumption and cantilever fluctuations [97].

We used nanomotion detection to provide a rapid and reliable determination of the response of bacteria to antibiotics [62]. The very same setup can be implemented to explore cancer cell sensitivity to chemotherapeutics [98]. Indeed, the potential application domains of this versatile technique are vast and the simplicity of its working principle allows foreseeing its proliferation in medical centers and research laboratories [64].
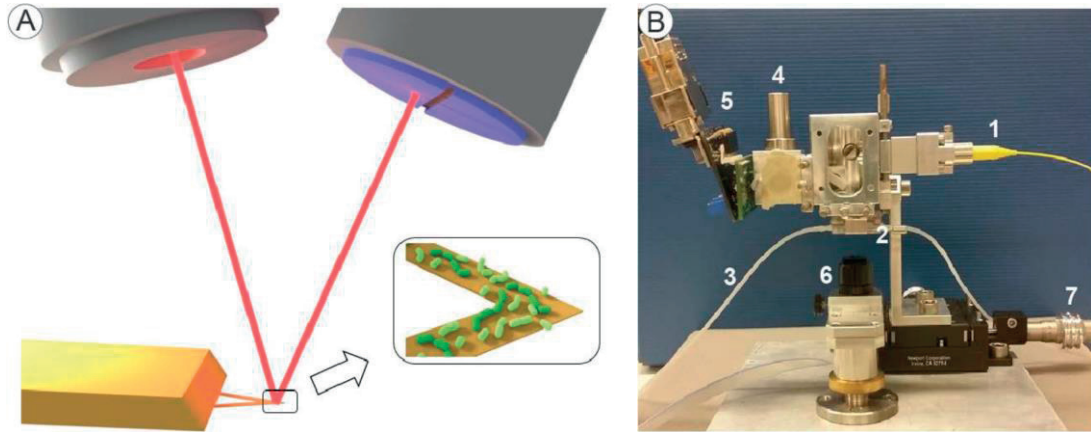

Fig. 5.2.1. Panel A: schematics of the technique's working principles: a laser beam is focused on the cantilever sensor and reflected back to the photo-diode detector, tracking the motion of the cantilever, induced by the presence of living specimens attached. Panel B: Custom-made device developed for simplicity and portability. A laser beam (1) is focused onto the cantilever, which sits in a closed fluid cell (2), where a gravity-driven fluid exchange (3) is possible. The laser beam is reflected back to a beam splitter (4) and finally to the photodiode detector (5). A small camera (6) allows easy leaser alignment, using translation stage (7).

However, despite the technical simplicity of the nanomotion sensor, the use of extremely sensitive cantilevers requires a certain number of precautions in order to obtain reliable results. Here, we present a step-by-step description of typical nanomotion experiments. The following protocols are the result of years of intensive use of the technique. In this short communication, we show the optimal experimental conditions and the overall working envelope of the technique.

5.2.2 Results

Instrument and cantilever selection

Any commercially available AFMs, equipped with custom liquid cells can be used to conduct nanomotion experiments [99]. Biologically oriented AFMs are the most convenient, since they are mounted atop of an inverted optical microscope. The optical image of the cantilever permits determination of the position and the number of specimens present onto the cantilever. In addition, a non-commercial

and dedicated apparatus performs similarly well [56,100,101]. As an example, a device developed in our lab has been used intensively (*Fig. 5.2.1, panel B*).

The choice of the cantilever is of utmost importance. Stiffer cantilevers give lower amplitude oscillations, whereas softer ones can break more easily during manipulation and are exposed to larger thermal drift. In most of our experiments, we used triangular silicon or silicon nitride (Si_3N_4) cantilevers (0.06 – 0.12 N/m by Bruker), but, when working with peculiar experimental setups (e.g. The SCALA hardware) we also used rectangular sensor arrays. In all our experiments, we employed commercial cantilevers directly from the packaging box, but we are working on the development of optimized sensors for nanomotion experiments.

Cantilever functionalization

Strong attachment of the specimens on the cantilever is of paramount importance in the setup of a nanomotion experiment. A specific chemical functionalization protocol must be chosen for each biological system [58,60], such as (3-aminopropyl)triethoxysilane (APTES) and/or glutaraldehyde for bacteria, poly-lysine or fibronectin for cells, concanavalin a for yeast, etc. Attention should be paid to the fact that some chemicals compromise the viability of the attached specimens. In case of bacterial samples, to assess their viability, a convenient option is the use of DEAD/LIVE BacLight stain. Naturally, the purity and quality of the chemicals must be taken into consideration: APTES and glutaraldehyde exposed to humidity lose their adhesive properties, whereas complex attaching media can be subjected to unwanted bacterial or yeast contaminations. Therefore, it is advisable to prepare a fresh solution for each experiment.

In most cases, the cantilever exposure time to the functionalizing agent determines the amount of chemical on its surface. A non-complete coating of the sensor can reduce the number of specimens and the strength of the attachment, while an excessive functionalization can lead to release of functionalizing agent in the solution, causing adverse effects on the living specimens throughout the measurements.

As an example, in the experiments involving bacterial samples, we coated the sensors by exposing them to 20 µl of 0.5% glutaraldehyde for 10 min, rinsing with ultrapure water, drying, and then incubating with 10 µl of a high-density bacterial suspension (OD600: 0.6 with 10 µl of suspension diluted in 1ml of phosphate buffer saline). When performing experiments with yeast, we obtained a good attachment using a 10-minute exposure to 1 mg/ml concanavalin a (ConA), or in other cases we chose 1-minute

exposure to 0.1% APTES. For the attachment of mammalian cells, the choice was fine-tuned for each particular cell line: osteoblasts and cancer cells (i.e. The NCI-H460 cells) were attached exposing the cantilever for 30 minutes to the medium containing 50 μg/ml fibronectin, while neurons required a 15-minute exposure to 1 mg/ml poly-l-lysine. In all cases, after the functionalization, the sensors were thoroughly and gently rinsed in ultra-pure water and used to approach on individual cells to promote the attachment (1 nN force).

Recently, more controlled functionalization procedures have been proposed. For instance, localized and highly controlled functionalization of surfaces can be obtained using ink-jet printing of the chemicals. This protocol can be extended to a direct printing and immobilization of the biological specimens on the sensor. These novel and controlled procedures could allow fast sensor preparation and will lead to more controlled parallelization of the nanomotion setup, and should be taken in high consideration in the case of industrial extension of some of these applications.

Sample attachment

The main goal of the preparation protocols involves the attachment of viable specimens on the cantilever surface. There are several possible protocols to ensure a reliable immobilization of the samples on the sensor, often depending on the sample's nature and abundance.

In the case of bacterial or yeast cells, a droplet (typically 10 - 20 μl) of medium bearing a high concentration of specimens is placed on the cantilever, left to incubate around 35 minutes and immersed into growth medium. After such preparation, the cantilever is mounted on the holder and inserted into the AFM. The procedure is depicted on the *Fig. 5.2.2*. Overall, such external method is relatively simple and requires only a small amount of functionalizing agent. The main drawback lays in the need for the transfer of the sensor from the preparation to the analysis chamber, and this manipulation can produce sensor damage or contamination of the sample. Furthermore, each subsequent immersion step can induce detachment of specimens from the sensor, due to capillary forces. Generally, such random attachment procedures are quite fast and easy to perform, but have a down-side in the loss of control in the number and positioning of the specimens on the sensor.
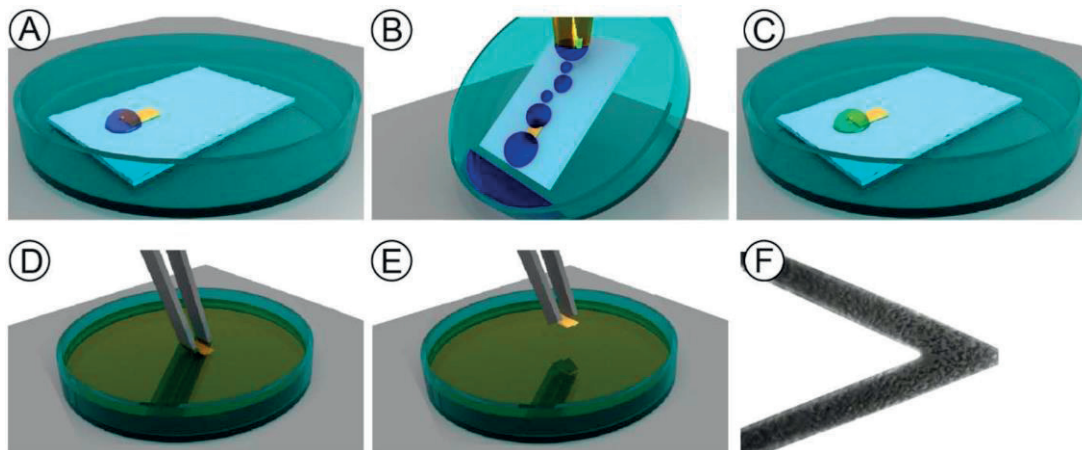
Fig. 5.2.2. Graphical representation of the functionalization and the attachment protocol. A) ~20 μl of functionalizing chemical is deposited on the cantilever side of the chip, for 10 minutes. B) One milliliter of ultrapure water is used to wash out the residual chemical. The cantilever is let to dry (5 min). C) ~20 μl of suspension of the sample is deposited on the cantilever side of the chip for 35 minutes. D, E) Chip is immersed in and out of the culture medium for few times and observed under optical microscope for validation of the sample attachment. This step has to be done carefully and is specific to each sample. F) A good attachment yield with sufficient number of bacteria and no loosely attached groups (clumps).

An alternative method for the sample attachment is to insert the functionalized sensor directly in the analysis chamber, which is then flushed with a sample-rich medium. The system is left to incubate 1- 15 minutes to ensure the immobilization of the viable specimens followed by gentle flushing with clean medium to remove the floating or loosely attached microorganisms. In some cases, even the very functionalization of the sensor can be performed in the analysis chamber, which must be then thoroughly washed to reduce the presence of dissolved chemicals. The main disadvantages of this procedure are the possible contamination of the analysis chamber or the possibility of the presence of debris or unattached organisms floating in the chamber.

Mammalian and plant cells requires some user intervention. In this direct attachment protocol, the cells are seeded on the analysis chamber and micrometer, high-precision motors are employed to place the sensor in the near proximity of a particular cell (the piezo-motors of an AFM are ideal for this kind of high-precision movement). The motors are then used to press the functionalized sensor on the cell, applying a controlled small pressure. Depending on the sample, a force in the range of 1 – 15 nN is employed for about 3-5 min, to promote cell adhesion to the sensor. In particular cases, this procedure can be repeated to immobilize more than one cell in selected locations. Once the sensor is retracted, and the cells appear to be firmly attached, the nanomotion experiments can begin.

To retain the chemical activity of the functionalizing layer, some precautions should be taken into consideration. For instance, complex molecules from some growth media, such as lysogeny broth (LB, also known as Luria broth) typically used to grow bacteria, can compete with bacterial proteins for active moieties on the surface functionalized with glutaraldehyde or APTES. In these cases, the bacterial suspension needs to be centrifuged and the LB replaced by the phosphate buffer saline (PBS). This washing step should be repeated at least three times, until the concentrated PBS-bacteria suspension can be used for the attachment.

Another important precaution is to obtain sample attachment only on the cantilever surface, without partially attached and floating species, as they may introduce additional noise to the signal. *Figure 5.2.2, panel F* illustrates an example of a good bacterial coverage.

Laser alignment

In most AFMs, the detection of the sensor fluctuations is obtained through a laser-based system. A laser is focused on the apical area of the cantilever and its reflection is collected using a low-noise photodetector. This allows a deflection sensitivity in the range of few angstroms. Due to such a high sensitivity, the alignment of the laser transduction system is fundamental to ensure the high resolution detection of the movements of the cantilever. This is valid for conventional AFM measurements as well as for the nanomotion analyses. The laser beam must be focused on the apical region of the cantilever and its reflection should be centered on the photodiode to ensure a dynamic range of detection.

In the case of nanomotion analyses, we noticed that a special care should be taken in keeping a correct alignment of the laser and the photodiode throughout the experiment. Indeed, thermal drift over longer period of measurements can induce a decrease in sensitivity and the resulting variation in amplitude of the fluctuation signal can be mistakenly interpreted as a biological response. As a test of the constant sensitivity of the setup, we often rely on the Fourier analysis of the resulting nanomotion signal by recording the amplitude and shape of the cantilever's resonance frequency before and after the measurement, we can determine if a misalignment has occurred.

Medium optical purity assessment

Closely correlated to the previous step is the need for an accurate control over the laser pathway inside the analysis chamber. Any small floating particles inside the analysis chamber, such as detached specimens, undiluted chemicals or small debris, can modify the laser pathway strongly affecting the results. Thus, a "purity" check of the medium should always be taken into consideration. Such a test can simply be accomplished by recording the oscillations of a cantilever with no living biological samples attached. Any fluctuation measured in this condition can be considered the baseline for the subsequent experiment and can influence greatly the outcome of a measurement.

Oscillations recording

The final outcome of a nanomotion experiment is a time-dependent graph of the fluctuations of the cantilever. The properties of this graph will indicate the metabolic activity of the biological specimens over time and their response to the exposed chemical agents. The oscillations are usually recorded by an external software and require a high acquisition rate, due to the innate variability of the measured signal. The collection of the nanomotion signal can be carried out in several ways. For instance, many commercial AFMs have dedicated software that can collect in real-time the deflection of the cantilever through built-in routines. In the experiments performed using the JPK Nanowizard III AFM, we exploited the Real-Time measurement option to visualize and store the nanomotion signal over time. In the cases in which such options are not available, we have employed I/O cards and developed custom LabVIEW routines to perform the measurements.

To measure the response of bacteria and cells, we have usually worked with acquisition rates of 20 kHz at 16 bits. Such a high sampling rate is chosen to record the resonance frequency of the cantilever. According to our experience, the most important information regarding the metabolic activity of the biological specimens is located at frequencies lower than the resonance frequency of the sensor (mainly up to 1000 Hz). Any noise of external origin can have a large impact for nanomotion experiments. Most noise sources can be reduced by confining the instrument in acoustic boxes and using vibration isolation tables. In addition to such vibrations, any electrical circuit bears an electrical noise that has a typical frequency fingerprint decreasing with the increase of the frequency (1/f noise). Luckily, high-level instrumentation and specific electronic filters can be used to reduce these unwanted signals, and to allow the extraction of the metabolically-relevant information.

Before starting the oscillations recording, we strongly recommend monitoring the cantilever with optical microscope at high magnification. Especially in the case of larger plant or mammalian cells, high magnification optical imaging of the sensor throughout the measurements allows correlating large scale cellular displacements with cantilever oscillations. We have demonstrated the importance of this combined characterization in our previous works [60,64], and in *Fig. 5.2.3* we illustrate the usefulness of such a correlation in the case of NCI-H460 cancer cells. In the latter case, one of the attached cells was undergoing cell division during a nanomotion experiment. By simultaneously collecting nanomotion signal and optical images, it was possible to correlate the increased oscillations with the cell replication. During division of eukaryotic cells, the actin cytoskeleton undergoes drastic changes and rearrangements. Entering mitosis, the extensive actin network is dismantled and rearranged, giving mitotic cells a characteristic round shape. Furthermore, microtubules play a crucial role by precisely organizing the establishment of the bipolar spindle and accurate segregation of chromosomes. In the experiment, cells were allowed to spread on a substrate coated with fibronectin, where integrin-mediated adhesion-dependent signaling supports cell cycle progression and survival. After some time, it entered mitotic phase and the signal increased substantially (variance plot on *Figure 5.2.3*). Looking at the timescale of the signal and corresponding images, the increase in variance can be attributed to the internal cellular rearrangements prior to division.
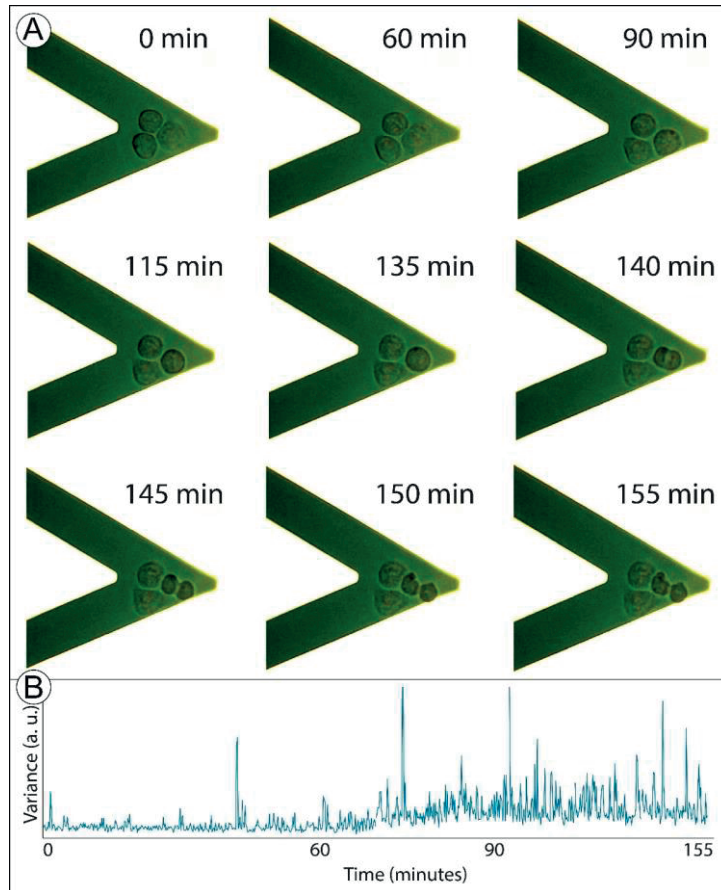
Fig. 5.2.3. Correlation between the optical images (A) and the variance (B) of the nanomotion signal. The increase in variance happens following the rearrangements of the cellular actin networks, before and during the division.

Fluid exchange system

In most nanomotion experiments, liquid exchange is a fundamental step to expose the specimens to a different chemical or physical condition, such as the introduction of a drug in the case of bacteria or cells. Unfortunately, the liquid flow can be an additional noise source and it may generate shear stress that can detach from the sensor some of the organisms under investigation. While a nanomotion experiment can be performed even in the presence of very slow liquid flow [97], we advise discarding the data collected during the liquid exchange and allowing 5-10 minutes for the medium to stabilize in the analysis chamber.

Numerous methods can be used to exchange liquids in the small analysis chamber. For most experiments, the use of slow, low-noise systems or dedicated devices [99] is advisable to ensure that the gentle liquid flow does not disrupt the experimental setup

and results. In order to determine the exact moment of the arrival of the new medium into the analysis chamber and the completion of the liquid exchange, we suggest using a timer if the flow rate has been previously determined [102]. An alternative consists in controlled injection with precisely graduated syringes [103]. In many cases, we have employed a gravity-driven flow, which generates even smaller disturbance to the sensor. In the case of experiments involving an open Petri dish, the direct manual injection of the drug or medium can replace the liquid exchange.

Data processing

To analyze the data collected in our experiments, we developed a MATLAB (Mathworks - Natick, Massachusetts, USA) software that accesses the raw data and performs the necessary analysis. This software was used to produce all the graphs and diagrams presented in this work. Once the nanomotion data has been collected as a raw deflection against time (*Figure 5.2.4, panel A*), the goal of the signal analysis is to extract the biologically-related information. Often, during the acquisition process, a thermal drift of the cantilever occurs. Most frequently, this happens at the beginning of the experiment or immediately after the liquid exchange procedure, when temperature differences are present in the analysis chamber. This phenomenon induces a slow bending of the cantilever, which behaves as a bimetal due to the metal coating present on one of its sides. If such long-term change in the mean level is present, it is advisable to remove it. In our experiments, we have often employed a windowed linear fit: we choose a window of 20 to 200 seconds (depending on the speed of the drift) and apply a linear fit to each window throughout the dataset and subtract it from the raw signal, as illustrated in *Figure 5.2.4, panel B*. After flattening, a moving average or a low pass filter (1000 Hz) can be applied, since most of the metabolically-related information is concentrated at lower frequencies.

After these preparation steps, the signal can be finally analyzed. While the more fundamental information (such as the specimens' viability) can be extracted, more complex analyses should be employed to achieve a more in-depth characterization of the biological system. The important information that can be extracted from the data requires the calculation of a windowed variance of the oscillations: the data is divided in small 10-30 second chunks and the variance for each of these blocks is calculated. The resulting plot, obtained using the software published in the appendix, depicts the evolution of the signal variance throughout the experiment (*Figure 5.2.4, panel C*). This can yield information on the strength of the oscillations and viability of the specimens over time and in different conditions. Also, it is a very useful representation, as it evidently points out any outliers, trends and, most importantly,

expected signal changes. Furthermore, the user can perform an additional averaging of the variance values in the different experimental conditions (e.g. before vs. after the exposure to antibiotics). An example of averaging is presented on *Figure 5.2.4*, *panel D*, where each bar represents the averaged variance of the deflection as a final quantitative measure that determines the outcome.
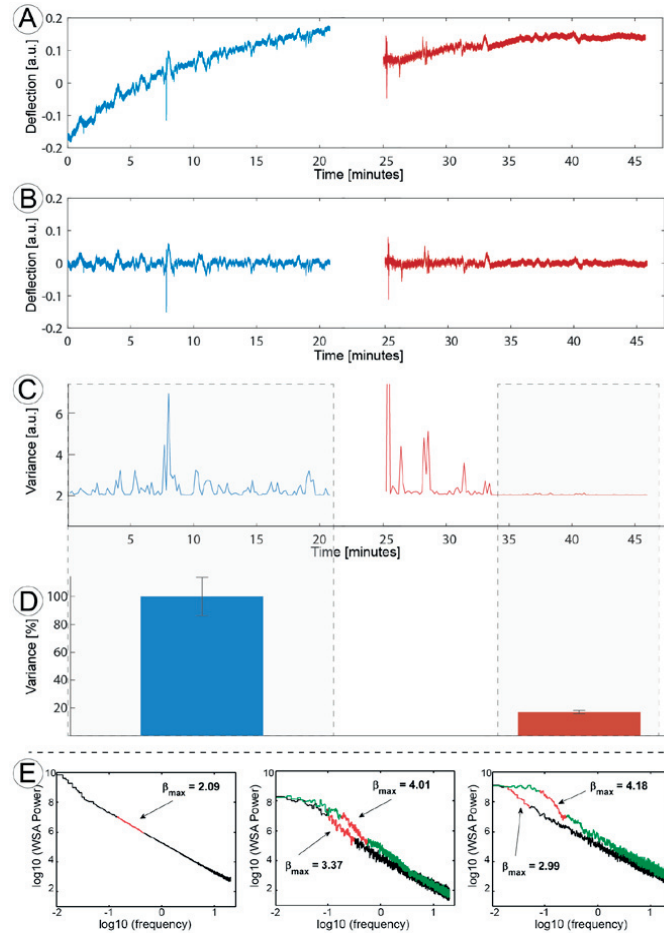
Fig. 5.2.4. Panel A: Nanomotion deflection signal recorded while the attached Bordetella pertussis were in growth media (blue) and in the presence of the antibiotic (red). Panel B: the same signal, flattened and centered around zero. Linear fit over 200s window has been applied. Panel C: Variance of the flattened deflection signal. For every 10s of the signal, variance has been calculated and plotted as it evolves in time for both conditions. Panel D: Normalized variance averages for the selected areas on variance plot. Blue bar shows 100% value, while the red bar represents the variance average calculated 10min after the drug exposure, and shows the reduction of fluctuations to less than 20%. Panel E: Another way of analyzing the signal. Log-log plots of deflection signals power spectra, obtained by applying Interval Weighted Spectral Averaging (IWSA) method for three cases: cantilever without living specimens (left); Bordetella pertussis (middle); Escherichia coli (right). Green curves refer to untreated, black to treated bacteria or bare cantilever. In all cases a sliding regression window was applied. Window positions with maximal values of exponent β were drawn in red, while the corresponding βmax values are indicated in each panel.

84

In addition to the variance, more complex signal analysis procedures can be taken into consideration. We have investigated different approaches to the characterization of the signal, producing other Matlab and Labview routines to perform more advanced characterizations, such as FFT analyses and signal filtering, but in this regard much work still must be done. Indeed, the nanomotion signal is mainly a colored noise, which contains a white noise component, peaked at the resonance frequency, electronic noise at low frequencies and the biological component in between. In this framework, a simple FFT analysis, a method generally used to detect putative frequency components of the oscillatory signal, might not be optimal. In our studies, we have seen that the multitude of specimens and oscillating sources yield no particular isolated frequency. The presence of living specimens on the sensor produces only an increased intensity of the lower frequencies in the power spectrum of the data (<1000 Hz). The result of the metabolic activity of the samples is spread over wider frequency regions. 1/f dependence noise is superimposed on frequency-independent white noise, and analysis of these factors will likely be important for the understanding of the cell-generated noise. There is evidence that a log-log power spectrum analysis is more suitable to allow the emerging and characterization of relevant peaks. Therefore, one could apply Interval Weighted Spectra Averaging (IWSA) method (*Figure 5.2.4, panel E*) instead of simple power FFT (*Figure 5.2.5*) [104]. In addition to this, other more refined spectral and non-linear analyses including multi-fractal [105], time-frequency using the Stockwell-transform [106,107], or multiscale entropy analyses [108] could be well suited.
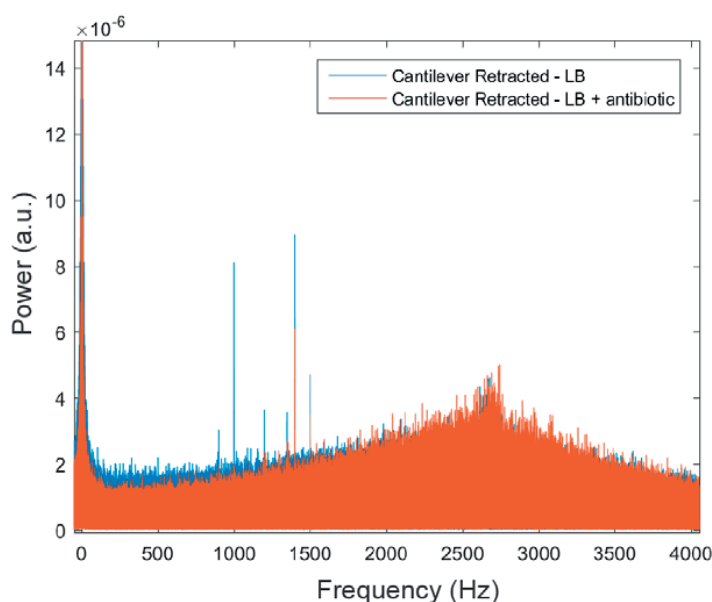

Fig. 5.2.5. FFT analysis of oscillatory movement in growth media (blue) and in the presence of the antibiotic (orange).

It must be noted that the response of living biological systems can be extremely variable. The phenotypic response of the specimens to a particular drug or condition can require long stabilization times. For example, when studying bacteria exposure to antibiotics, we identified several cases in which the initial nanomotion response did not reflect the effective susceptibility to the particular drug. In some cases, resistant species reduced their fluctuations, only to return to a normal oscillation after tens of minutes. Also, care should be taken when averaging, to avoid the initial part of the signal, as the drug might still not take its effect.

5.2.3. Conclusion

Nanomotion analysis of microscopic samples is a simple and rapid method to assess the viability and metabolic response of a wide range of simple organisms in different conditions. Here, we have detailed the best practice to achieve successful measurements with this innovative technique. We described all the steps required to determine the best protocols for the experiments, while also highlighting some of the problems that can occur during measurement and, for most of them, the way to avoid them.

Due to the young age of this technique, its limitations and development possibilities are still unexplored. For instance, the laser-photo-detection system is extremely simple and efficient but also a major source of noise. Electronic noise, susceptibility to impurities in the analysis chamber or from laser misalignment can affect a good nanomotion experiment. Such problems would be in part reduced by employing other kinds of high-sensitivity fluctuation detection, such as piezo resistive sensors or capacitive transduction systems.

Overall, the nanomotion sensor is a very versatile and powerful instrument which can be the base for new investigation tools. Indeed, we have already combined nanomotion and fluorescence microscopy analyses and the increasing control over the grafting of micro fluidics or micro contacts directly on the cantilever can open the way to even more complex characterization platforms, merging, on the same sensor, nanomotion and conventional tools. This would be a step towards integrated diagnostic tools, Lab-on-a-Lever sensors, which can deliver an unprecedented view of the overall activity of biological specimens and of their response to external stimuli.

5.3. Calibration

Cantilever calibration

The calibration experiments were conducted to quantify the amount of energy added by the bacteria to the motion of the cantilever. The experiments consist of the following procedure.

Cantilever is inserted into an AFM head and scans a calibration grating of known height, thus providing voltage versus the deflection relation (V/m).

The first stage is then used to calibrate a piezo actuator stack to obtain the relation for applied voltage versus the piezo element displacement (V/m).

Then the calibrated piezo is used to actuate the cantilever in the open fluid cell of the nanomotion device with a known amplitude. Knowing the amplitude of the motion the final relation of the photodiode voltage versus the deflection is known.

Other methods of calibration are possible using interferometry to measure the cantilever deflection. There are other ways to calibrate the piezo element that could be used.

There is another aspect of the calibration of the cantilever that is important. Due to manufacturing processes the resultant cantilevers have dispersion in their dimensions and thus properties, especially the spring constant. To compare the cantilevers it is necessary to measure their resonant frequency.

Low-pass filter

The biologically significant phenomena in the experiments according to comparison of the power spectra are happening in the low frequency region, under 100 Hz (see *Fig. 2.4*).

Experiments conducted in our Laboratory proved that the use of the low-pass filters with a cut-off frequency set to 100 Hz increases the difference between the variance of the signal of viable bacteria in comparison to non-viable by a factor of 2.5. Without the filter the single-to-noise ratio is approximately 2 and when using the filter it increases to approximately 5. The variance of the signal of viable bacteria drops by a factor 2, however the baseline drops by a factor of 5.

5.4. Nanomotion AST of slow-growing bacteria

This section has been published.

María Ines Villalba‡, Petar Stupar‡, Wojciech Chomicki, Massimiliano Bertacchi, Giovanni Dietler, Laura Arnal, María Elena Vela, Osvaldo Yantorno*, Sandor Kasas*, **Nanomotion Detection Method for Testing Antibiotic Resistance and Susceptibility of Slow-Growing Bacteria**, Small.

‡ Authors contributed equally

5.4.1. Introduction

Infectious diseases are one of the most important causes of human mortality worldwide. Therefore, rapid detection and identification of microbial pathogens are mandatory in order to treat patients appropriately. It is important to realize that antimicrobial susceptibility testing (AST) should be carried out for all pathogens recovered from an infectious process, since therapeutic measures cannot be consistently predicted based exclusively on the knowledge of the identity of the infecting microorganisms. Consequently, it is evident that physicians require rapid and reliable AST that allows them to make a fast decision and, as a result, improve patient outcomes and reduce health care associated costs. A number of laboratory methods are currently available to characterize the in vitro susceptibility of microorganisms against antibiotics. Current culture-based methods include disk diffusion methods, antimicrobial gradient diffusion tests and broth dilution techniques as those recommended by the Clinical and Laboratory Standards Institute (CLST) or by the European Committee on Antimicrobial Susceptibility Testing (EUCAST) [109,110]. However, results obtained by these techniques are time consuming, needing at least 20 hours, or up to a month in case of tuberculosis. During the last decades, automated and semi-automated devices, such as: Becton Dickinson Phoenix, Siemens MicroScan Walk Away or Vitek 2, have been extensively used at hospital level [18,20,111]. Nevertheless, they are currently used for the AST determination of fast growing organisms, have a high cost and, in addition, are not available for the full spectrum of bacteria.

Although it has been reported that antibiotics exert specific effects on growing microorganisms, few studies have attempted to quantify the dynamic changes induced by antibiotics in microbial growth patterns [112]. We previously reported that atomic force microscope (AFM) based nanomotion sensors can be used to characterize

metabolic activity of living bacteria within minutes, needing only 10^2 bacteria to have a measurable signal (*Figure 2.2* and *Figure 2.3*) [23,58,64].

Furthermore, we have described the use of such a device to determine the Minimal Inhibitory Concentration (MIC) and Minimal Bactericidal Concentration (MBC) of ampicillin, and the effects of kanamycin, ciprofloxacin and caspofungin, for different kinds of fast growing organisms, such as *Escherichia coli*, *Staphylococcus aureus* and *Candida albicans* [23,64]. Nevertheless, it has not yet been determined whether this device is sensitive enough to detect cantilever fluctuations produced by slow growing bacteria, when incubated in culture media and in the presence of antibiotics. In this work, we explored the nanomotion sensor's ability to determine the MIC and MBC of macrolides antibiotics in slow growing bacteria (SGB).

We have previously assessed the growth kinetic of *Bordetella pertussis*, the etiological agent of whooping cough or pertussis, in both Stainer Scholte (SS) liquid medium as planktonic cells, and adhered to surfaces as sessile populations forming biofilm [113,114]. B. pertussis can adhere and live attached to different surfaces (polypropylene, glass) where it shows a specific growth rate (μ) of 0.03 h^{-1} [114]. This growth rate is very slow compared to the one of *E. coli* (MG1655), which displayed a μ value of 1.09 h^{-1}, growing on polyethylene terephthalate (PET) surfaces [115]. Accordingly, we decided to use *B. pertussis* as a representative organism of SGB in order to assess the impact of different antibiotic concentrations on its metabolic activity and to evaluate the time nanomotion detection requires to sense susceptibility to different antibiotics. Macrolides such as erythromycin or clarithromycin are regarded as antibiotics of choice in the treatment of pertussis. Co-trimoxazole (1:19 Trimethoprim /sulfamethoxazole) is often cited as an alternative where macrolides cannot be tolerated [116]. In this work, we have focused on bacteriostatic antibiotics, for which bacteriostatic activity has been defined as a MBC/MIC ratio > 4 [117]. Finally, the results obtained with the nanomotion sensor for AST analysis were compared with the ones coming from traditional techniques as broth dilution method [109].

5.4.2. Materials and Methods

B. pertussis Tohama I strain (Collection of Institute Pasteur, Paris, France -CIP 8132-); BPSM, a streptomycin resistant (Smr) strain derivative from *B. pertussis* Tohama I [118]; and *B. pertussis* clinical strain (Bp2723) collected at La Plata Children's Hospital (Hospital Sor Maria Ludovica, La Plata, Argentina), were employed throughout this study. The antibiotics used in the experiments were: erythromycin (Sigma- E6376); clarithromycin (Sigma A3487),

trimethoprimsulfamethoxazole, also known as co-trimoxazole, 1:19 (Sigma T7883 and Sigma S7507, respectively) [TMP-SMX] and ampicillin (Sigma- A0166). In the case of BPSM strain, streptomycin (Sigma S6501) was employed. SS liquid medium was used to culture *B. pertussis* strains [114,115]. Bacteria were deposited onto triangular silicon nitride (Si$_3$Ni$_4$) cantilevers with spring constants typically 0.06 or 0.12 N/m. Before deposition, in order to promote bacterial attachment, the cantilevers were incubated with 10 μL of 0.5% glutaraldehyde for 10 min, rinsed with ultrapure water, dried, and then incubated with 10 μL of a high-density bacterial suspension (OD595: 0.5 with 100 μl of suspension diluted in 1mL of phosphate buffer saline). The cantilevers with adhered bacteria were inserted into the analysis chamber of a home-made nanomotion device to analyze their vibrational response in growth medium and upon exposure to antibiotics [62]. For each tested condition, 40 minutes measurements of the cantilever oscillations were done at room temperature. Variance of the deflection signal was calculated to define the variation in the amplitude of the sensor´s movements. The evident outliers were removed in cases of inevitable non-biological signal. The information was recorded using custom software optimized for this application to register the cantilevers movement, and the Matlab R2013bTM software was employed to analyze the data.

5.4.3. Results

The standard method of broth dilution was used to evaluate the MIC and MBC values for *B. pertussis* Tohama I reference strain and the clinical strain Bp2723 grown as planktonic cells. We found that the MIC values of planktonic cells for erythromycin and clarithromycin were between 0.06-0.12 μg/mL and the MBC between 2.5-5.0 μg/mL. The respective MBC/MIC ratios were greater than 4 for erythromycin, clarithromycin and co-trimoxazole. Thus, these antimicrobials could be considered as bacteriostatic [117]. We found that the MIC value for each antibiotic tested was the same for both the clinical strain and the reference strain, grown under planktonic condition. Similar results were found for the MBC values of the two strains. Tohama I strain showed MIC and MBC values of 3 and 10 μg/mL of streptomycin, respectively, while BPSM strain survived the exposure to 200 μg/mL of the same drug. In the first set of experiments, nanomotion measurements were done on Bp Tohama I reference strain in SS liquid media. The aim of the measurement was to assess the survivability of bacteria on a cantilever. Therefore, the cantilever oscillations were monitored during 13h of incubation under non-stressing conditions. After six hours from the start of the experiment, the oscillations continuously increased with time. This phenomenon could be associated with the beginning of replication of the adhered cells, since they are entering the exponential phase of

90

growth, as we have previously reported for B. pertussis biofilm growth [113,114]. *Figure 5.4.1* shows the variance of the cantilever oscillations during the time course of the experiment. In further experiments, we explored cantilever oscillations after the antibiotic exposure.
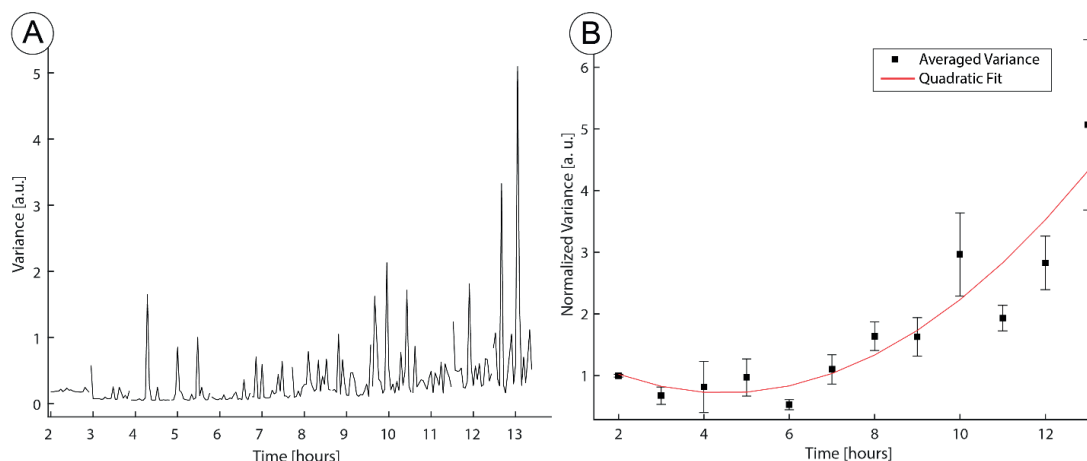

Fig. 5.4.1. Variance of the cantilever oscillation signal in time. B. pertussis cells were attached to the cantilever and tracked during 13h of incubation in SS media. Panel A: Line plot of the variance against time. Panel B: Variance averages of 1h window better reflect the increase in oscillations throughout time.

We chose clarithromycin´s and erythromycin's MBC values previously determined by the broth dilution method to test the outcome on metabolic activity of B. pertussis Tohama I strain during three hours of incubation. Reduction of the sensor's oscillation amplitudes and of the corresponding variance took place after the antibiotic exposure (*Figure 5.4.2*).
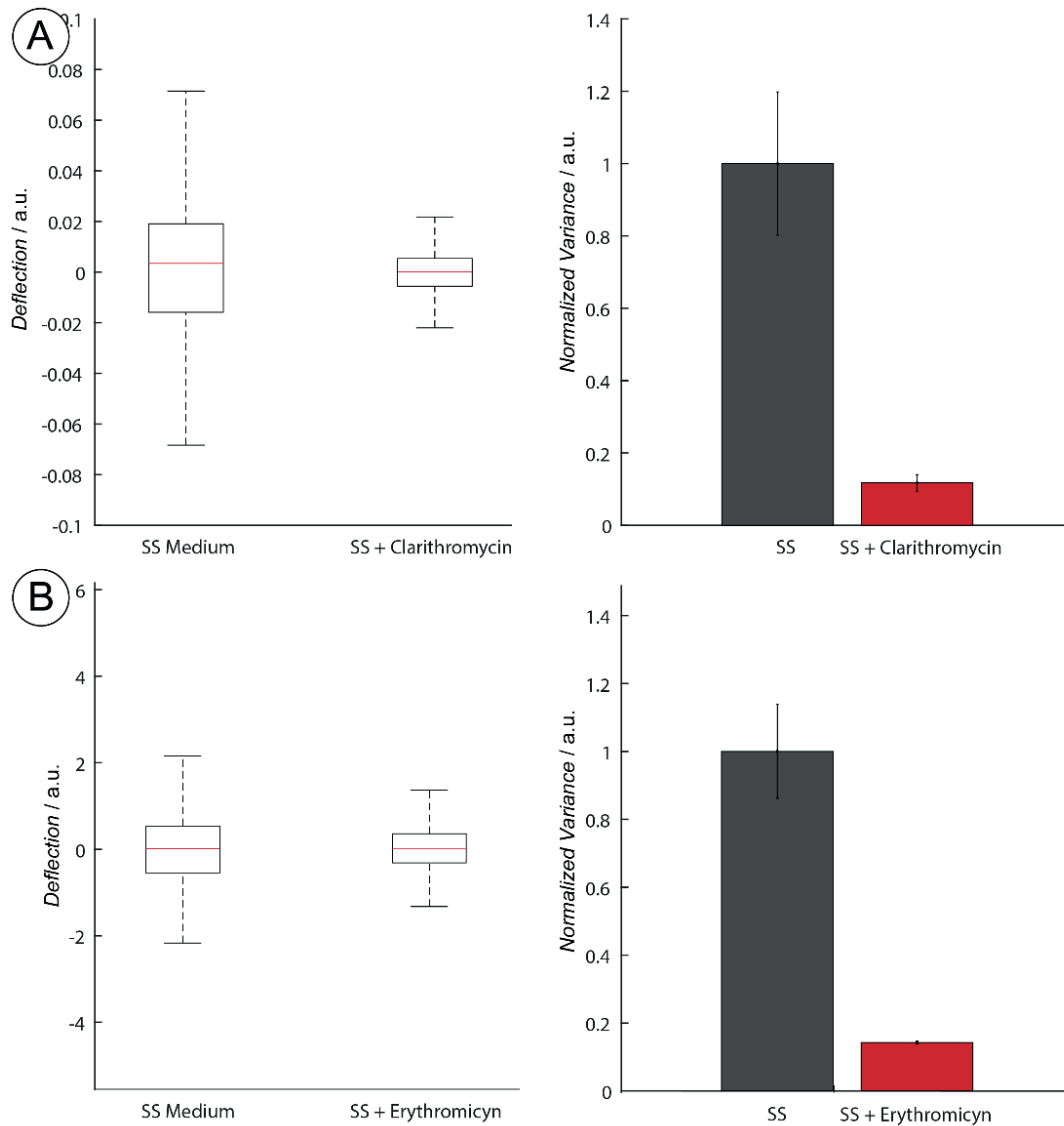
Fig. 5.4.2. Panel A: Boxplots of the cantilever oscillation movement with B. pertussis cells adhered and incubated in SS medium with and without the addition of clarithromycin (5µg/mL). Panel B: Normalized variance averages across 15 minutes of incubation time (15 minute averages were taken after 40 minutes of incubation in the medium or antibiotic).

We have observed that 40 min incubation time is sufficient to register the effect of the clarithromycin and erythromycin, and less than 20 min for ampicillin. This result is in agreement with those previously reported with this device but using fast growing bacteria [62]. In addition, we monitored the cantilever oscillations when B. pertussis BPSM, a Smr strain resistant to streptomycin, was incubated in presence and absence of specific antibiotics. The variance was higher for BPSM in SS medium with the addition of streptomycin at 50 µg/mL, indicating that the metabolic activity was not reduced. The variance of the signal decreased significantly when the bacteria were

exposed to SS medium with co-trimoxazole, which suggests a drop in metabolic activity in such environment (*Fig. 5.4.3*).
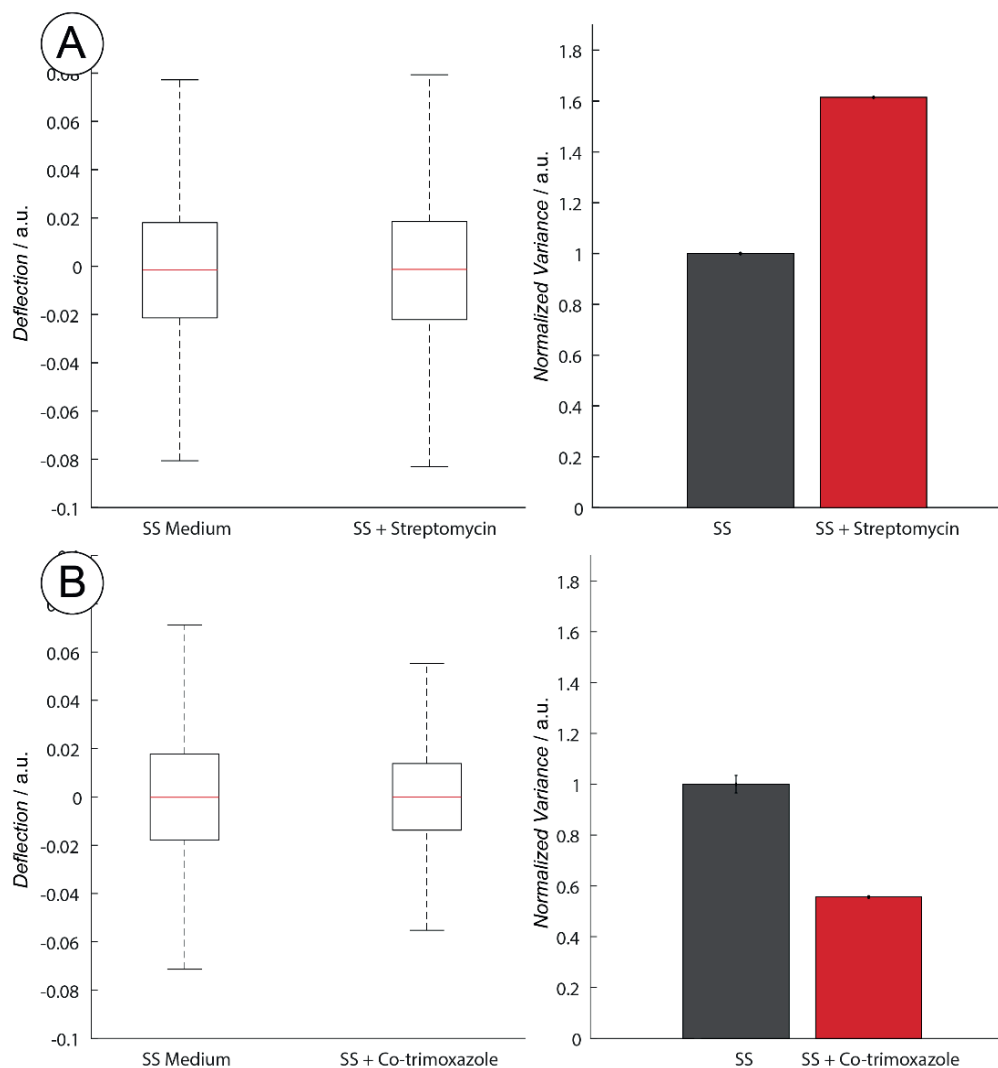

Fig. 5.4.3. Boxplots of cantilever movement with BPSM (streptomycin resistant) strain adhered and their corresponding variance averages. Panel A: After the introduction of streptomycin, boxplots suggest higher oscillation amplitudes, and variance bars confirm an increase in the movement. Panel B: Signal comparison between the exposure to medium and co-trimoxazole. Boxplots show a decrease in oscillation amplitudes, and variance bars support the same conclusion. The responses are connected with resistance (A) and susceptibility (B) of bacteria to the applied antibiotics. Variance bars are 15 min averages, taken after 40 min of incubation in the medium or the antibiotic).

To monitor the effect of different antibiotic concentrations on the reference strains and the clinical isolate, we incubated each strain in SS medium alone and in the presence of increased antibiotic concentrations from 0.002 μg/mL to 10.0 μg/mL. Macrolide clarithromycin and β-lactam ampicillin were employed for this set of experiments.

The used concentration range includes MIC and MBC values. Surprisingly, we registered that the larger variance values correspond to the MIC in cases of clarithromycin. The metabolic activity of B. pertussis cells adhered to the cantilever increased when it was exposed to antibiotic concentrations lower than MIC in all cases. Culture experiments suggest high viability of the attached cells at MIC values. After reaching MIC, the variance values drastically decreased as the concentration of antibiotic in the culture medium was increased. This behavior was observed until the antibiotic concentration reached MBC value. Above MBC point, the variance of the oscillation signal (which reflects the cellular metabolic activity) dropped to the lowest values measured in the experiment (*Figure 5.4.4*). Finally, we compared the MIC and MBC concentrations obtained with the device with the ones obtained by the conventional method and we found similarities between these two methodologies using the clinical strain and B. pertussis reference strain.
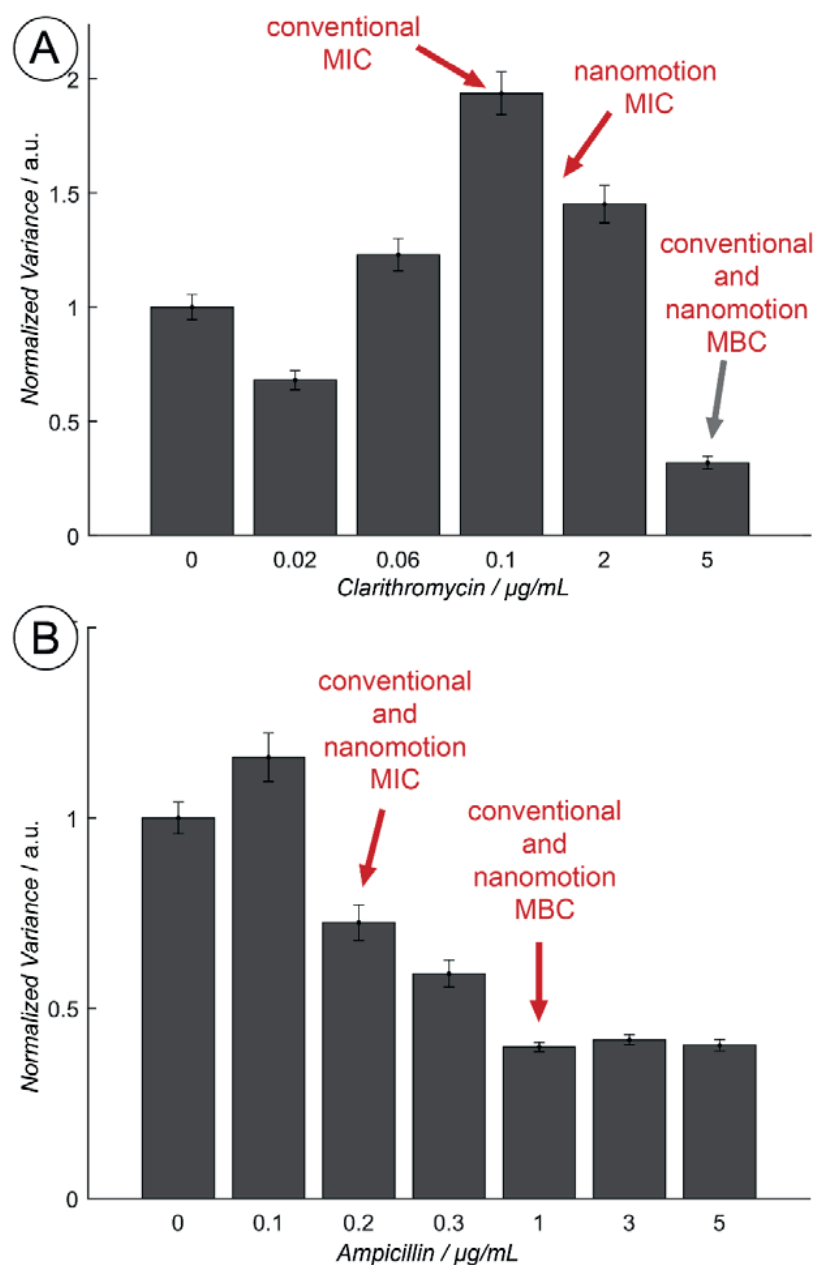
Fig. 5.4.4. Normalized variance of the cantilever movement obtained when B. pertussis was exposed to different concentrations of clarithromycin (Panel A) and ampicillin (Panel B). MIC and MBC values obtained by the conventional methods in parallel are marked in red. Results suggest a potential application of such a method for obtaining MIC and MBC values in a much shorter time frame. Each bar corresponds to 30-minute average. Considering that clarithromycin and erythromycin need at least 40 minutes of exposure for an effect to take place, the variance average is shown to be higher, whereas in case of ampicillin, the MIC action takes place within the variance average and the resulting value at MIC is lower that on the condition without the antibiotic.

5.4.4. Conclusion

A first set of experiments measuring living *B. pertussis* cells on a cantilever during a prolonged period of time confirm the sensitivity of the device to register small signal changes originating from the increase in metabolic activity (from lag to log phase) and multiplication. In further experiments, we showed that a decrease in variance of the signal, compared to the one in growth media, suggests the action of clarithromycin and erythromycin on *B. pertussis* cells on the sensor. In case of resistance to streptomycin, the signal's variance does not decrease with the addition of the drug. However, on incubation with co-trimoxazole, the signal's variance reduction is apparent.

As in the case of resistance (BPSM strain's response to streptomycin), the high variance before and close to MIC values is possibly a consequence of the stress condition imposed by the presence of the antibiotic in the cellular environment. This observation is consistent with previously reported studies. Compensatory response to antibiotics has been observed in *Pasteurella multocida* under subMIC conditions [119].

The above results confirm that the nanomotion sensor not only detects the metabolic activity of a SGB like *B. pertussis*, but permits also to determine the MIC and MBC values in a shorter time than the traditional methods. It constitutes a great advantage for the SGB infectious diseases treatment. Such a rapid antibiotic susceptibility test could reduce treatment costs, and more importantly, diminish health risks. The new strategy for detecting antimicrobial resistance would be particularly useful in cases of infectious disease where the treatment lasts several weeks or months, thus helping to avoid the illness recurrence.

5.5. Nanomotion monitoring of mitochondrial activity

This section has been published.

5.5.1. Introduction

Mitochondria are 0.7-3 micrometer sized sub-cellular organelles that contain their own DNA, and it is nowadays believed that they were independent prokaryotic cells that long time ago colonized eukaryotes [120]. Mitochondria live with eukaryotes in an endosymbiotic manner and are involved in numerous key physiological processes, such as energy production and regulation, signaling and programmed cellular death. Altered mitochondrial function is a key underlying mechanism of many pathological states, such as cardiac diseases, diabetes and numerous other neurological conditions [121]. Precise assessment of mitochondrial function is necessary to understand those underlying mechanisms and the aging process. Furthermore, growing literature indicates that mitochondria are also targeted by environmental pollutants, making them an important subject in environmental toxicology and health research [122]. However, the diagnosis of mitochondrial diseases is a complicated, expensive, and time-consuming process that involves mitochondrial isolation, DNA extraction and sequencing. Among the tools for probing mitochondrial properties, measurements of oxygen consumption and ATP production have been used to assess the function of freshly isolated mitochondria [123].

Few years ago, our team noticed that atomic force microscopy (AFM) cantilevers can be used as nanomotion sensors to detect subtle oscillations that characterize living organisms. Despite the fact that the origin of these oscillations is still not fully understood, we could observe that the amplitude (variance) of these oscillations reflect the metabolic state of the organism of interest. We also noticed that these nanoscale oscillations exist in every living biological sample we tested so far (bacteria, yeast, vegetal and mammalian cells) [23,58,64,97]. In an attempt to simplify mitochondrial disease diagnostic, we carried out preliminary experiments to explore the putative nanoscale oscillation pattern of native mitochondria. The experiments consisted in attaching isolated mitochondria onto an AFM cantilever and recording its oscillations as a function of exposure to different chemicals.

Enzymes within the mitochondrial matrix (*Figure 5.5.1.a*) are designed to oxidize the added substrates, in a cyclic manner (*Figure 5.5.1.b*), so that every product of a reaction is a potential substrate for another reaction. In our experiments, human embryonic kidney cell mitochondria were submitted to malate, pyruvate, ADP, sodium azide and rotenone. Malate and pyruvate are the substrates involved in the citric acid cycle (Kerbs' cycle), and their oxidation provides energy conserved in the structure of molecules like NADH and FADH2. These energy carriers lose energy by interacting with complexes embedded in the mitochondrial inner membrane. Complexes (I-IV) transfer energy by passing along the electrons in a process called the electron transport system. Starting with re-oxidation of a NADH molecule, a pair of electrons is passed through a series of carriers to coenzyme Q, forcing protons from the matrix into the intermembrane space. The electrons are then passed through Complex III, forcing more protons out, and finally to Complex IV, where oxygen is reduced to water by using the electrons. In this process, some energy is released as heat, while the majority is conserved within the created proton gradient. The last link in the chain of complexes is the ATP synthase (F0 and F1 subunits). It holds a proton channel, where protons are pumped through, allowing energy for the synthesis of ATP by rotating F1 subunit and changing the conformation of binding sites where ADP molecules react with available phosphate.
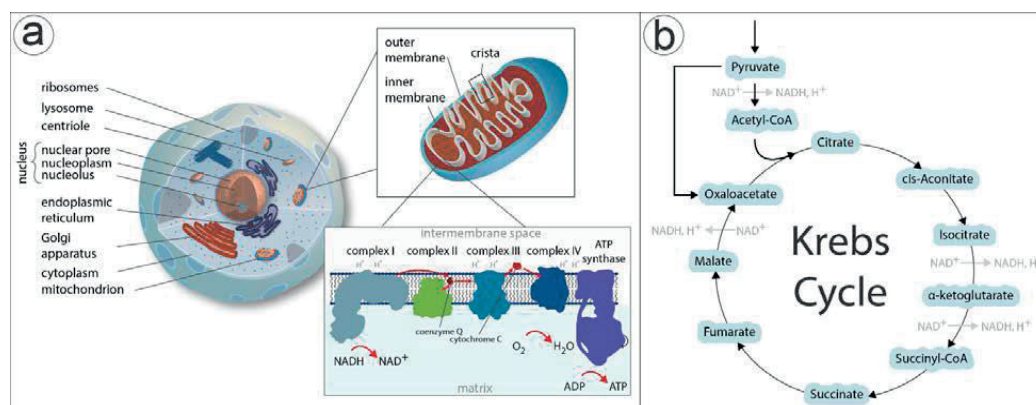

Fig. 5.5.1. Panel (a): Schematic of a mammalian cell with labelled organelles, zoom on the mitochondrion showing its structure and most important components of the inner membrane (Complexes I-IV and ATP synthase). Panel (b): Krebs cycle (citric acid cycle) showing the sequence of metabolic reactions that generate energy within mitochondria.

Apart from the substrates, our experiments consisted in adding inhibitors, sodium azide and rotenone. Sodium azide inhibits the ATPase activity of F1 subunit, but has no inhibitory effect on ATP synthesis [124]. Rotenone is another inhibitor and it acts by inhibiting NADH dehydrogenase or Complex I of the electron transport chain [125].

98

The oscillation patterns that we observed with mitochondria on the cantilever were highly dependent on the chemicals to which they were exposed. These preliminary experiments indicate that mitochondria, similarly to bacteria, yeast, vegetal and mammalian cells also promote oscillations of the cantilever to which they are attached.

5.5.2. Materials and Methods

Solutions and buffers. Buffer 1 (HB): 210 mM mannitol, 70 mM sucrose, 5 mM HEPES (pH 7.12). Buffer 2 (HBS): HB + 1 mM EGTA + 1x Roche's Complete Mini EDTA-free protease inhibitor cocktail (1 tablet dissolved in 10 ml of buffer). 50 % Percoll: Percoll (Sigma P1644) diluted 1 to 1 with HB. Percoll solutions (22 % and 15 %): the 50 % Percoll stock is used to prepare all other Percoll solutions; to that effect dilutions of the 50 % Percoll solutions are done in HBS.

Substrate solutions were prepared in advance and stored at -20 oC. All substrates were dissolved in the working buffer (125 mM KCl, 10 mM TRIS, 0.1 mM EGTA, 1 mM KH_2PO_4, pH 7.4), while rotenone was initially dissolved in 50 % ethanol and then diluted with the buffer. Malate and pyruvate were used in 5 mM final concentration, while ADP was added in 1 mM final concentration. Sodium azide was used in 10 mM, while rotenone in 1 µM.

Mitochondria isolation. Mitochondria were isolated according to a modified protocol [126]. Human embryonic kidney cells (293T) were grown to approximately 85 % in DMEM. Plates were placed on ice and washed twice with 8 ml of ice cold HB. Cells were collected by scraping directly in the Dounce Tissue Grinder and homogenized well. The obtained homogenate was spun at 1500g for 3 minutes. The supernatant was spun at 13000g for 17 minutes and the pellet was re-suspended in 1.4 ml of HBS. 5ml centrifuge tubes with a discontinued Percoll gradient were used (1 ml of 50 % Percoll solution followed by layering 3 ml of 22 % Percoll solution). To the re-suspended pellet, 0.6 ml of 50 % Percoll (final concentration of Percoll 15 %) was added and layered 1 ml of the 15 % Percoll sample on top of the described 50-22 % gradient. This was spun at 30700g for 6 minutes and mitochondria were recovered from 50-22 % Percoll interface. Mitochondria were finally washed by making 1 to 10 dilution with HBS and centrifuging at 15600g for 30 minutes.

AFM imaging. Atomic Force Microscopy measurements were made using Nanowizard III AFM from JPK Instruments (Berlin, Germany), coupled with a Zeiss Axiovert inverted optical microscope. A fluid cell was incorporated and all the images were obtained in buffered conditions. Images were collected using DNP (Bruker) cantilevers, with a nominal spring constant of 0.06 N/m. Quantitative imaging mode

has been used for the image acquisition, Gwyddion (v. 2.36) software for flattening and no further image processing has been carried out.

Mitochondria attachment procedure. Mitochondria were attached to cantilevers using glutaraldehyde functionalization and the following procedure. Conventional NP-O cantilevers (Bruker) were functionalized using 0.5 % glutaraldehyde for 10 minutes. All cantilevers were washed afterwards, and placed to dry for the following 4 minutes. A droplet of solution containing concentrated mitochondria was placed onto the functionalized cantilevers and left for 30 minutes. After the attachment, the cantilevers were mounted and positioned inside a fluid cell, together with the working buffer.

Data acquisition and processing. Real time deflection of the cantilever was collected at the sampling frequency of 20 kHz. The signal was first flattened using a running window of 200 seconds. A linear fit was applied to each window and the raw signal was subtracted, so the outcome is a detrended signal, centered around zero. Such signal was further processed by applying the moving average of 4 seconds. Finally, variance was calculated in the similar manner, using a running window of 10 seconds. Variance signal was used for line and bar plots in the presented figures. Error bars in *Figure 5.5.5* represent the standard error of the mean.
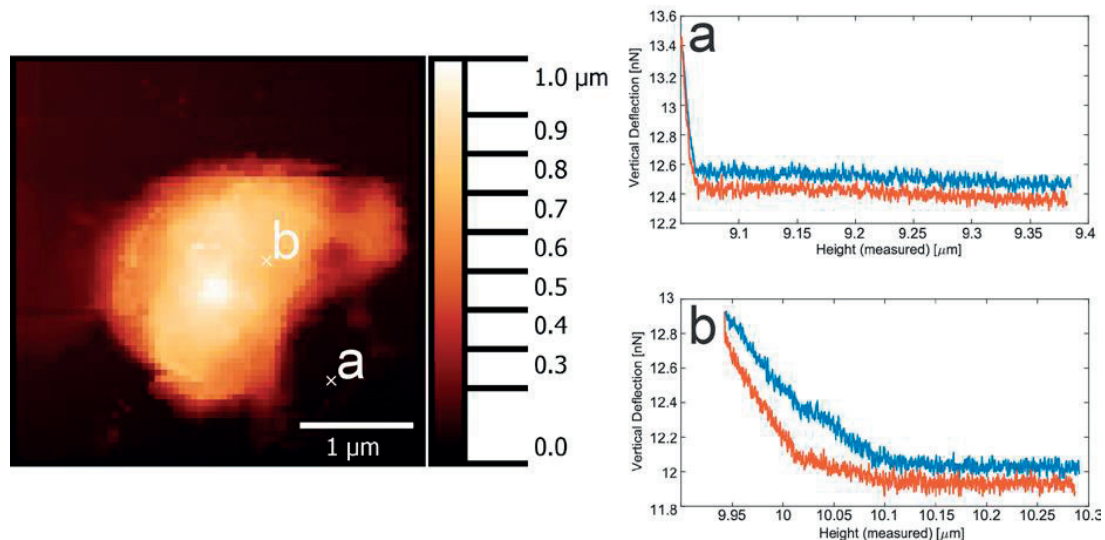

Fig. 5.5.2. The AFM image of isolated mitochondrion attached to glass, in buffered conditions. Structure shows 2.5 μm length, 2 μm width and 1.1 μm height. Force-distance curves from positions marked on the AFM image are shown on the right. The top figure (a) shows the stiffness of the substrate, while the other one (b) shows the softness of the biological structure.

Before exploring the mitochondrial sample with our technique, we imaged the attached mitochondria on a glass substrate in liquid media. *Figure 5.5.2* shows the obtained image with examples of force-distance curves at two different positions, one on the mitochondrion and the other one on the support. Curves show a typical response of the cantilever in contact with a soft and a hard sample, respectively.

Next, freshly isolated mitochondria were attached to the cantilever sensor and introduced into the analysis chamber. Real-time cantilever deflection recordings were made while mitochondria were submitted to different conditions by using the fluid cell that allowed us the fluid exchange. The first media to make a measurement was a plain buffer, after which we introduced substrates: malate and pyruvate. With introduction of the substrates, the oscillations increased, as presented on the variance plot in *Figure 5.5.3*. Oxygen consumption in this condition reflects state 2 respiration of mitochondria, specific to Complex I. Then, we introduced ADP to the medium to stimulate further the respiration in the presence of malate and pyruvate. In this condition, state 3 respiration, specific to Complexes I and II, appears to keep oscillations of the sensor increased. The example of oscillations, plotted as a real-time deflection, is presented on *Figure 5.5.4*. We continued the experiment by adding sodium azide and measuring the response. The oscillations showed a slow decrease, and were completely reduced only after the injection of media containing rotenone.
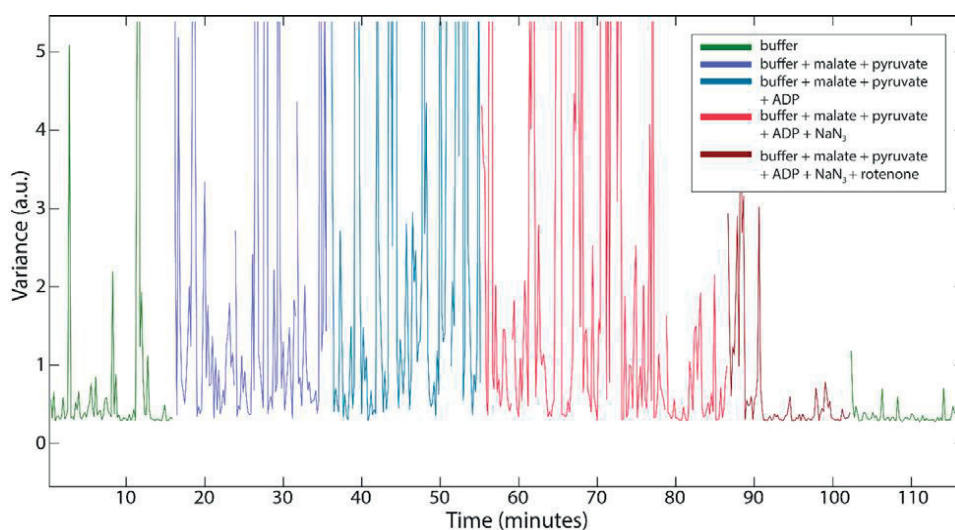

Fig. 5.5.3. The evolution of variance throughout the experiment. Variance was calculated from the deflection data for each measurement. Different colors represent different conditions to which mitochondria were subjected. In each condition, a new substance was added (substrates: malate, pyruvate, ADP; inhibitors: NaN3, rotenone). Variance increases with the addition of substrates and decreases in presence of the inhibitors.
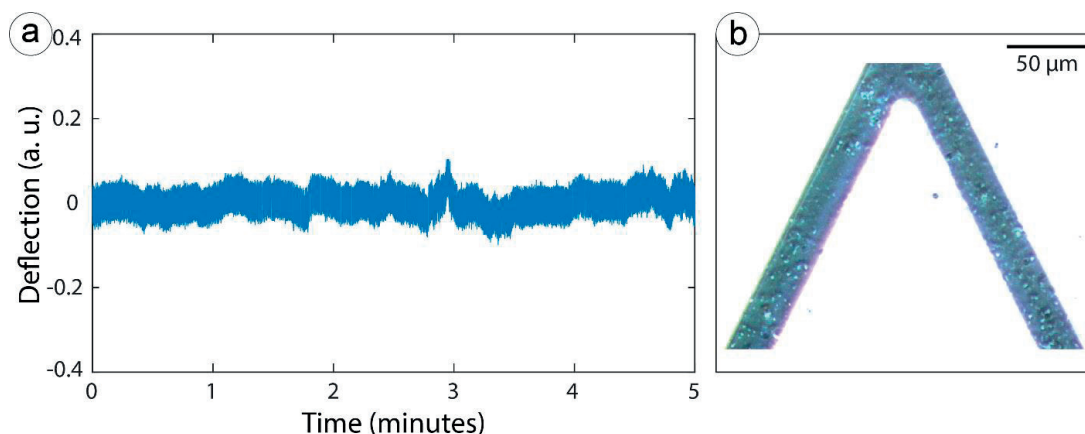
Fig. 5.5.4. Panel a: Deflection of the cantilever with mitochondria attached. The recordings were made while the buffer with substrates (malate, pyruvate, ADP) was present in the analysis chamber. Figure shows a section of 5-minute oscillations. Panel b: A typical image of mitochondria attached to the cantilever.

Lastly, *Figure 5.5.5* shows the variance averaged over 15-minute intervals within different conditions. Two sets of bars are presented, one with the control cantilever (functionalized, but with no mitochondria attached), and the other one with mitochondria attached. Each set is normalized to the first measurement (buffer) separately, and represents the percentage change of variance once the substrates (and the inhibitor) are added. While the control cantilever oscillations remained within the error interval, the one with mitochondria attached showed more than two times increase in oscillations in the presence of metabolic substrates compared to the buffer only. Values suggest that mitochondria do couple with the cantilever and induce oscillations greatly above the baseline thermal motion, when activated by substrates. These oscillations dropped with the introduction of the inhibitor, suggesting the complete inhibition of mitochondrial activity.
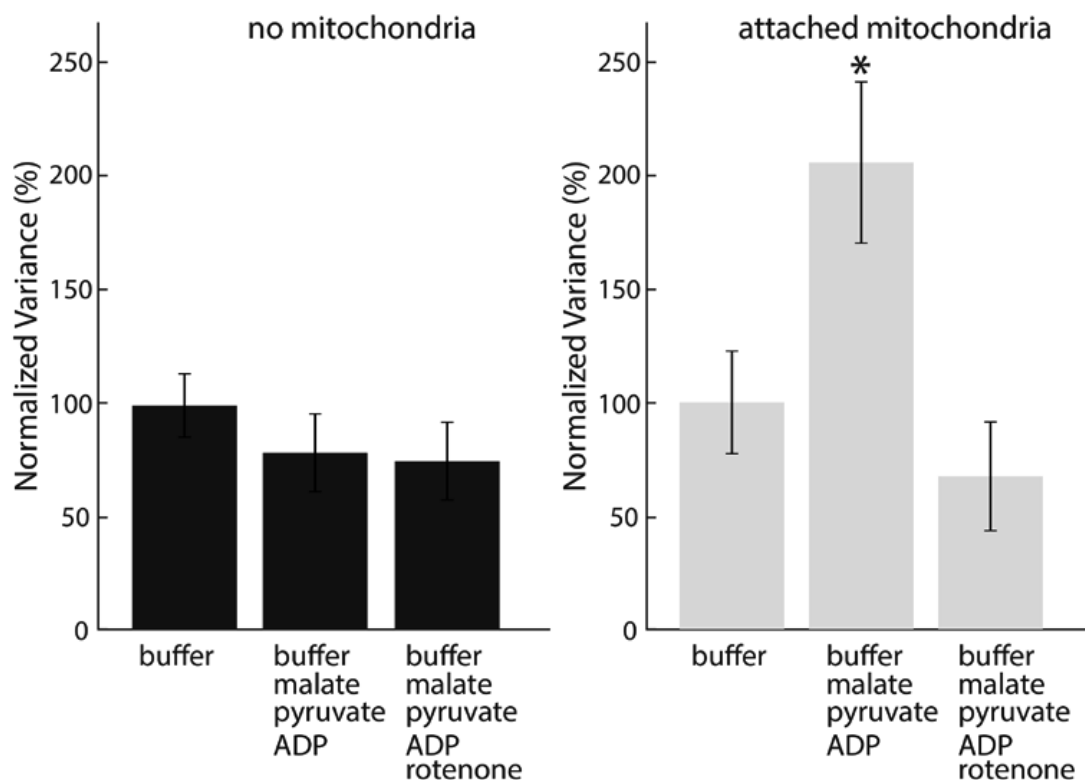
Fig. 5.5.5. Normalized and averaged variance over the 15-minute intervals in conditions of a plain buffer, buffer with substrates and lastly, with the inhibitor. Dark grey represents values without any mitochondria on the cantilever as a control, while light grey values show variance changes with the attached mitochondria. The two-sample t-test rejected the null hypothesis at the 5% significance level ($p \leq 0.05$) only in the case of attached mitochondria with the addition of substrates.

In this work, we showed how nanometer scale oscillations arising from mitochondrial processes coupled with the cantilever and produced motion. Conventional FFT analysis, unfortunately, could not produce any distinct frequency components specific to the oscillations in different metabolic conditions. Therefore, we believe variance evolution is the best parameter to describe dynamic changes in oscillations. As showed on *Figure 5.5.3*, switching from plain buffer into a buffer with metabolic substrates caused oscillations to increase. Those oscillations were amplified with the addition of a diphosphate necessary for the series of conformational changes that precedes the ATP synthesis. Sodium azide is an inhibitor that acts by confining the activity of ATPase, without stopping the ATP synthesis coupled mechanically to the proton motive force across the inner membrane by the rotation of the subdomain ensemble [127]. Furthermore, some reports show that the presence of inorganic phosphate could tamper the ability of azide as an inhibitor [128]. Therefore, the observed slow and incomplete decrease of variance could be attributed to azide

not being as potent inhibitor in our experimental setup. Rotenone, a specific NADH dehydrogenase inhibitor, stops the electron transfer to coenzyme Q. This creates reactive oxygen species which can damage DNA and other components of mitochondria. This could suggest why in the presence of rotenone in our experiments, oscillations of the cantilever dropped to the lowest values.

Considering our previous work, it is not surprising that a cantilever with the attached mitochondria oscillates more than a control in the presence of metabolic substrates. The observed increase could be attributed to the complex dynamics of the mitochondrial metabolic system.

5.5.4 Conclusion

Mitochondrial diseases are a public health issue nowadays and their diagnostic is unfortunately still a complicated, long, and expensive process. In these experiments, we demonstrated that the activity of native mitochondria can be detected, like in the case of other prokaryotes. We have also shown that their oscillation pattern is affected by the chemicals to which they were exposed. Having in mind these two facts, it can be speculated that the oscillation pattern of "healthy" and "diseased" mitochondria could also differ. Likewise, it could be expected that they react differently upon appropriate chemical exposure. Such a possibility would open novel avenues in mitochondrial disease diagnosis and research. Even if for the moment we did not explore these interesting hypotheses, the present work suggests that continuing the investigation might lead to a great benefit in terms of diagnostic speed and cost. The next step is to extend our studies to mitochondria isolated from patients suffering from mitochondrial diseases.

5.6. Conclusion

The results presented in this chapter bring suggestions to help explain the origins of the observed effect that will be discussed in the next chapter.

The results presented in this chapter show the possible applications of the method with the slow-growing bacteria infection. Compared to the standard methods of AST the nanomotion provides the result on the same day.

Chapter VI

Discussion

6.1. Effect explanation

In the third chapter of this thesis we proposed few possible causes of the observed effect. Some of the considered effects were discarded based on a simple model and calculation of the forces, momenta and energies involved.

We proposed and discussed the imposturous effects. Some of the imitating effects were also discriminated against based on the simple model and the calculation of the forces, momenta and energies involved. Based on the experiments presented in the fifth chapter the possible contributing effects are discussed here.

As noted in the conclusion to the third chapter (section 3.5) the causes that contribute to the observed effect most significantly are:

- flagellar motility,

- local pH changes,

- bacteria induced surface strain.

The main imitating effects that are needed to be controlled for are:

- the antenna effect,

- freely swimming bacteria bumping into the cantilever.

Flagellar contribution

It has been observed that if flagella are present on the bacteria and active, their contribution is significant. One of the experiments showed that the lack of flagella caused a drop in the variance to about half of the value of the same strain possessing flagella. It has also been observed that the variance of the bacteria lacking flagella (e.g. *Staphylococcus aureus*) is lower compared to the bacteria possessing active flagella (e.g. *Escherichia coli*). The flagellar activity can provide more energy transferred to the motion of the cantilever than is observed in the experiment under the assumption of a perfect alignment in the direction of the cantilever motion of all the flagella that are operating at their full capacity in all of the bacteria present. However under reasonable assumptions of random directionality, random capability and random number of working flagella the transferred energy can reach the value in agreement with experiment.

Local pH effect

It has been observed in an experiment with bulk changes of pH that the cantilever covered with gold on one side is prone to a static deflection. The hydrogen ions interact with the surface of the silicon nitride. The local change in pH is assumed to be capable of causing the observed deflection, and through diffusion it is possible for the effect to present a dynamic character. The local change in pH in our experiments is attributed to the metabolic activity of the living microorganisms. However it is unknown if the cantilever with attached bacteria covering about 10% of the surface area behaves in a similar manner. Furthermore, in a series of experiments with cantilevers coated with a reflective gold coating at the apex and viable bacteria attached the oscillations were still observed. Uncoated silicon nitride cantilever is assumed not to bend as a result of the interaction between hydrogen ions and its surface because the surface stress of both sides compensate. This argument puts the contribution of the local pH effect into question. Moreover in the experiments with slow growing bacteria *Bordetella pertussis* the oscillations of the cantilever are present, yet their metabolism [129] does not supplement enough NH_4 for the observed oscillations.

Surface stress contribution

It has been observed in few experiments with eukaryotic cells and cancer cells in our Laboratory that e.g. spreading of the cell visible with an optical microscope can be correlated with the variance of the deflection signal, the same is true for recent experiments with T cells that were activated, which causes softening of their cytoskeleton and the variance of the deflection signal was observed to decrease.

Changes in the stiffness of the membranes due to fluctuating hydration can also contribute to the surface stress.

Flagella that are attached to the surface of the cantilever and the motors winding them up might also exert some additional surface stress.

Summary

The vertical deflection of the cantilever can be achieved with the surface stress applied along the length of the cantilever with the help of mechanical means and local pH fluctuations.

The torsional bending of the cantilever can be supplemented by an uneven distribution of the number of bacteria, the activity of bacteria in both applying a surface strain through mechanical means and local pH fluctuations.

Both of those effects tend to increase in time with bacteria growing and multiplying and both can last for hours in accordance with the constraints outlined in the introduction to the third chapter (section 3.1). Bacteria metabolize nutrients and continue to change the pH in their vicinity. Bacteria crawl on the surface of the cantilever through continually attaching and detaching their bodies, moreover bacteria regularly extend and compress their fimbria that being attached to the surface induce additional stress.

Both of the aforementioned effects due to their random nature reproduce the 1/f noise.

6.2. Device motorization and automation

The device has been motorized to achieve a better alignment precision. The automation of the device helped to simplify the alignment procedure through removing the tedious task of coarse and fine manual adjustment. Another advantage over the manual version is the ability to control it remotely, thus removing the necessity to remain in the same place as the device is located. The achieved precision and reproducibility allows those devices to be used by other groups to conduct their research and to be placed in a hospital environment. One device is at the Desert Research Institute in Nevada, US where it is used for COLDTECH project as a life detector in extremely cold environments analogue to conditions on the Europa moon. One device is at Lausanne University Hospital – CHUV, with the second one planned to be moved there as well. Moreover the knowledge and experience gained with the development of the automated device will be used for future developments.

Chapter VII

Conclusion

The observed development of the last few decades in the field of biophysics contributed to the improvement of the medical diagnostics. Despite the quick progress, increasingly precise knowledge about the pathogenesis, diagnosis and disease therapy still there are many problems that remain unresolved. For centuries we are witnessing helplessness towards numerous infectious diseases. In spite of the milestone which was the invention of the antibiotics, science encountered another problem the antimicrobial resistance. Modern science therefore poses a challenge which is to quickly diagnose infectious diseases and to identify indispensable, targeted therapy. A step towards creating a medical procedure that is a tool to combat microbes is the creation of a device that detects the nanomotion induced by living microorganisms on a cantilever. These experiments are significantly shorter than standard methods used in hospital laboratories for the antibiogram determination. It should also be noted that there are microorganisms that are reluctant to grow in which case the determination time difference is even greater.

The creation of a tool for fast and precise indication of pharmacotherapy is necessary from the point of view of the patient as an individual and in the context of the global health protection. The delayed use of the right antibiotic is a life-threatening condition for a patient who develops bacteremia, sepsis or septic shock. The increase in the drug resistance, if no action is taken against that, will put people's life in danger. Today the WHO warns against the growing problem of bacterial diseases, against rapidly spreading tuberculosis, and talks about the great return of syphilis, which has almost been forgotten. It is important to look for the AMR origin, however it is equally important to develop rapid, accurate, reliable, cost-effective, easy-to-use and ready-to-use commercial tools.

The two main goals of this study have been the development of the improved device that could assess the viability of microorganisms through detection of the cantilever oscillations induced by the viable microorganisms attached to it, the other goal was to understand the physical origins of this phenomenon.

The current version of the device offers a number of advantages over the previous device iterations. First of all the motorization enables higher precision of the adjustment, combined with finer laser power adjustment. Another advantage is the ability to remotely control the device. Another advantage is the ability to simplify the pre-experiment operation with the software automation. The graphical user interface was also significantly improved for simplicity, ease-of-use and low barrier entry. The repeatability of the alignment and the reproducibility of the experiment was improved.

The current understanding of the observed effect origins involves the combination of few effects:

- microorganisms exerting a surface stress on the cantilever via fimbria, membrane or immobilized flagella,
- microorganisms causing surface strain due to local pH changes due to their metabolism,
- microorganisms exerting forces on the cantilever due to flagellar drive if present on the bacteria.

The other discussed effects play a lesser, insignificant roles as shown previously. This work also stresses the importance of controlling for factors that can imitate viable bacteria causing false positive results. This work attempts to lay a groundwork in explaining the effect and proposing further experiments helpful in quantifying the answer.

Future outlook for science

Multiple experiments should be made to thoroughly investigate the ultimate explanation of the observed effect.

This method has the potential to be used for the basic research in microbiology to quantitatively asses the viability, motion and surface interactions of living microorganisms.

As proposed in [64] this method might be useful in discovering life on other planets, moons, asteroids, comets, in the interplanetary dust or water plumes. This method might be useful for the detection of life in extreme conditions as can be found in the Antarctic Ocean or on the dry highlands exposed to high doses of UV light.

Future outlook for application

This method has the potential to be widely used in the hospital laboratory environment to help to find the proper drug to treat bacteremia, sepsis, septic shock, urosepsis, and lung infection. This method might be used to select the specific drug for targeted therapies. This method might also be useful in the development of pharmaceutics.

Appendices

Control program description
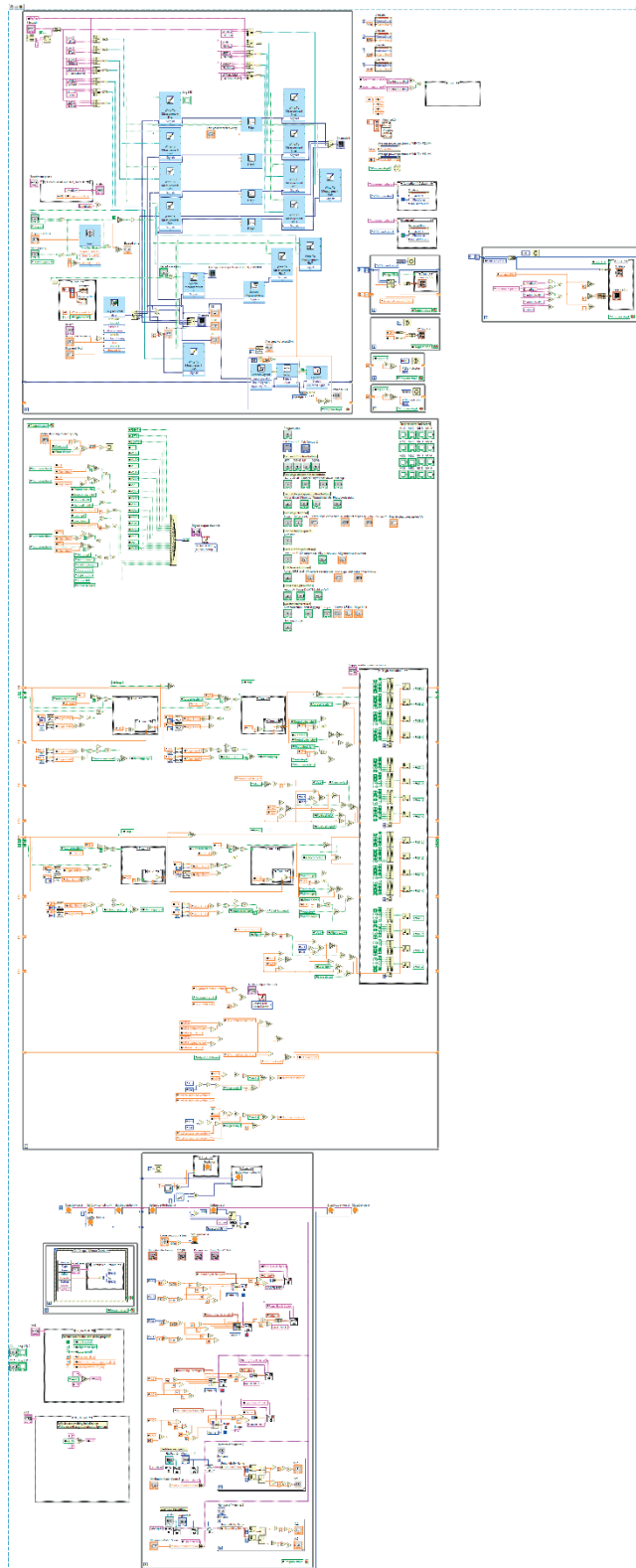
The program controls the alignment of the Nanomotion device (measurement device) and enables acquisition of signals, its analysis and allows for graphical representation of the results.

Program is coded with G-code in LabVIEW environment. It combines the easy to use programming interface, code blocks, data lines, ready-to-use functions and device libraries in Block Diagram with the simple graphical user interface design suite in Front Panel. Each Front Panel element corresponds to an element in Block Diagram, however some of the Block Diagram elements are not represented in the Front Panel. The Front Panel can be thought as a data input and data output interface.

The whole program code is shown on the left. At the very top left is a While Loop that contains data acquisition, treatment, presentation and saving. Below that is a While Loop containing the part of the program that enables to control stepper motors, laser and light. Below that is a While Loop containing image acquisition and treatment functions. On the left side of that loop there are three structures: the top one is used to handle Event Structure responsible for obtaining coordinates by clicking on the image preview, the two others are the Case Structures that are responsible for two stages of automatic alignment. The first contains 13 steps that recognizes the cantilever and the laser spot and afterwards controls the stepper motors. The second one contains 13 steps that controls the centering of the laser spot on the quadrant photodiode.

The code comprises of structures, constants, variables, functions, property invokes and Virtual Instruments (VIs).

In the first part of the Apendix the definitions of the constituents are given followed by the functional description of the parts of the program.

121

Definitions

Structures

The code encompassed by the **While Loop** is executed at least one time and repeats itself until a specific condition is fulfilled. The indicator **i** returns the number of cycles elapsed from the initialization of the structure. Boolean input of the Conditional Terminal controls the While Loop. For programs which code is meant to be executed more than once the whole code is placed inside the main While Loop.
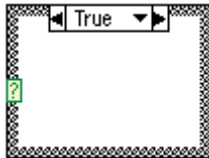
The code encompassed by the **Case Structure** is executed with each iteration of the parent loop (e.g. main While Loop) or constantly if the structure is not nested.
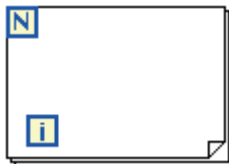
The code encompassed by the **For Loop** is executed **N** times each time it is invoked. The indicator **i** returns the number of cycles elapsed from the initialization of the structure.
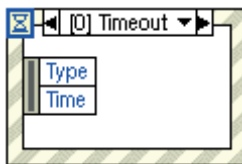
The **Event Structure** awaits until a specified event happens, then executes accordingly. This structure features the Timeout terminal that allows to apply specific time (in milliseconds) after which the event is no longer acted upon.

122

Numeric functions

`0` (blue)	Integer constant representation.
`0` (orange)	Floating point constant representation.

x, y → **+** → x+y — Returns the sum of two inputs.

x, y → **−** → x-y — Returns the difference of two inputs.

x, y → **×** → x*y — Returns the product of two inputs.

x, y → **÷** → x/y — Returns the quotient of two inputs.

x → **+1** → x+1 — Returns the input value increased by 1.

x → **-1** → x-1 — Returns the input value decreased by 1.

x → **||** → abs(x) — Returns the absolute value of the input.

x → **[-x]** → -x — Returns the negative value of the input.

x, y → **÷R IQ** → x-y*floor(x/y), floor(x/y) — Return the remainder and the integer quotient of the input.
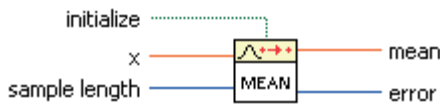
initialize, x, sample length → **MEAN** → mean, error — Returns the mean value of the input, initialization terminal enables control, the sample length terminal allows for calculating the mean value of requested sample number.
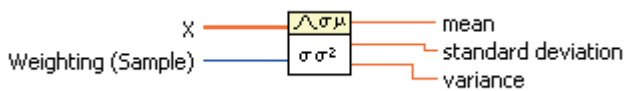
X, Weighting (Sample) → **σ σ²** → mean, standard deviation, variance — Returns the mean value, standard deviation and the variance of the input, the Weighting (Sample) terminal allows for calculating the output values for the requested sample number.

Comparison function

<table>
<tr><td>x = y?</td><td>Returns TRUE if x is equal to y, returns FALSE otherwise.</td></tr>
<tr><td>x != y?</td><td>Returns TRUE if x is not equal to y, returns FALSE otherwise.</td></tr>
<tr><td>x > y?</td><td>Returns TRUE if x is greater than y, returns FALSE otherwise.</td></tr>
<tr><td>x >= y?</td><td>Returns TRUE if x is greater than or equal to y, returns FALSE otherwise.</td></tr>
<tr><td>x < y?</td><td>Returns TRUE if x is less than y, returns FALSE otherwise.</td></tr>
<tr><td>x <= y?</td><td>Returns TRUE if x is less than or equal to y, returns FALSE otherwise.</td></tr>
<tr><td>x > 0?</td><td>Returns TRUE if x is greater than 0.</td></tr>
</table>
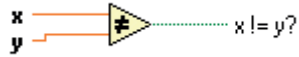
Boolean functions

TRUE constant representation.

FALSE constant representation.
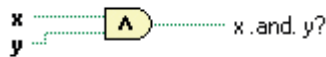
x .and. y? — Returns Boolean value of AND operation of inputs.
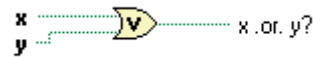
x .or. y? — Returns Boolean value of OR operation of inputs.
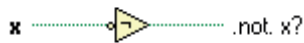
.not. x? — Returns the logical negation of the input

s? t:f — Select function returns one of the input values depending on the input value of the **s** terminal, value of the **t** terminal if the **s** value is TRUE and value of the **f** terminal if the **s** value is FALSE.

124
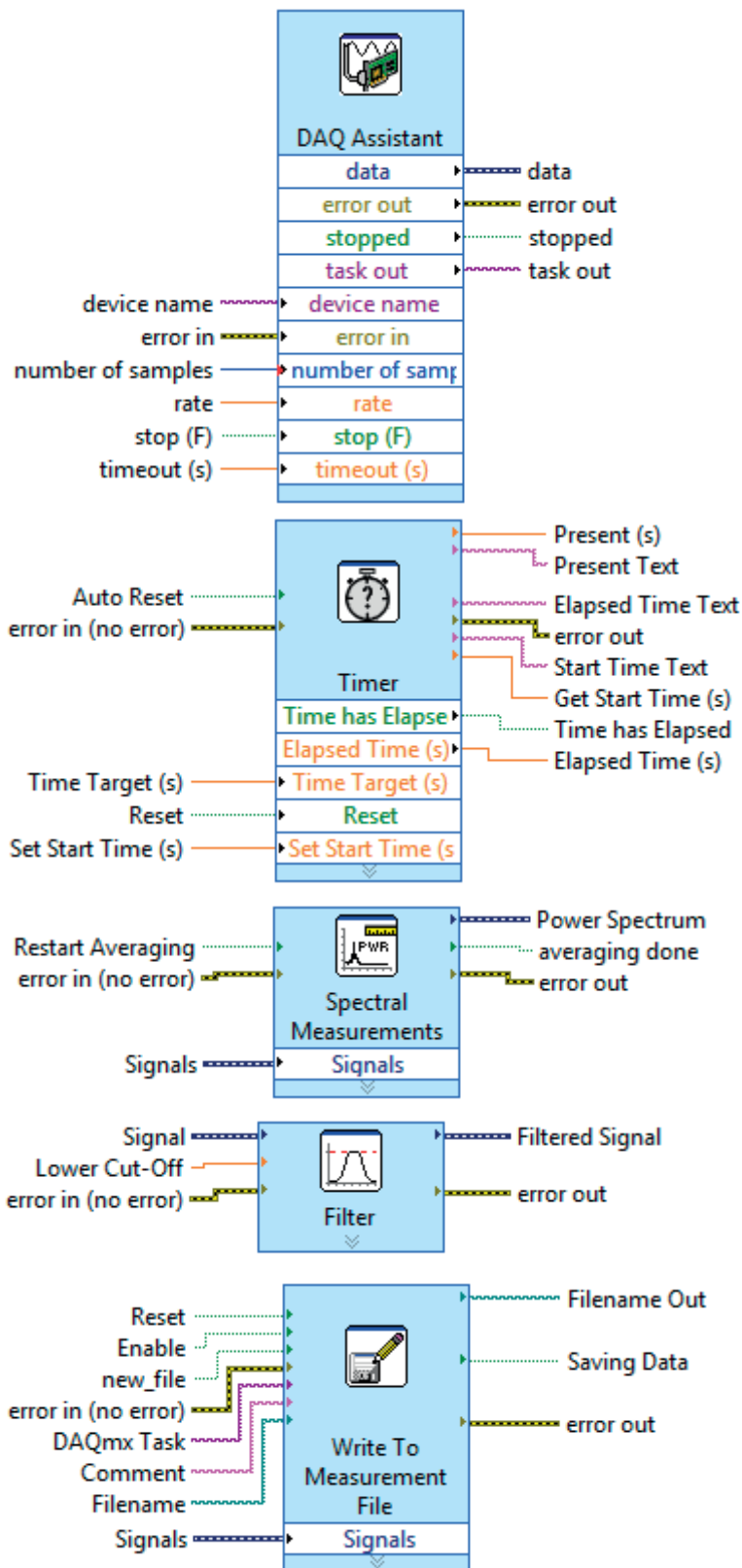
Express Vis

DAQ Assistant is an express VI that is used to configure NI-DAQmx tasks (analog and digital input and output channels) that enables connecting the computer that is running LabVIEW program with physical device that is controlling the experiment and acquiring signals.

Timer express VI is used to indicate the time that passed since the specified event.

Spectral Measurements express VI is used to calculate power spectrum, specific settings (averaging, weighting, window, etc.) can be accessed through options.

Filter express VI can be used to filter the collected signals. Available are low-pass, high-pass and band-pass filters with multiple topologies to choose from.

Write To Measurement File express VI can be used to record the acquired signals to a file in the data storage. This express VI enables to choose the file type and divide multiple signals by recording time and file size into separate files. Adding a header into the file is also possible.
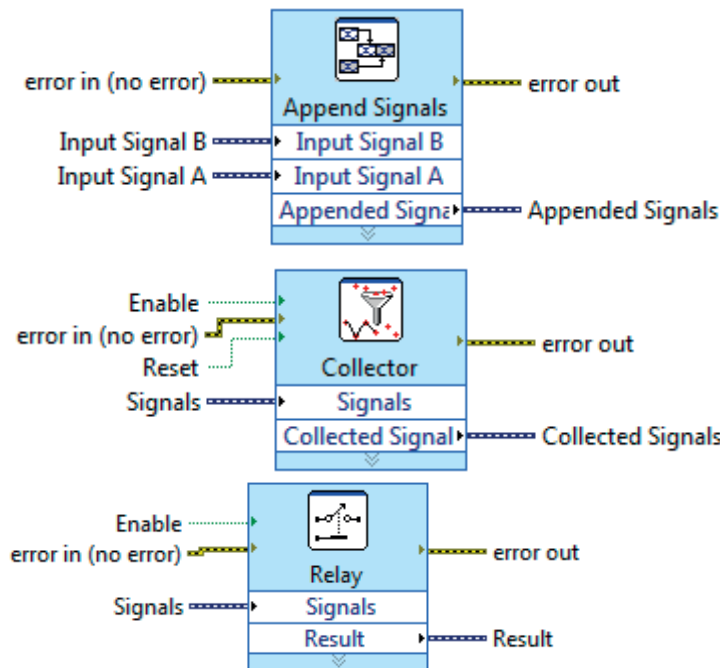
Append Signals express VI used to join two signals one after the other.

Collector express VI is used to collect and store data to a set size limit and releases it when the limit is reached.

Relay express VI is used to switch between two output options: transferring the original input signals unchanged or creating empty data in its place.

## Input and output channel and signal functions
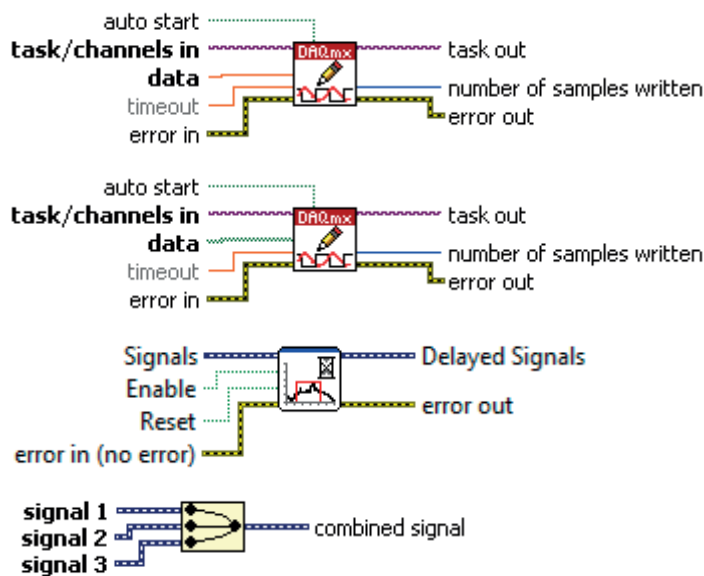
DAQms Write (Analog DBL 1Chan 1Samp) is a DAQms task that is configured to operate 1 analog digital output channel of the acquisition device.

DAQmx Write (Digital 1D Bool NChan 1Samp 1Line) is a DAQms task collection that is configured to operate 28 digital output channels of the acquisition device.

Delay Values stores the data from previous iterations of the structure it is placed in, the data is further released after a specified number of iterations.

Merge Signals function combines separate signal into one combined signal containing the data in parallel.

String functions
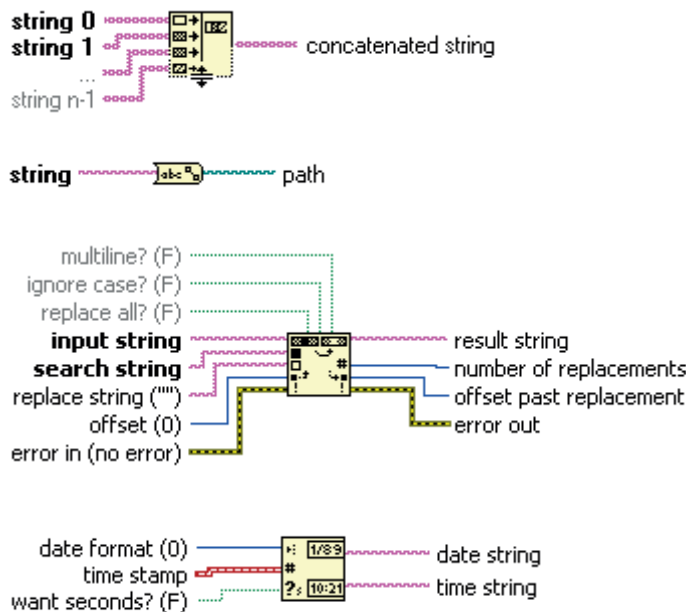
Concatenate Strings function combines input strings and converts them into one string containing the input strings in sequence.

String To Path function transforms string input into a path-type output.

Search and Replace String function searches the input string for search string and replaces it with replace string, offset parameter is used to exclude given number of characters from the beginning of the input string from searching and replacing, the function returns the result string.

Get Date/Time String function returns date string and time string, the time stamp input is used to return specific time and data, otherwise the function returns system time.

Array and cluster functions
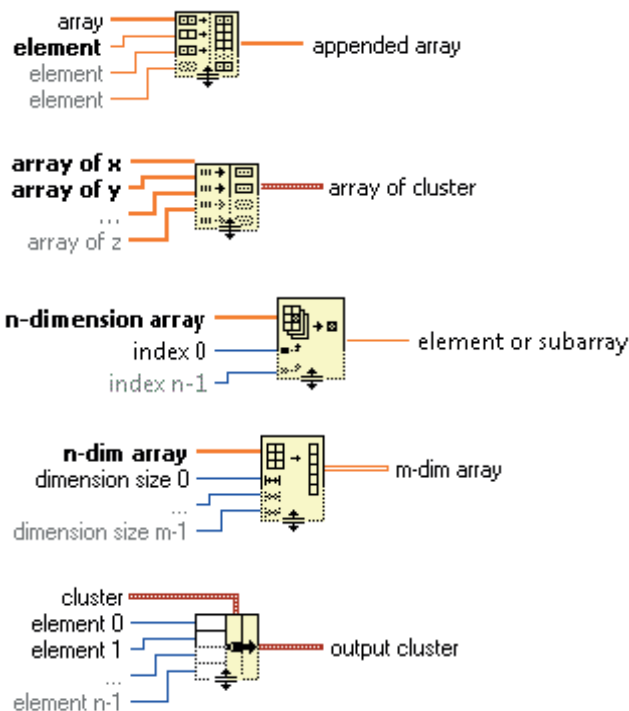
Build Array is a function that appends array or elements to an array.

Index & Bundle Cluster Array indexes input arrays and creates an array.

Index Array function returns element or subarray of the input array specified by index or indices.

Reshape Array is a function that reads the data from n-dimension input array row-by-row and writes to m-dimension output array row-by-row.

Bundle is a function that combines elements into a cluster. There is a input for a cluster constant to provide cluster model for this function.
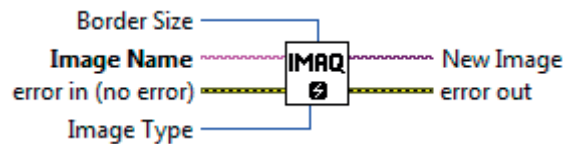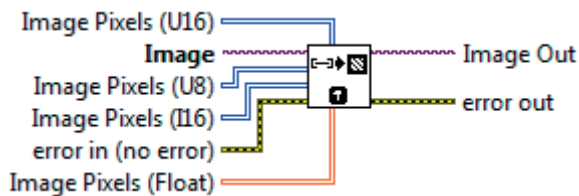
Image functions

Group
Image
Bounding Rectangle
Drawing Mode (Frame)
error in (no error)
Color
Image Out
error out
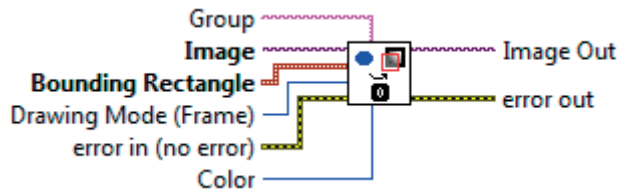
IMAQ Overlay Oval is a function that imposes oval shape on the input image.

Group
Font, Size & Style
Image
Origin
String
error in (no error)
Text Color (black)
BG Color (Transparent)
Image Out
error out
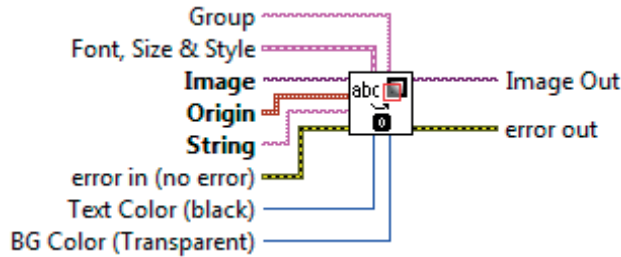
IMAQ Overlay Text is a function that imposes text on the input image.

Border Size
Image Name
error in (no error)
Image Type
New Image
error out

IMAQ Create is a function that temporarily allocates memory for an image.

Image Pixels (U16)
Image
Image Pixels (U8)
Image Pixels (I16)
error in (no error)
Image Pixels (Float)
Image Out
error out

IMAQ ArrayToImage function transforms a 2D array into an image.

File Path
Image
Load Color Palette? (No)
File Options
error in (no error)
Color Palette out
Image Out
File Type out
File Data Type out
error out
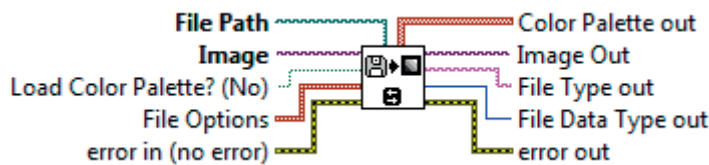
IMAQ ReadFile is a function that reads into memory an image from a file.

Algorithm
Image
Mask
Angle Range
error in (no error)
Advanced Options
Template Image Out
Template Report
error out
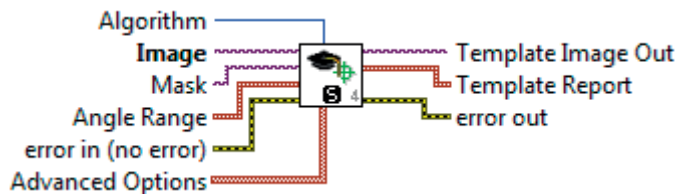
IMAQ Learn Pattern 4 is a function that reads an **Image** from a file. Then this file is used as an input to pattern learning algorithm that results in creation of **Template Image**.

Algorithm
Image
Template Image
ROI Descriptor
Parameters
error in (no error)
Advanced Options
Image (duplicate)
Matches (pixel)
Matches (real-world)
Number of Matches
error out
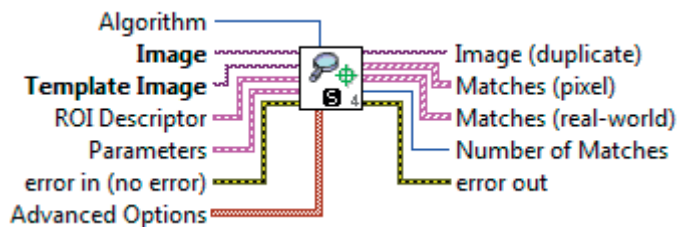
IMAQ Match Pattern 4 is a function that uses **Template Image** as an input to matching algorithm that is looking for a match in an input **Image**.

128
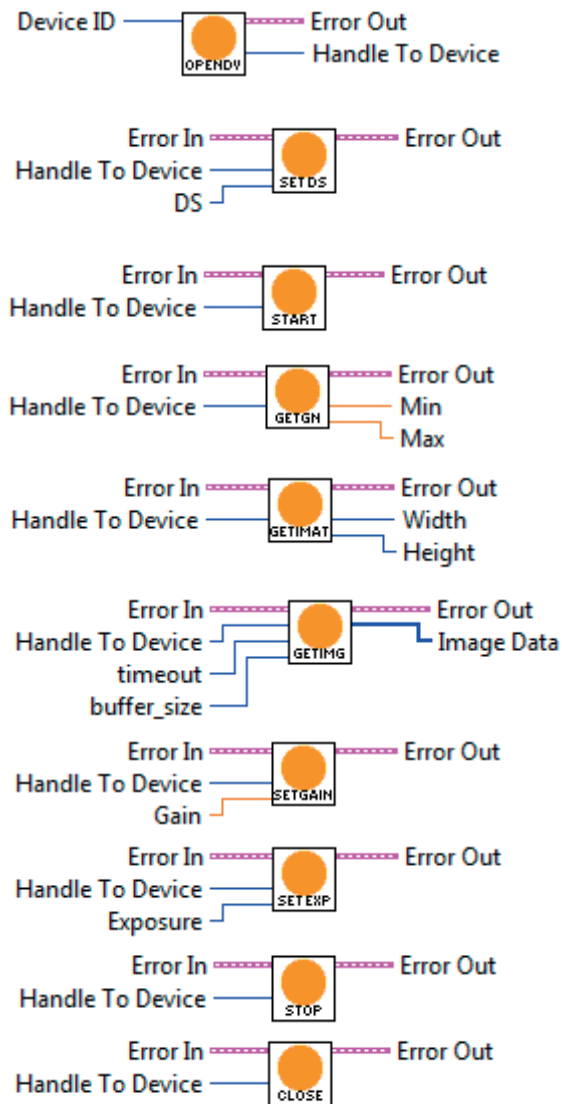
Camera functions

OpenDevice function initializes the camera and return the device handle.

SetDownsampling function allows to decrease the resolution of the acquired image by averaging squares of multiple pixels given by the downsampling factor (binning) or by skipping pixels off the multiples of the downsampling factor (skipping).

StartAcquisition function starts the data acquisition from the handle specified camera.

GetGainInfo function acquires the gain value from the camera.

GetImageAttributes function acquires the size of the image from the camera after downsampling if enabled.

GetImage function acquires image and transforms it into an array.

SetGain function sets gain of the camera.

SetExposure function sets exposure of the camera.

StopAcquisition function stops the data acquisition of the camera.

CloseDevice function uninitializes the camera and closes the device handle.

Other functions

Wait function allows to set a specific time in milliseconds for the structure to execute and proceed with the next task.
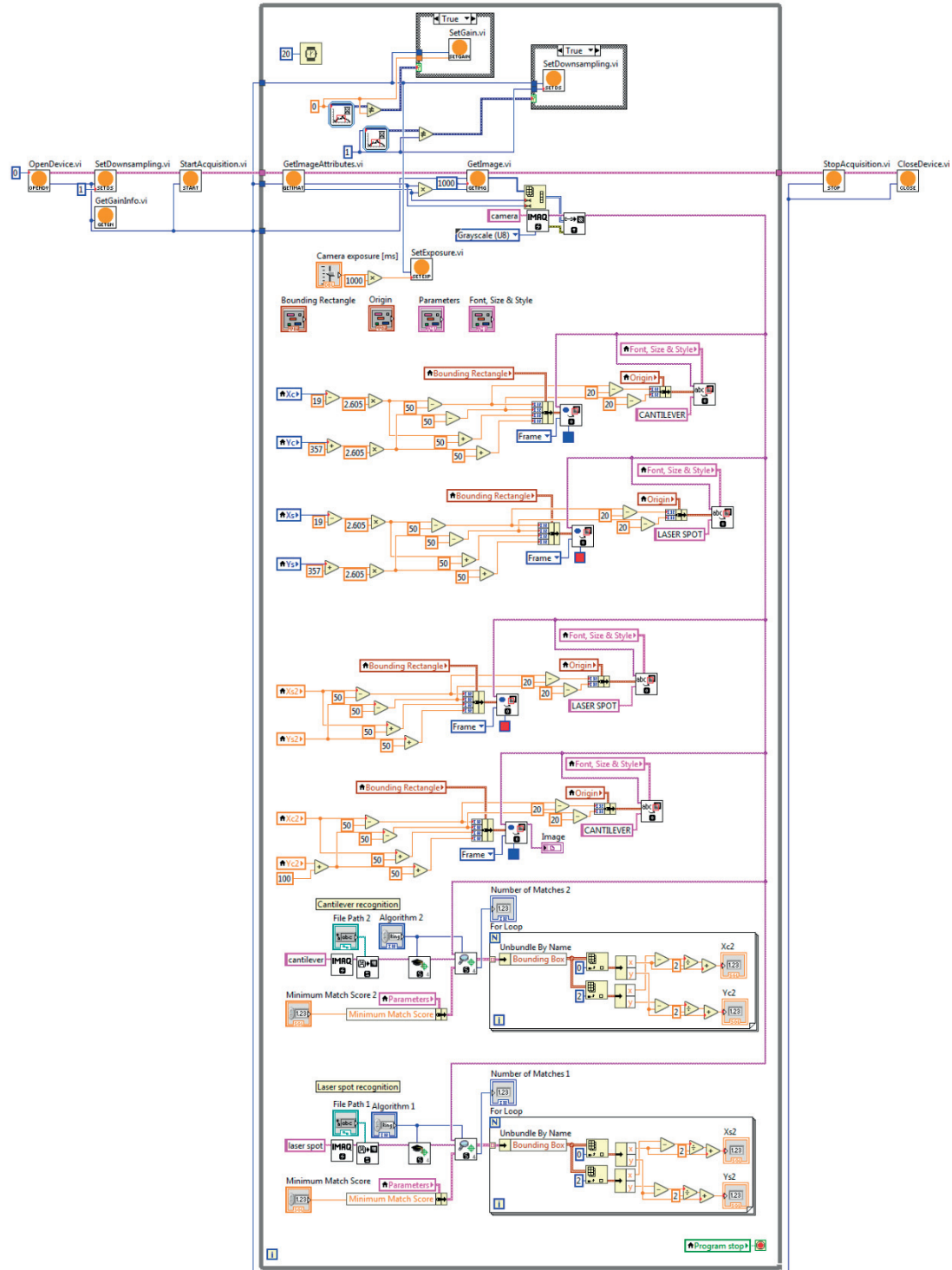
Code

Top While Loop

This part of the program is contained within one **While Loop** that enables the acquisition of analog signals through input channels of the acquisition device connected with the help of **DAQ Assistant**, there are 5 channels acquired: bottom – top, left – right, sum, (bottom – top)/sum, bottom – top filtered with a hardware low-pass filter and the laser diode voltage. The upper part of the structures sets the paths and the names for the files that are being saved with the help of 11 **Write To Measurement File** express VIs, 4 of those are filtered with **Filter** express VIs that are configured as low-pass filters. The **Timer** express VI controls the time related tasks, such as timing the experiment. There are two **Spectral Measurements** express VIs, one is used for calculating and plotting online spectrum of the bottom – top signal. At the bottom right of the structure there is a part of the program calculating the variance of the bottom – top signal. All the photodiode signals are plotted in raw and filtered. Power spectrum is also plotted.
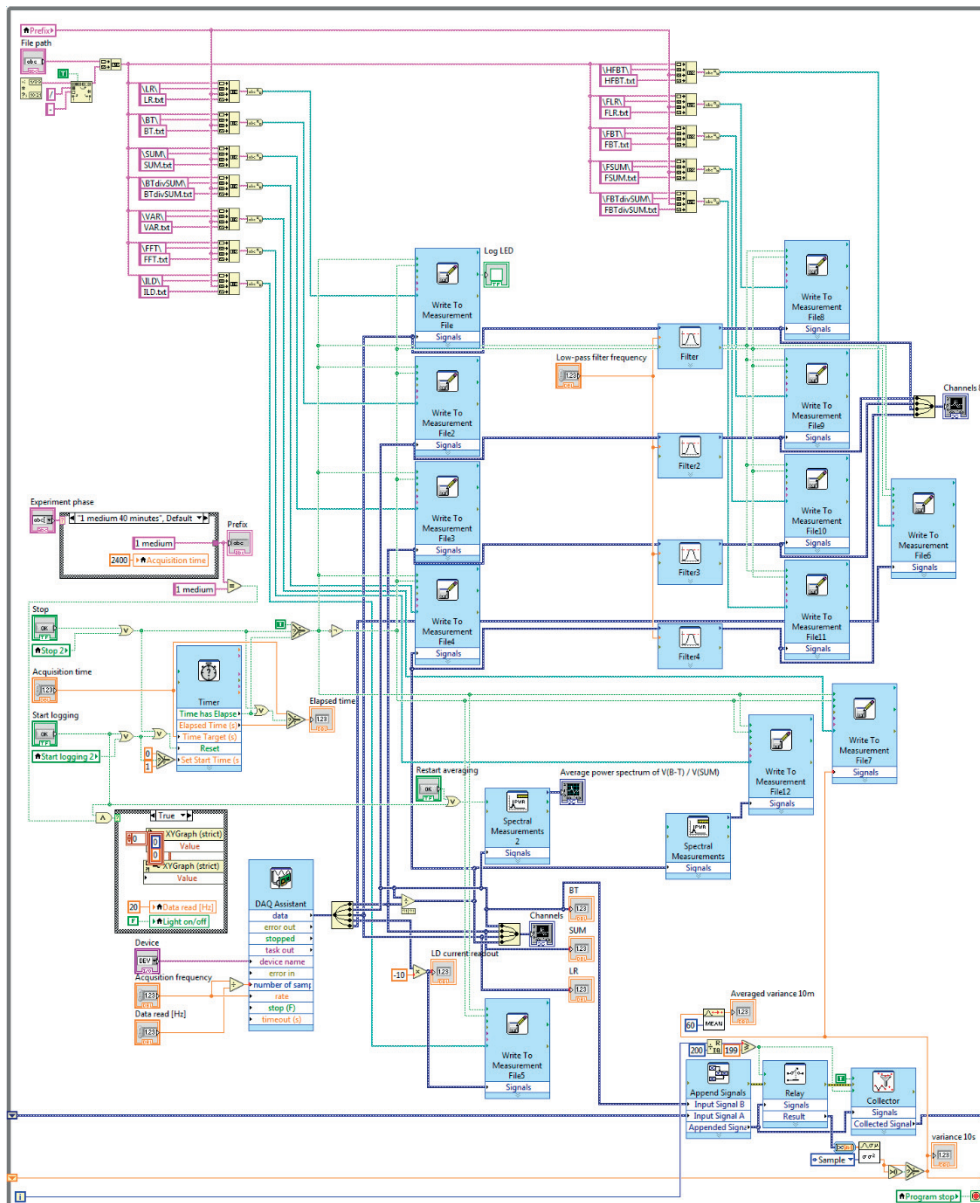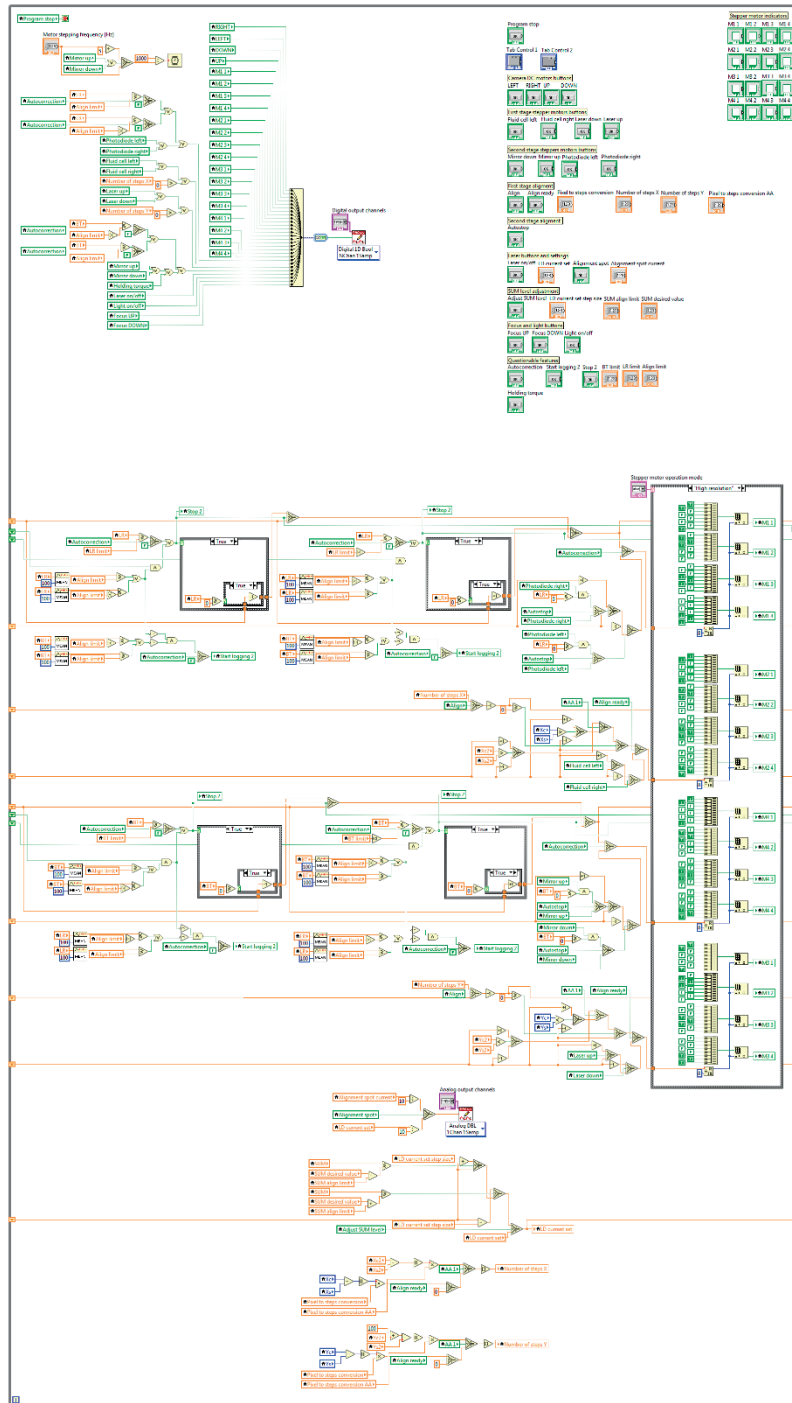
This part of the program enables the control of the stepper motors of the device. It consists of loop iteration frequency and digital output channels control at the top left. At the top right variable controls are created and invoked in this structure and the whole program. Below there is stepper motor control logic tree on the left and the **Case Structure** that holds controls for stepper motor operation mode. On the bottom of the **While Structure** there are laser intensity analog output channel control, **Adjust SUM level** control tree and at the very bottom two parts calculating the number of steps required for the first stage of the **Automatic Alignment**.

This part of the program enables acquisition and processing of the image from the camera. On the left outside of the While Loop the camera is initialized and the data from the camera is acquired, on the right outside the data acquisition is halted and the camera is uninitialized. Inside the While Loop the camera data is being process to obtained image. Variables are created below and invoked inside this structure. There are 4 parts responsible for drawing circles and adding text overlays on the image preview in the middle. The bottom 2 parts are used to learn template images and recognize the templates on the image from the camera.
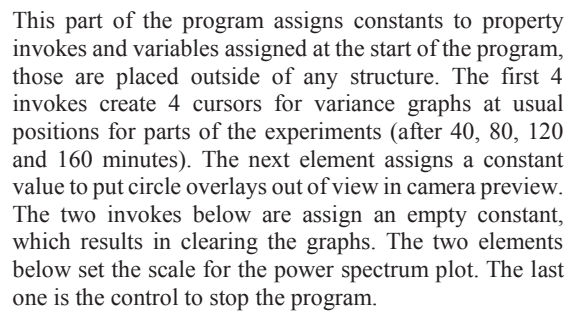

132
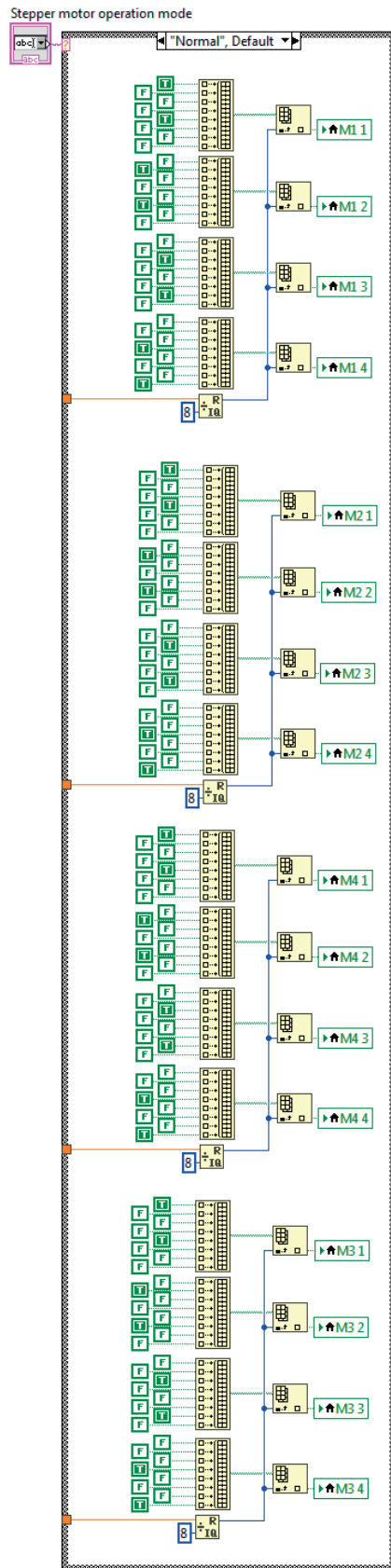
This part of the code is responsible for the operation of the normal stepper motor mode. The code is placed in a **Case Structure** that permits to choose different operation modes. In the Case Structure there are 4 parts, each responsible for one stepper motor (M1, M2, M3 and M4). From the left side of each part there are Boolean constants which are connected with the **Build Array** function and the created array is connected to **Index Array** function. The index is taken as a reminder of step count (floating point number terminal) divided by 8 (array contains 8 elements). Choosing the direction of the stepper motor rotation will result in increase or decrease in step count and the result of the **Remainder** function will point to specific Boolean value from the arrays for all 4 stepper motor control/indicators (MX 1, MX 2, MX 3 or MX 4, where X is the motor number). This results in sending signals to H-bridges that control the motors in sequence that can rotate the stepper motor in one direction and counter-rotate in counter-sequence. This operation mode uses one TRUE Boolean value per step per motor which results in normal, low-torque, 4 substeps per step operation.
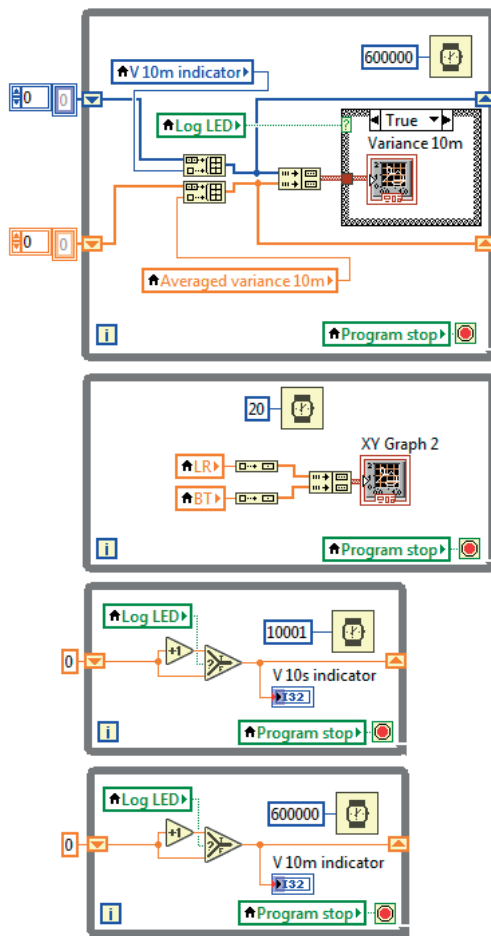
Stepper motor operation mode
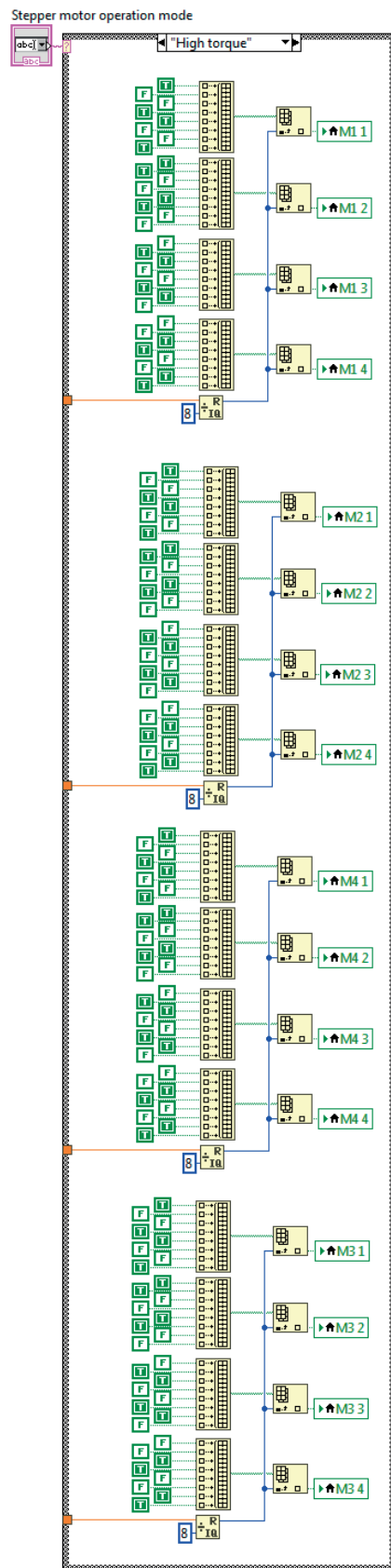
This operation mode uses two TRUE Boolean value per step per motor which results in high-torque, 4 substeps per step operation.
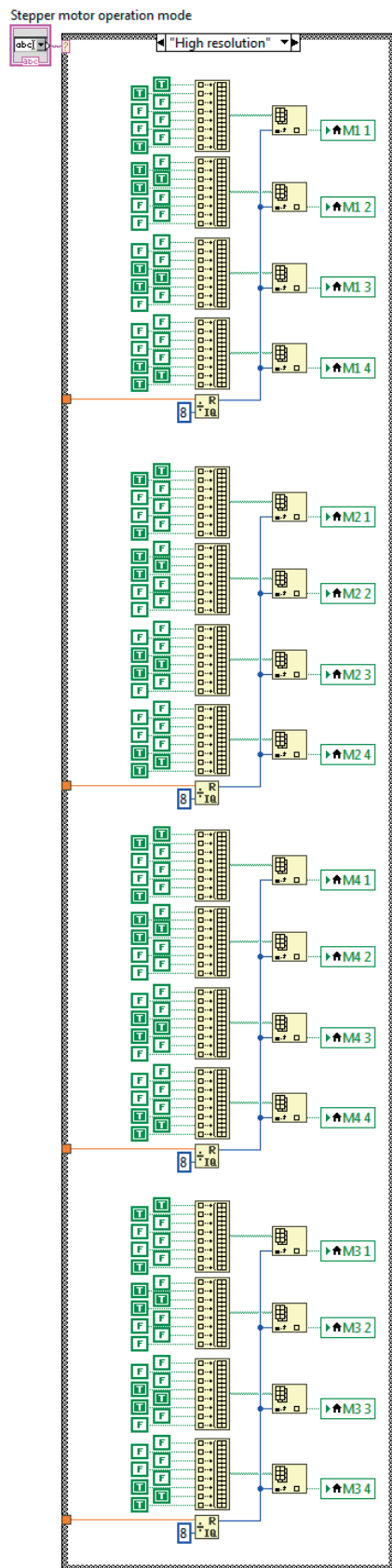
This operation mode uses one and two TRUE Boolean values alternately per step per motor which results in high-resolution, 8 substeps per step operation. Because of this mode of operation the arrays contain 8 elements.

135

V delete

0 → Cursor.Index
2400 → Cursor.PosY

V delete

1 → Cursor.Index
4800 → Cursor.PosX

V delete

2 → Cursor.Index
7200 → Cursor.PosX

V delete

3 → Cursor.Index
9600 → Cursor.PosX

-200 → Xc2
→ Xs2
→ Yc2
→ Ys2

Variance 10m

0 0
   0 → Value

V delete

→ Value

Average power spectrum of V(B-T) / V(SUM)

5E-7 → YScale.Maximum

Average power spectrum of V(B-T) / V(SUM)

5E-9 → YScale.Minimum

Program stop ▶ ⋯⋯ STOP

This part of the program assigns constants to property invokes and variables assigned at the start of the program, those are placed outside of any structure. The first 4 invokes create 4 cursors for variance graphs at usual positions for parts of the experiments (after 40, 80, 120 and 160 minutes). The next element assigns a constant value to put circle overlays out of view in camera preview. The two invokes below are assign an empty constant, which results in clearing the graphs. The two elements below set the scale for the power spectrum plot. The last one is the control to stop the program.

136

The top structure is responsible for plotting the variance graph in 10 minute averaging window. The next one contain graph that is showing the values of BT and LR signals in volts (-10 to +10 V) representing the position of the laser spot on the photodiode. The next two structures are counters for the variance plotting in 10 seconds and 10 minutes averaging windows.

Point select for the cantilever and laser spot

This section of the program is used to get the coordinates of the cantilever and laser spot with the help of the operator using a cursor. There is a "Point select" **String Combo Box** that enables to choose either the cantilever or the laser spot to be selected. The coordinates are written as **Xc** and **Yc** for the cantilever and **Xs** and **Ys** for the laser spot. The first event case is timeout which is not set, thus the **Event Structure** will not expire. The second event case contains **Case Structure** with two possible cases: the "Cantilever", which is default and the "Laser spot". The **Event Structure** is always in this case, thus each click on the image preview will result in coordinates being written, only through **Case Structure** the coordinates are written in different variables. The third event case is a stop condition that is never fulfilled.
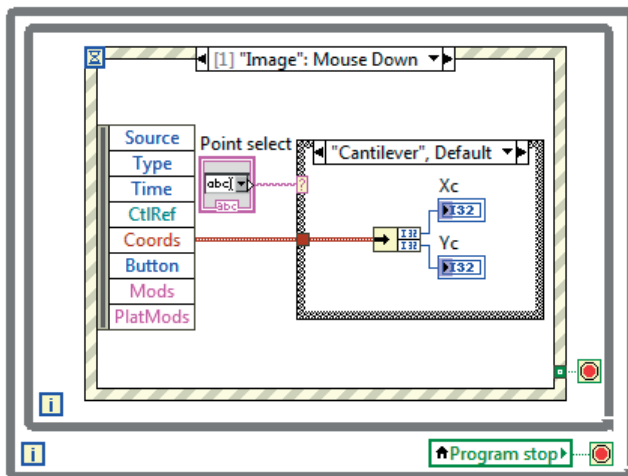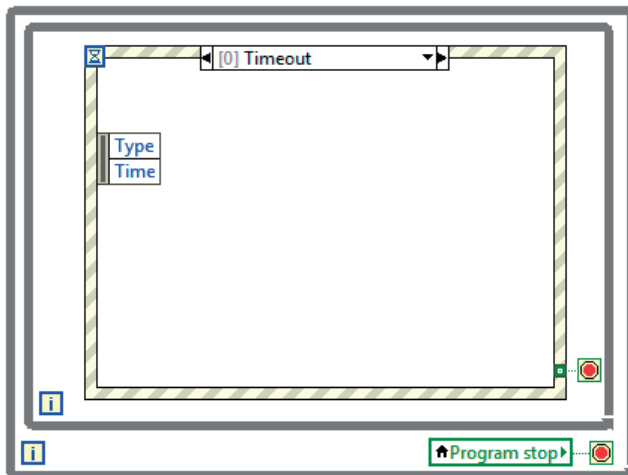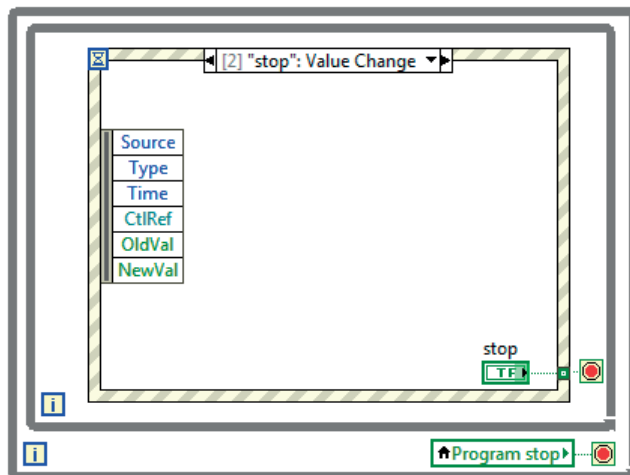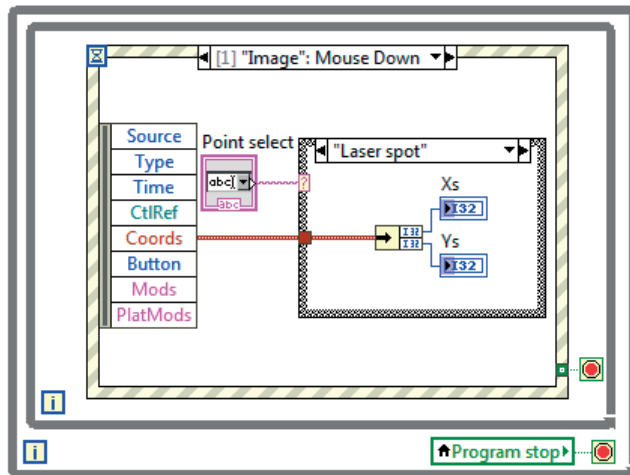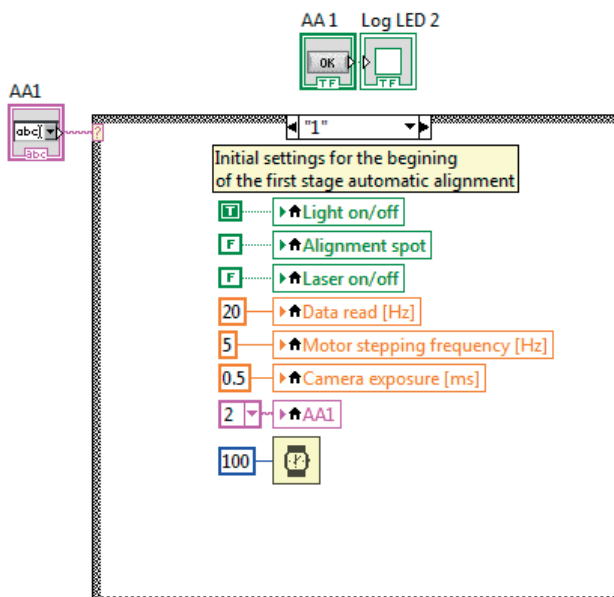
First stage of automatic alignment

This part of the program is used to control the first stage of automatic alignment – aligning the laser spot on the cantilever. This part of the program is placed in a multiple choice case structure that allows for skipping, repeating and direct linking of steps in contrast to stacked sequence structure that once began follows all steps until the end of the structure.

Case 0
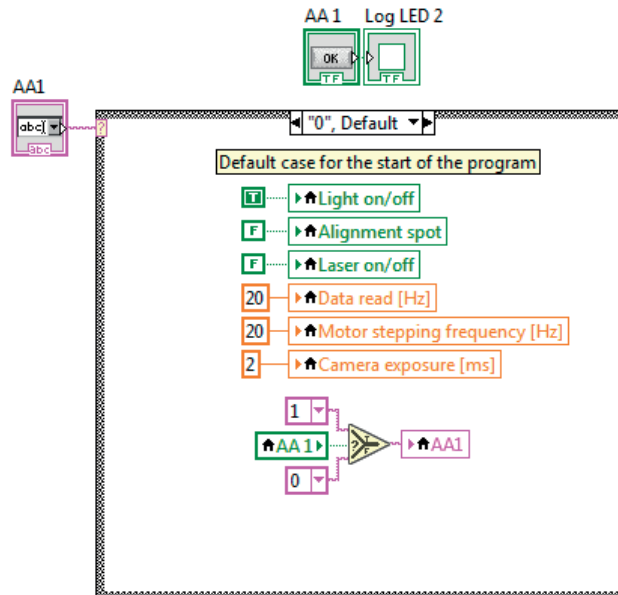
The case 0 is the default one that the program starts with. It inputs Boolean and numeric values to variables. Once the Boolean variable **AA1** is changed to TRUE the **Select** function changes the constant from 0 to 1 and sends it to string variable **AA1**, thus changing the case to the next one. Additionally the TRUE value of the Boolean variable **AA1** turns on **Log LED 2** on the front panel in graphical user interface to notify that the first stage of alignment is in progress. The LED is turned on illuminating the fluid chamber for better camera visibility. Laser and the laser alignment spot are turned off. Data read frequency (topmost **While Loop/DAQ Assistant**) is set to 20 Hz, motor stepping frequency (middle **While Loop**) is set to 20 Hz and camera exposure is set to 2 ms. Those settings are set as default for ease of use in manual mode.

Case 1

The case 1 is the first one after the initialization of automatic alignment. The LED is kept on, laser is kept off, data read frequency is kept at 20 Hz. The motor stepping frequency is changed to 5 Hz and the camera exposure is changed to 0.5 ms. **Wait** function is set to 100 ms, this time is enough for all the changes to take place. After this time elapses the string variable **AA1** is changed to 2a.
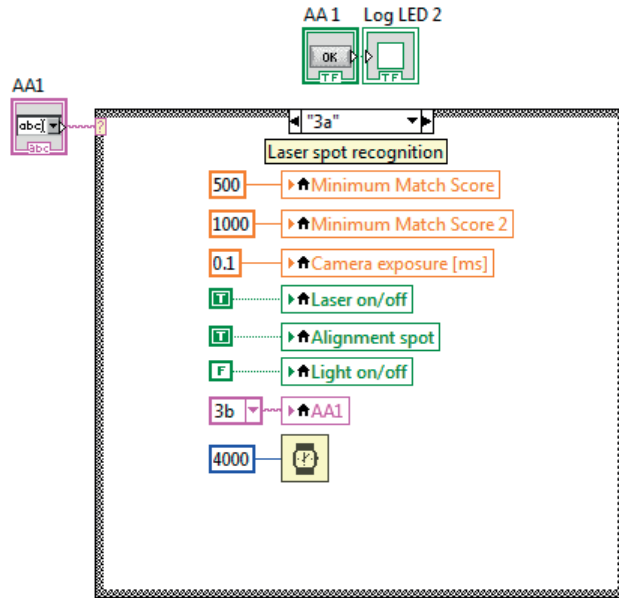
140
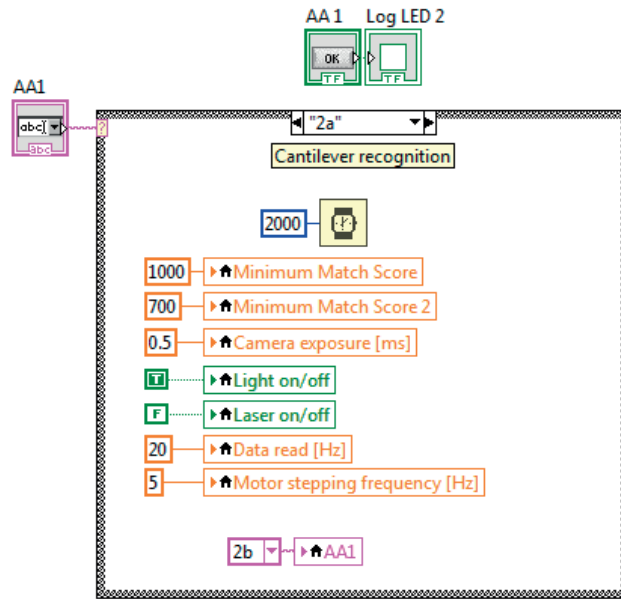
Case 2a

The case 2a changes the parameters used for detection of the cantilever. Values of **Minimum Match Score** (laser spot) and **Minimum Match Score 2** (cantilever) are changed for cantilever recognition. Those values are determined experimentally. The **Wait** function is set to 2000 ms, which is enough for the process of the cantilever recognition. Other parameters are kept at the previously set values. The string variable **AA1** is changed to 2b.
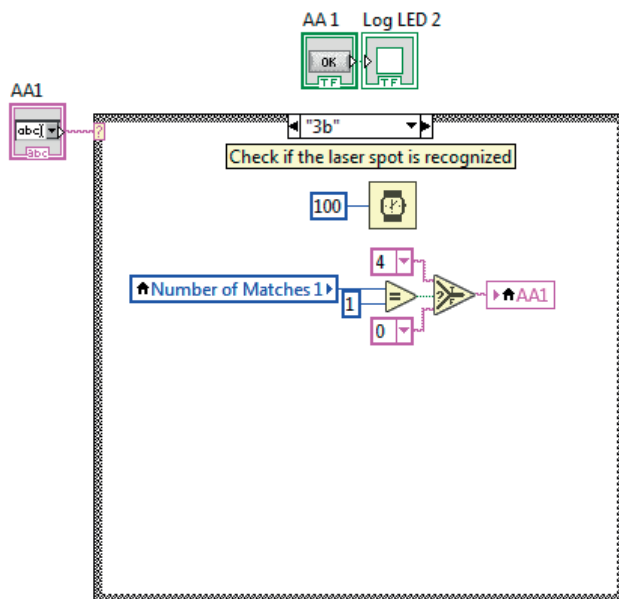
Case 2b
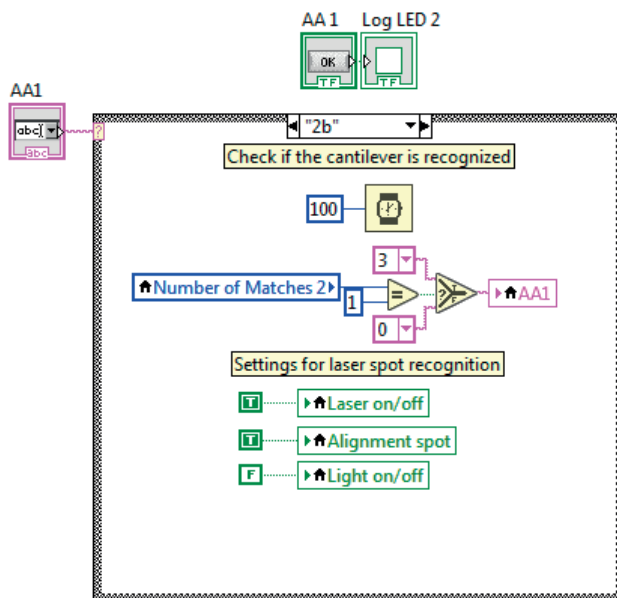
The case 2b is used to check if the cantilever was found by the recognition algorithm. To accomplish that the **Number of Matches 2** is checked, if it is equal to 1 the **Case Structure** is shifted to case 3a. Additionally the laser and the alignment spot are turned on. If the number of matches found is different than one the **Case Structure** is moved to case 0 and the process starts from the beginning.

Case 3a

The case 3a is analogous to case 2a, this one adjusts the parameters for laser spot detection. Values of **Minimum Match Score** (laser spot) and **Minimum Match Score 2** (cantilever) are changed for laser spot recognition. Those values are determined experimentally. The camera exposure is lowered to accommodate the intensity of the laser that would otherwise saturate neighboring pixels. The **Wait** function is set to 4000 ms, which is enough for the process of the laser spot recognition. Other parameters are kept at the previously set values. The string variable **AA1** is changed to 3b.

Case 3b

The case 3b is analogous to case 2b, which is used to check if the laser spot was found by the recognition algorithm. To accomplish that the **Number of Matches 2** is checked, if it is equal to 1 the **Case Structure** is shifted to case 4. If the number of matches found is different than one the **Case Structure** is moved to case 0 and the process starts from the beginning.

Case 4
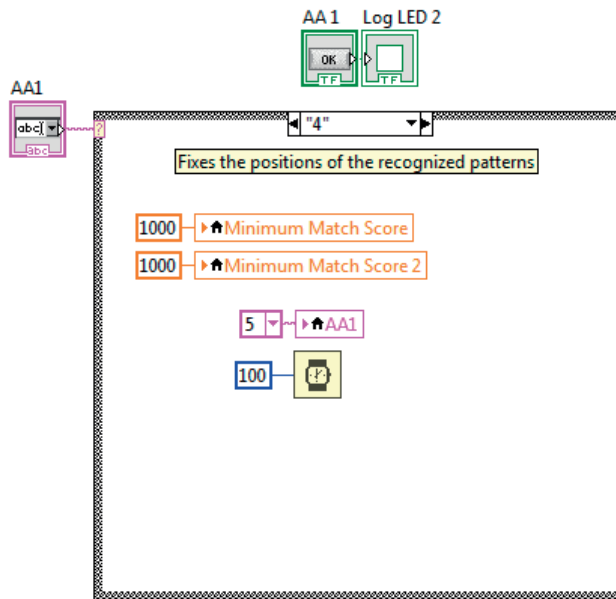
In the case 4 the values of **Minimum Match Score** (laser spot) and **Minimum Match Score 2** (cantilever) are changed to highest values. This is done to lock the recognized coordinates of the cantilever and the laser spot. The **Wait** function is set to 100 ms. The string variable **AA1** value is changed to 5.

Case 5
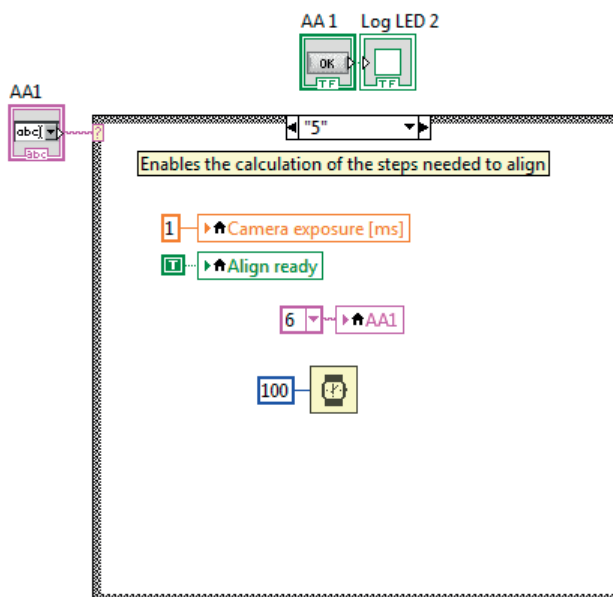
In the case 6 the calculation of the stepper motor steps needed to move the laser spot in vertical direction and cantilever in horizontal direction is accomplished. The Boolean value for the **Align ready** variable invoke is changed to TRUE. This enables the calculation in the middle **While Loop**. Additionally the camera exposure is changed to 1 ms to allow for better visibility for the human operator. The **Wait** function is set to 100 ms. The string variable **AA1** is changed to 6.

Case 6
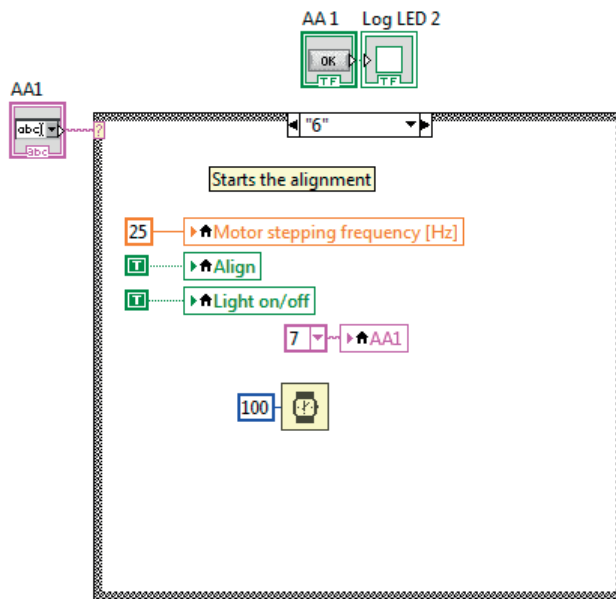
The case 6 starts the alignment of the laser spot and the cantilever. The stepper motor operation frequency is set to 25 Hz. The Boolean variable **Align** that is used to release the number of steps in both the X and Y direction into the middle **While Loop**. The LED is turned on as it is no longer interfering with the cantilever and laser spot detection and allows to follow the alignment by human operator. The **Wait** function is set to 100 ms. The string variable **AA1** is changed to 7.

Case 7
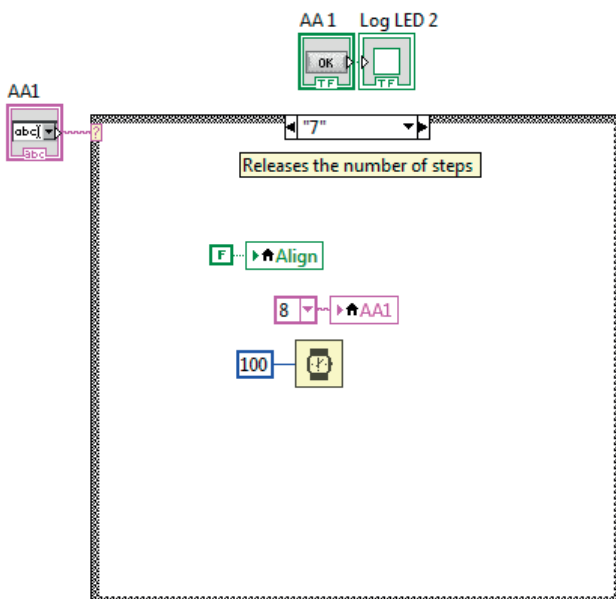
The case 7 allows to decrease the number of steps left with each iteration of that loop. The **Align** that was used to release the number of steps into the middle **While Loop** needs to change its value to FALSE to allow **Select** function to connect the data line through **Shift Register** to allow the number of steps left to decrease with each iteration of the **While Loop**.

Case 8
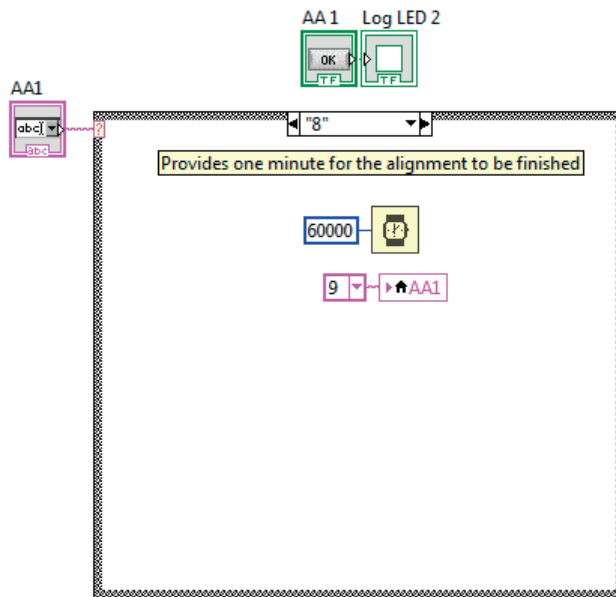
The case 8 provides the time necessary for the alignment to be finished. The **Wait** function is set to 60 000 ms. The string variable **AA1** value is changed to 9.

Case 9
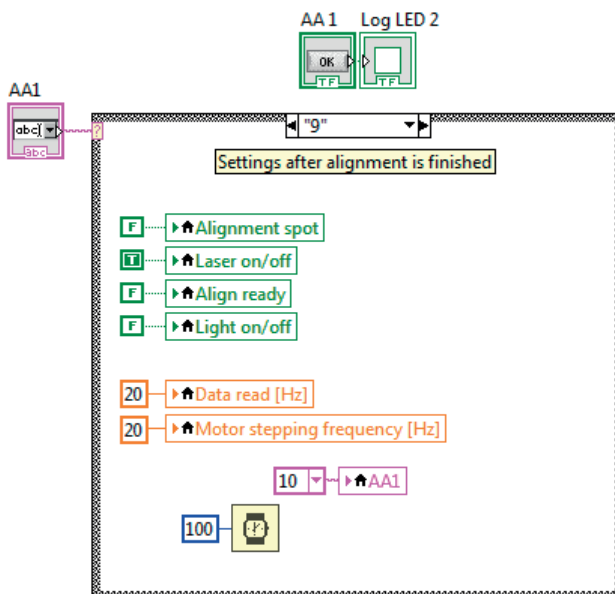
The case 9 prepares the parameters for the second stage of the alignment. The laser is kept on. The **Align Ready** is turned off. The LED illumination is turned off, because that light would interfere with the second stage of alignment and the following experiment. The data read frequency is kept at 20 Hz. Motor stepping frequency is changed back to default 20 Hz. The **Wait** function is set to 100 ms. The string variable **AA1** is changed to 10.

Case 10
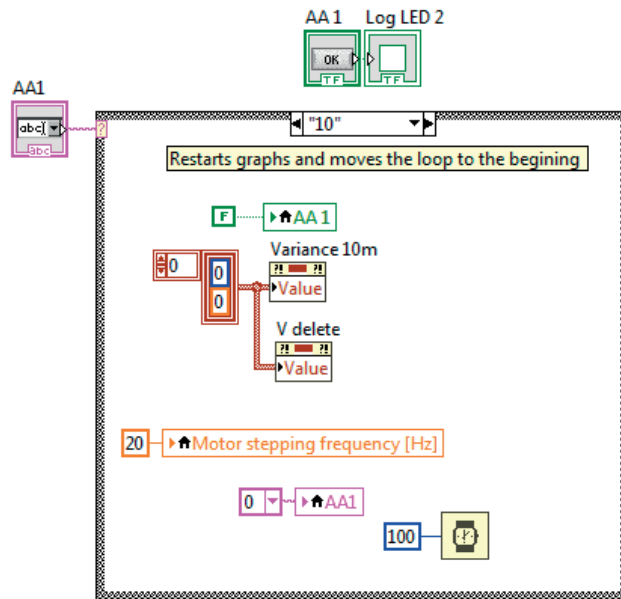
The case 10 is used to restart plotting the Variance graphs. The **Wait** function is set to 100 ms. The Boolean **AA1** is changed to FALSE. The string variable **AA1** is changed to 0. This structure returns to the default case 0 and awaits for the activation through the **AA1** Boolean variable. Additionally the FALSE value of the Boolean variable **AA1** turns off **Log LED 2** on the front panel in graphical user interface to notify that the first stage of alignment is not in progress as in the default case.

Second stage of automatic alignment

This part of the program is used to control the second stage of automatic alignment – aligning the reflected laser spot in the center of the quadrant photodiode. Similarly to the first stage of automatic alignment, this part of the program is placed in a multiple choice case structure.

Case 0
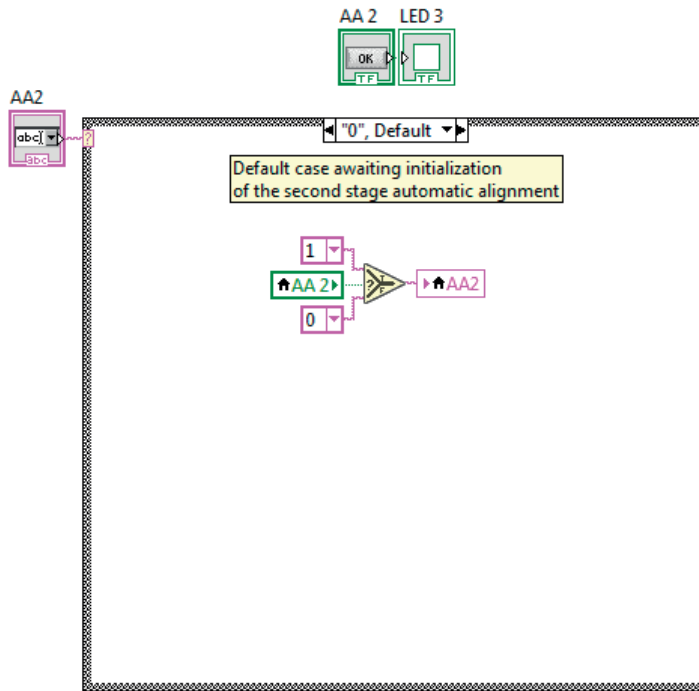
The case 0 is the default one that the program starts with. Once the Boolean variable **AA2** is changed to TRUE the **Select** function changes the constant from 0 to 1 and sends it to string variable **AA2**, thus changing the case to the next one. Additionally the TRUE value of the Boolean variable **AA2** turns on **LED 3** on the front panel in graphical user interface to notify that the second stage of alignment is in progress.

Case 1
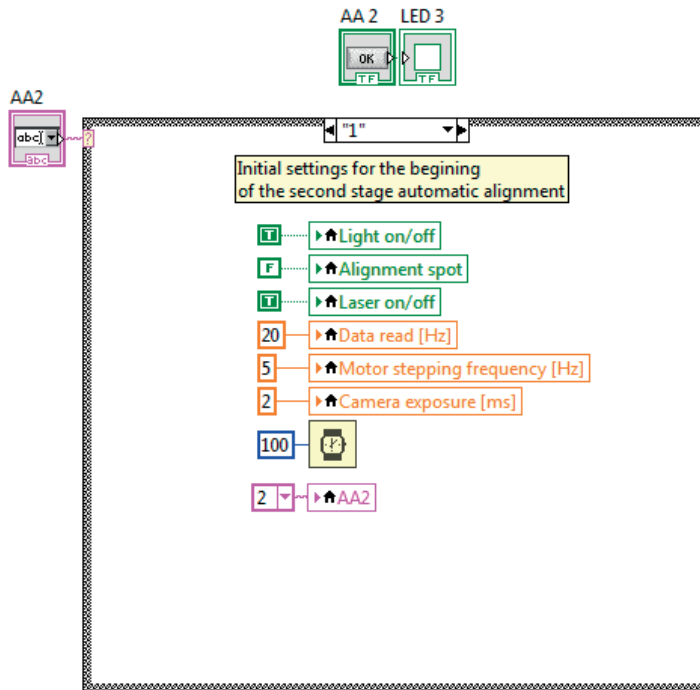
The case 1 is the first one after the initialization of the second stage of automatic alignment. The LED is kept off, laser is kept on, data read frequency is kept at 20 Hz. The motor stepping frequency is changed to 5 Hz and the camera exposure is changed to 2 ms. **Wait** function is set to 100 ms. The string variable **AA2** is changed to 2.

Case 2

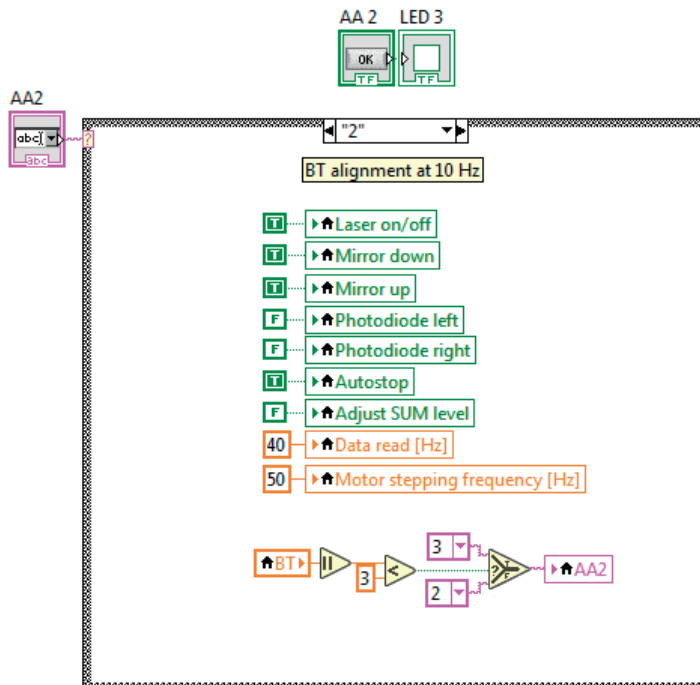The case 2 is moving the reflected laser spot in the vertical direction (Y) on the quadrant photodiode with the help of a mirror fixed on to the output shaft of the gearbox of a stepper motor. The laser is kept turned on, the **Autostop** and both the **Mirror up** and the **Mirror down** variables are assigned TRUE Boolean values. The autostop feature finds the BT signal sign and allows only one of the up or down movements to take place based on the sign. If BT is above 0 it allows it only to go down and if below 0 it allows only to go up. This feature works only if the spot of the laser is placed close to the center of the quadrant photodiode (usual experimental conditions). Other Boolean variables are set as FALSE. Data read frequency is set at 40 Hz and the motor operation frequency is set at 50 Hz for coarse alignment. The case is executed until the BT signal is within ±3 V, then the string variable **AA2** is changed to 3.

Case 3
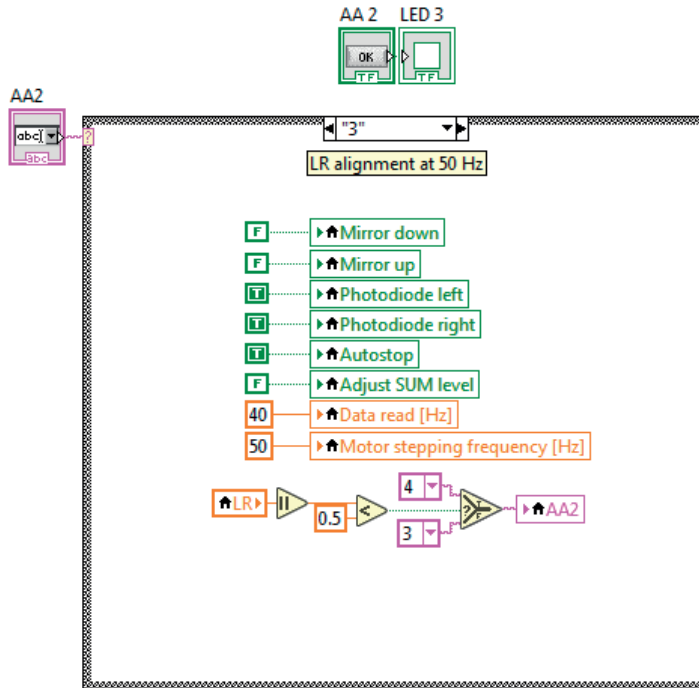
The case 3 is analogous to case 2, however it aligns the laser in horizontal (X) direction. Both the **Photodiode left** and **Photodiode right** variables are assigned TRUE Boolean values, and both the **Mirror up** and the **Mirror down** FALSE values. Other parameters have the same values. The case is executed until the LR signal is within ±0.5 V, then the string variable **AA2** is changed to 4.

Case 4
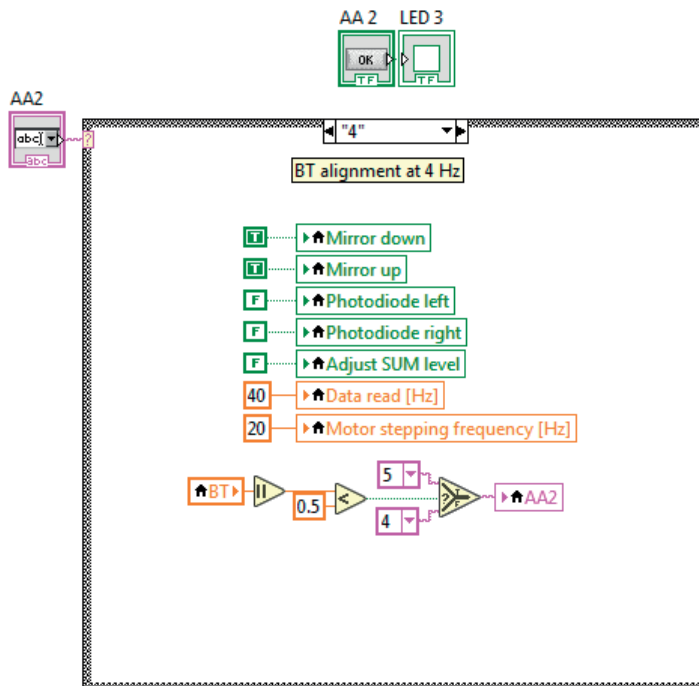
The case 4 is analogous to case 2, however with lower frequency of the motor operation and lower signal boundaries for finer adjustment. The case is executed until the BT is within ±0.5 V, then the string variable **AA2** is changed to 5.

149
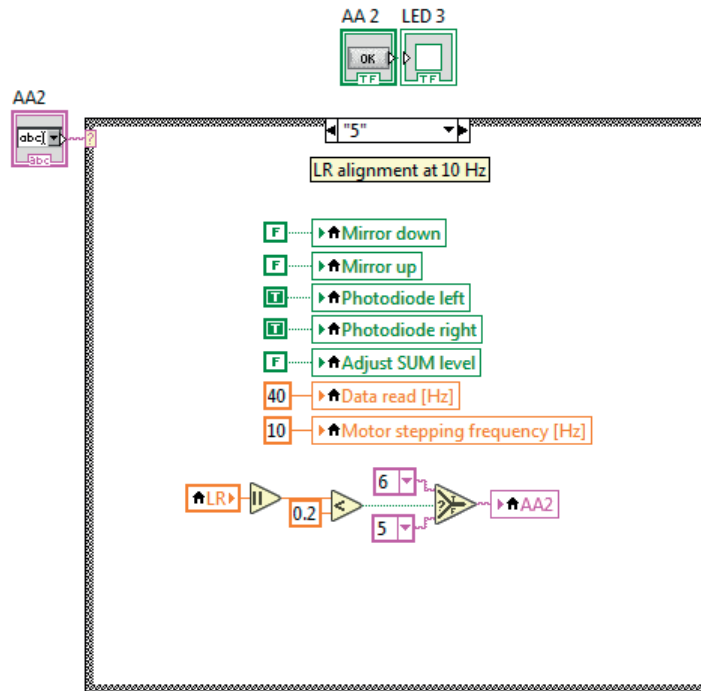
Case 5

The case 5 is analogous to case 3, however with lower frequency of the motor operation and lower signal boundaries for finer adjustment. The case is executed until the LR is within ±0.2 V, then the string variable **AA2** is changed to 5.

Case 6
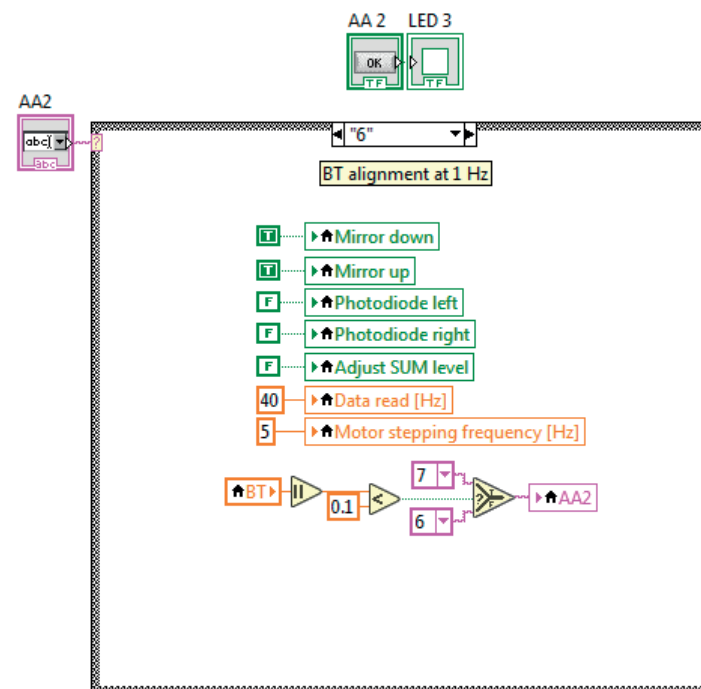
The case 6 is analogous to case 2, however with still lower frequency of the motor operation and still lower signal boundaries for even finer adjustment. The case is executed until the BT is within ±0.1 V, then the string variable **AA2** is changed to 7.

Case 7

The case 7 is analogous to case 3, however with still lower frequency of the motor operation and stiller lower signal boundaries for even finer adjustment. The case is executed until the LR is within ±0.1 V, then the string variable **AA2** is changed to 8.

Case 8

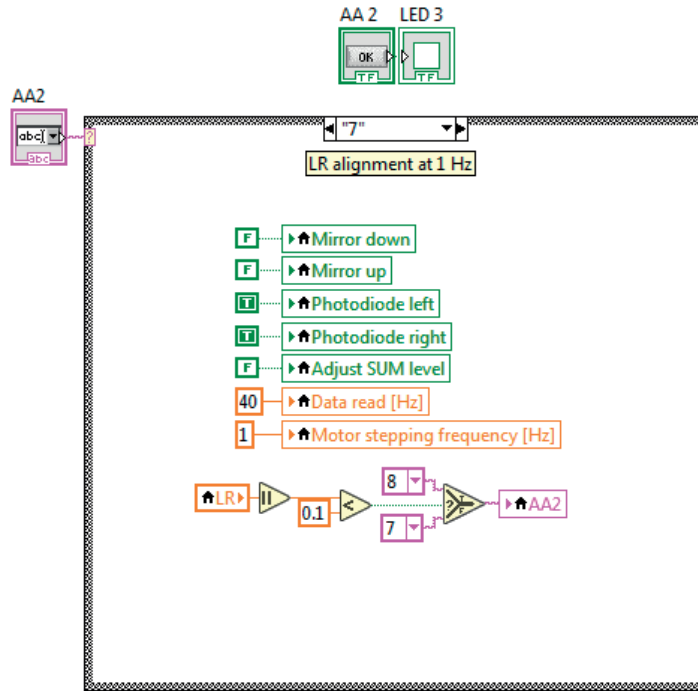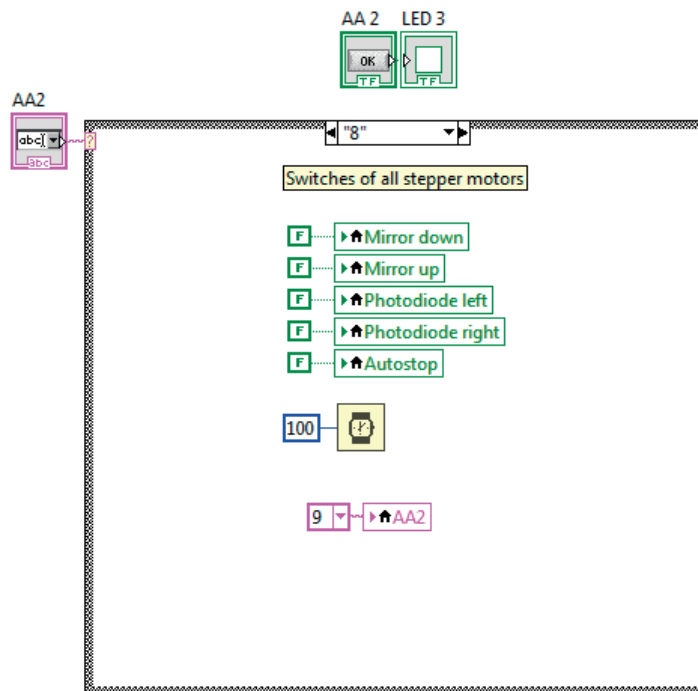The case 8 is used to turn off all the stepper motor operation. All the Boolean variables related to the motors and autostop feature are assigned FALSE Boolean values. The **Wait** function is set to 100 ms. The string variable **AA2** is changed to 9.

Case 9
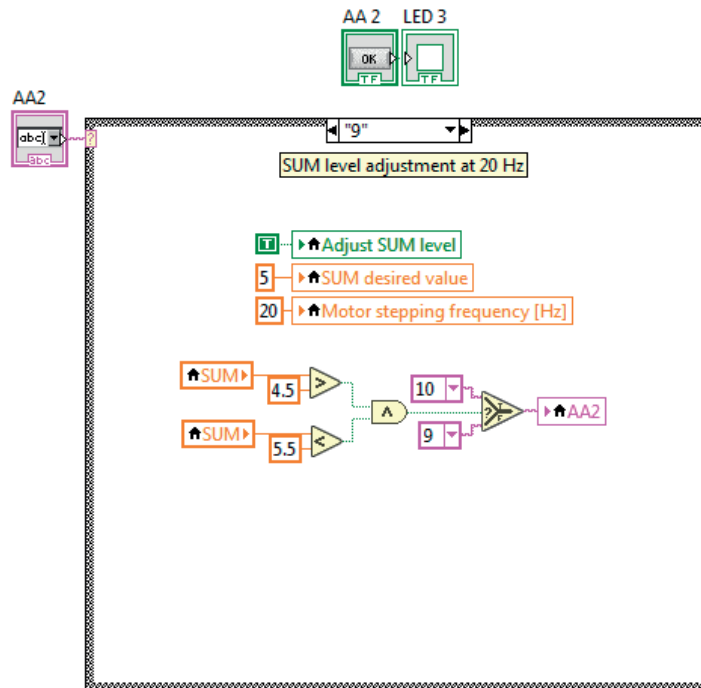
The case 9 is used to start the process of coarse adjustment of the SUM signal value through laser intensity change. The middle **While Loop** iteration frequency is set at 20 Hz. The SUM signal desired value is set to 5V. **Adjust SUM value** variable is assigned TRUE Boolean value. The laser intensity is adjusted with voltage sweep of the laser diode and simultaneous comparison of signal value and the desired value in the middle **While Loop**. The case is executed until the SUM is between 4.5 – 5.5 V, then the string variable **AA2** is changed to 10.

Case 10
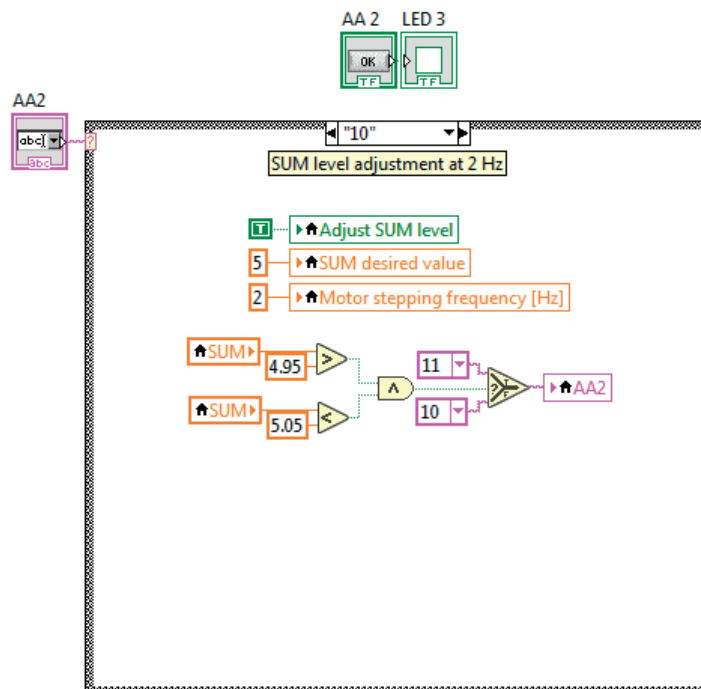
The case 10 is analogous to case 9, however the adjustment is finer. Both the loop iteration frequency and the boundaries are changed. The case is executed until the SUM is between 4.95 – 5.05 V, then the string variable **AA2** is changed to 11.

152
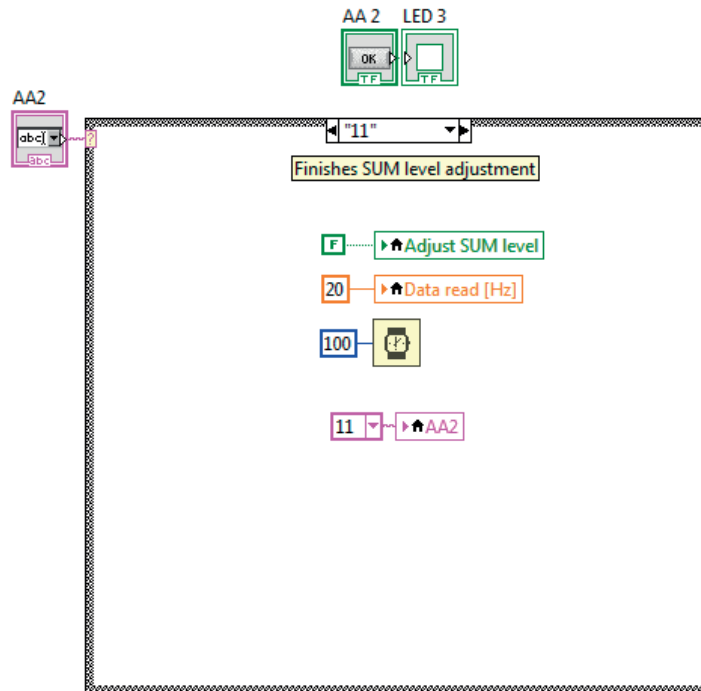
Case 11

The case 11 ends the automatic laser intensity adjustment. The **Adjust SUM value** is assigned FALSE Boolean value. **Data read** is changed to default value of 20 Hz. The **Wait** function is set to 100 ms. The string variable **AA2** is changed to 12.

Case 12
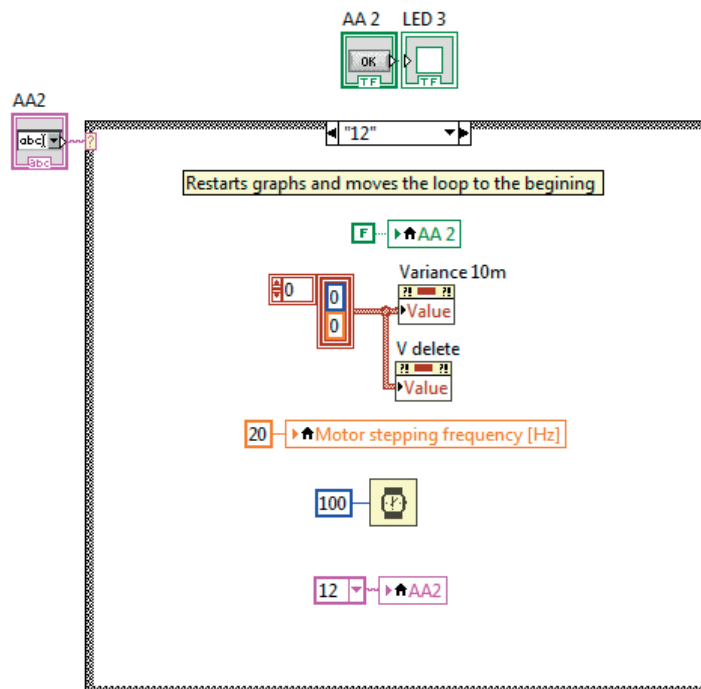
The case 12 finishes the second stage of alignment. The variance graphs are restarted. The **Wait** function is set to 100 ms. The Boolean **AA2** is changed to FALSE. The string variable **AA2** is changed to 0. This structure returns to the default case 0 and awaits for the activation through the **AA2** Boolean variable. Additionally the FALSE value of the Boolean variable **AA2** turns off **LED 3** on the front panel in graphical user interface to notify that the second stage of alignment is not in progress as in the default case.

References

1. Prestinaci F, Pezzotti P, Panto sti A. *Antimicrobial resistance: a global multifaceted phenomenon*. Pathogens and Global Health. 2015 Oct; 109(7):309–18.

2. Laxminarayan R, Duse A, Wattal C, Zaidi AKM, Wertheim HFL, Sumpradit N, et al. *Antibiotic resistance—the need for global solutions*. The Lancet Infectious Diseases. 2013 Dec 1; 13(12):1057–98.

3. World Health Organization. *Antimicrobial resistance: global report on surveillance.* Geneva, Switzerland: World Health Organization; 2014. 232 p.

4. The PLOS Medicine Editors, *Antimicrobial Resistance: Is the World UNprepared?* PLoS Medicine 13(9): e1002130.

5. Shallcross LJ, Howard SJ, Fowler T, Davies SC. *Tackling the threat of antimicrobial resistance: from policy to sustainable action.* Philosophical Transactions of the Royal Society B: Biological Sciences, 2015 Jun 5; 370(1670): 20140082.

6. European Centre for Disease Prevention and Control. *Annual epidemiological report on communicable diseases in Europe 2008: report on the state of communicable diseases in the EU and EEA/EFTA countries*. Stockholm, European Centre for Disease Prevention and Control, 2008.

7. Savey A, Lepape A, Palomar M, Agodi A, Hiesmayr M, Magiorakos AP, Kinross P, Kärki T, Plachouras D, Suetens C. S*urveillance of healthcare-associated infections and prevention indicators in European intensive care units.* European Centre for Disease Prevention and Control; 2015.

8. Pumart P, Phodha T, Thamlikitkul V, Riewpaiboon A, Prakongsai P, Limwattananon S. *Health and economic impacts of antimicrobial resistance in Thailand.* Vol. 6. 2012. 352 p. (abstract only)

9. Frieden T et al., *Antibiotic Resistance Threats in the United States, 2013.* Centers for Disease Control and Prevention Office of Infectious Diseases, 2013.

10. Jim O'Neill et al., *Antimicrobial Resistance: Tackling a crisis for the health and wealth of nations.* 2014 Dec.

11. de Kraker MEA, Stewardson AJ, Harbarth S. *Will 10 Million People Die a Year due to Antimicrobial Resistance by 2050?* PLoS Medicine 2016 Nov; 13(11): e1002184.

12. Adeyi OO, Baris E, Jonas OB, Irwin A, Berthe FCJ, Le Gall FG, et al. *Drug-resistant infections: a threat to our economic future (Vol. 2): final report (English)*. The World Bank 2017 Apr, p. 1–172. Report No.: 114679.

13. Adeyi OO, Baris E, Jonas OB, Irwin A, Berthe FCJ, Le Gall FG, et al. *Drug-resistant infections: a threat to our economic future: executive summary (English)*. The World Bank; 2017 Apr, p. 1–20. Report No.: 114679.

14. Koch A, Cox H, Mizrahi V. *Drug-resistant tuberculosis: challenges and opportunities for diagnosis and treatment.* Current Opinion in Pharmacology. 2018 Oct 1;42:7–15.

15. Opota O, Croxatto A, Prod'hom G, Greub G. *Blood culture-based diagnosis of bacteraemia: state of the art.* Clinical Microbiology and Infection, 2015 Apr; 21(4):313–22.

16. Opota O, Jaton K, Greub G. *Microbial diagnosis of bloodstream infection: towards molecular diagnosis directly from blood*. Clinical Microbiology and Infection, 2015 Apr; 21(4):323–31.

17. Fleischmann C, Thomas–Rueddel DO, Hartmann M, Hartog CS, Welte T, Heublein S, et al. *Hospital Incidence and Mortality Rates of Sepsis: An Analysis of Hospital Episode (DRG) Statistics in Germany From 2007 to 2013.* Deutsches Ärzteblatt International. 2016 Mar; 113(10):159–66.

18. Chatzigeorgiou K-S, Sergentanis T, Tsiodras S, Hamodrakas S, Bagos P. *Phoenix 100 versus Vitek 2 in the Identification of Gram-Positive and Gram-Negative Bacteria: a Comprehensive Meta-Analysis.* Journal of clinical microbiology. 2011 Jul; 49:3284–91.

19. Gherardi G, Angeletti S, Panitti M, Pompilio A, Di Bonaventura G, Crea F, et al. *Comparative evaluation of the Vitek-2 Compact and Phoenix systems for rapid identification and antibiotic susceptibility testing directly from blood cultures of Gram-negative and Gram-positive isolates.* Diagnostic Microbiology and Infectious Disease. 2012 Jan; 72(1):20–31.

20. Mittman S, Huard R, Della-Latta P, Whittier S. *Comparison of BD Phoenix to Vitek 2, MicroScan MICroSTREP, and Etest for Antimicrobial Susceptibility Testing of Streptococcus pneumoniae.* Journal of clinical microbiology. 2009 Sep; 47:3557–61.

21. Martínez-Martín D, Fläschner G, Gaub B, Martin S, Newton R, Beerli C, et al. *Inertial picobalance reveals fast mass fluctuations in mammalian cells.* Nature. 2017 25; 550(7677):500–5.

22. van Belkum A, Dunne WM. *Next-Generation Antimicrobial Susceptibility Testing.* Journal of Clinical Microbiology. 2013 Jul; 51(7):2018–24.

23. Longo G, Alonso-Sarduy L, Rio L, Bizzini A, Trampuz A, Notz J, et al. *Rapid detection of bacterial resistance to antibiotics using AFM cantilevers as nanomechanical sensors.* Nature nanotechnology. 2013 Jun; 8.

24. Binnig G, Rohrer H, Gerber C, Weibel E. *Surface Studies by Scanning Tunneling Microscopy.* Physical Review Letters. 1982; 49:57-61.

25. Binnig G, Rohrer H, Gerber C, Weibel E. *7 × 7 Reconstruction on Si(111) Resolved in Real Space.* Physical Review Letters. 1983 Jan; 50(2):120–3.

26. Binnig G, Quate CF, Gerber C. *Atomic Force Microscope.* Physical Review Letters. 1986 Mar; 56(9):930–3.

27. Dufrêne YF. *Atomic Force Microscopy, a Powerful Tool in Microbiology.* Journal of Bacteriology. 2002 Oct; 184(19):5205–13.

28. Dufrêne YF, Ando T, Garcia R, Alsteens D, Martinez-Martin D, Engel A, et al. *Imaging modes of atomic force microscopy for application in molecular and cell biology.* Nature Nanotechnology. 2017 06; 12(4):295–307.

29. Möller C, Allen M, Elings V, Engel A, Müller DJ. *Tapping-mode atomic force microscopy produces faithful high-resolution images of protein surfaces.* Biophysics Journal. 1999 Aug; 77(2):1150–8.

30. Zhong Q, Inniss D, Kjoller K, Elings VB. *Fractured polymer/silica fiber surface studied by tapping mode atomic force microscopy.* Surface Science. 1993 Jun; 290(1):L688–92.

31. Meyer E., Heinzelmann H., Grütter P., Jung Th., Weisskopf Th., Hidber H.-R., et al. *Comparative study of lithium fluoride and graphite by atomic force microscopy (AFM).* Journal of Microscopy. 1988 Oct; 152(1):269–80.

32. Albrecht TR, Grütter P, Horne D, Rugar D. *Frequency modulation detection using high-Q cantilevers for enhanced force microscope sensitivity.* Journal of Applied Physics. 1991 Jan; 69(2):668–73.

33. Bauer AW, Perry DM, Kirby WMM. *Single-Disk Antibiotic-Sensitivity Testing of Staphylococci: An Analysis of Technique and Results.* A.M.A. Archives of Internal Medicine. 1959 Aug; 104(2):208–16.

34. Bauer AW, Kirby WM, Sherris JC, Turck M. *Antibiotic susceptibility testing by a standardized single disk method.* Technical bulletin of the Registry of Medical Technologists. 1966 Mar; 36(3):49–52.

35. Bauer AW, Kirby WM, Sherris JC, Turck M. *Antibiotic susceptibility testing by a standardized single disk method.* American Journal of Clinical Pathology. 1966 Apr; 45(4):493–6.

36. Joyce LF, Downes J, Stockman K, Andrew JH. *Comparison of five methods, including the PDM Epsilometer test (E test), for antimicrobial susceptibility*

testing of Pseudomonas aeruginosa. Journal of Clinical Microbiology. 1992 Oct; 30(10):2709–13.

37. Davies D. *Cell separations by flow cytometry.* Methods in Molecular Biology. 2012; 878:185–99.

38. Givan AL. *Flow cytometry: an introduction.* Methods in Molecular Biology. 2011; 699:1–29.

39. Adan A, Alizada G, Kiraz Y, Baran Y, Nalbant A. *Flow cytometry: basic principles and applications.* Critical Reviews in Biotechnology. 2017 Mar; 37(2):163–76.

40. Costa-de-Oliveira S, Teixeira-Santos R, Silva AP, Pinho E, Mergulhão P, Silva-Dias A, et al. *Potential Impact of Flow Cytometry Antimicrobial Susceptibility Testing on the Clinical Management of Gram-Negative Bacteremia Using the FASTinov(®) Kit.* Frontiers in Microbiology. 2017; 8:2455.

41. Silva AP, Faria-Ramos I, Ricardo E, Miranda IM, Espinar MJ, Costa-de-Oliveira S, et al. *Rapid Flow Cytometry Test for Identification of Different Carbapenemases in Enterobacteriaceae.* Antimicrobial Agents and Chemotherapy. 2016 May; 60(6):3824–6.

42. von Ah U, Wirz D, Daniels AU. *Isothermal micro calorimetry--a new method for MIC determinations: results for 12 antibiotics and reference strains of E. coli and S. aureus.* BMC Microbiology. 2009 May; 9:106.

43. Lerchner J, Mueller-Hagen D, Roehr H, Wolf A, Mertens F, Mueller R, et al. *Chip-calorimetric evaluation of the efficacy of antibiotics and bacteriophages against bacteria on a minute-timescale.* Journal of Thermal Analysis and Calorimetry. 2011 Apr; 104(1):31–6.

44. Russel M, Yao J, Chen H, Wang F, Zhou Y, Choi MM, et al. *Different technique of microcalorimetry and their applications to environmental sciences: A review.* Journal of American Science. 2009; 5:194–208.

45. Guosheng L, Yi L, Xiangdong C, Peng L, Ping S, Songsheng Q. *Study on interaction between T4 phage and Escherichia coli B by microcalorimetric method.* Journal of Virological Methods. 2003 Sep 1;112(1):137–43.

46. Sato M, Toda M, Inomata N, Inoue Y, Ono T, Ishijima A. *3PS013 Quantitative analysis of heat production of brown adipocytes using bimetal cantilever (The 50th Annual Meeting of the Biophysical Society of Japan).* Seibutsu Butsuri. 2012; 52(supplement):S148.

47.   Toda M, Inomata N, Ono T, Voiculescu I. *Cantilever beam temperature sensors for biological applications.* IEEJ Transactions on Electrical and Electronic Engineering. 2017; 12(2):153–60.

48.   Voiculescu I, Liu F, Ono T, Toda M. *Investigation of bimaterial cantilever beam for heat sensing in liquid.* Sensors and Actuators A: Physical. 2016; 242:58–66.

49.   Buchholz F, Lerchner J, Mariana F, Kuhlicke U, Neu TR, Harms H, et al. *Chip-calorimetry provides real time insights into the inactivation of biofilms by predatory bacteria.* Biofouling. 2012; 28(3):351–62.

50.   Lerchner J, Schulz A, Poeschel T, Wolf A, Hartmann T, Mertens F, et al. *Chip calorimetry and biomagnetic separation: Fast detection of bacterial contamination at low cell titers.* Engineering in Life Sciences. 2012; 12(6):615–20.

51.   Jurinke C, Oeth P, van den Boom D. *MALDI-TOF mass spectrometry.* Molecular biotechnology. 2004; 26(2):147–63.

52.   Machen A, Drake T, Wang YFW. *Same day identification and full panel antimicrobial susceptibility testing of bacteria from positive blood culture bottles made possible by a combined lysis-filtration method with MALDI-TOF VITEK mass spectrometry and the VITEK2 system.* PloS one. 2014; 9(2):e87870.

53.   Burckhardt I, Zimmermann S. *Using MALDI-TOF mass spectrometry to detect Carbapenem resistance within one to two and a half hours.* Journal of clinical microbiology. 2011; JCM. 00287-11.

54.   Fairchild A, Lee MD, Maurer JJ. *PCR basics.* PCR methods in foods. Springer; 2006. p. 1–25.

55.   Radu S, Ling OW, Rusul G, Karim MIA, Nishibuchi M. *Detection of Escherichia coli O157: H7 by multiplex PCR and their characterization by plasmid profiling, antimicrobial resistance, RAPD and PFGE analyses.* Journal of Microbiological Methods. 2001; 46(2):131–9.

56.   Lissandrello C, Inci F, Francom M, Paul MR, Demirci U, Ekinci KL. *Nanomechanical motion of Escherichia coli adhered to a surface.* Applied Physics Letters. 2014 Sep; 105(11):113701.

57.   Burg TP, Godin M, Knudsen SM, Shen W, Carlson G, Foster JS, et al. *Weighing of biomolecules, single cells and single nanoparticles in fluid.* Nature. 2007 Apr; 446(7139):1066–9.

58. Aghayee S, Benadiba C, Notz J, Kasas S, Dietler G, Longo G. *Combination of fluorescence microscopy and nanomotion detection to characterize bacteria.* Journal of molecular recognition. 2013 Nov; 26:590–5.

59. Longo G, Kasas S. *Effects of antibacterial agents and drugs monitored by atomic force microscopy.* Wiley interdisciplinary reviews. Nanomedicine and nanobiotechnology. 2014 Jun; 6(3):230–44.

60. Stupar P, Chomicki W, Maillard C, Mikeladze D, Kalauzi A, Radotić K, et al. *Mitochondrial activity detected by cantilever based sensor.* Mechanical Sciences. 2017 Mar 14;8(1):23–8.

61. Stupar P, Opota O, Longo G, Prod'hom G, Dietler G, Greub G, et al. *Nanomechanical sensor applied to blood culture pellets: a fast approach to determine the antibiotic susceptibility against agents of bloodstream infections.* Clinical Microbiology and Infection. 2017 Jun; 23(6):400–5.

62. Villalba MI, Stupar P, Chomicki W, Bertacchi M, Dietler G, Arnal L, et al. *Nanomotion Detection Method for Testing Antibiotic Resistance and Susceptibility of Slow-Growing Bacteria.* Small. 2018 Jan; 14(4).

63. Kasas S, Ruggeri FS, Benadiba C, Maillard C, Stupar P, Tournu H, et al. *Detecting nanoscale vibrations as signature of life.* Proceedings of the National Academy of Sciences of the United States of America. 2014 Dec; 112.

64. Ruggeri FS, Mahul-Mellier A-L, Kasas S, Lashuel HA, Longo G, Dietler G. *Amyloid single-cell cytotoxicity assays by nanomotion detection.* Cell Death Discovery. 2017 Aug; 3:17053.

65. Blair David F. *Flagellar movement driven by proton translocation.* FEBS Letters. 2003 Apr; 545(1):86–95.

66. Purcell EM. *The efficiency of propulsion by a rotating flagellum.* Proceedings of the National Academy of Sciences of the United States of America. 1997 Oct; 94(21):11307–11.

67. Fenchel T, Thar R. *"Candidatus Ovobacter propellens": a large conspicuous prokaryote with an unusual motility behaviour.* FEMS Microbiology Ecology. 2004 May; 48(2):231–8.

68. Thwaites JJ, Mendelson NH. *Mechanical properties of peptidoglycan as determined from bacterial thread.* International journal of biological macromolecules. 1989; 11(4):201–6.

69. Mortezaei N, Epler CR, Shao PP, Shirdel M, Singh B, McVeigh A, et al. *Structure and function of enterotoxigenic Escherichia coli fimbriae from differing assembly pathways.* Molecular microbiology. 2015; 95(1):116–26.

162

70. Ohashi A, Koyama T, Syutsubo K, Harada H. *A novel method for evaluation of biofilm tensile strength resisting erosion.* Water science and technology. 1999; 39(7):261–8.

71. Aggarwal S, Hozalski RM. *Determination of biofilm mechanical properties from tensile tests performed using a micro-cantilever method.* Biofouling. 2010; 26(4):479–86.

72. Poppele EH, Hozalski RM. *Micro-cantilever method for measuring the tensile strength of biofilms and microbial flocs.* Journal of microbiological methods. 2003; 55(3):607–15.

73. Alvarez O, Gonzalez C, Latorre R. *Counting channels: a tutorial guide on ion channel fluctuation analysis.* Advances in physiology education. 2002; 26(4):327–41.

74. Ji H-F, Hansen KM, Hu Z, Thundat T. *Detection of pH variation using modified microcantilever sensors.* Sensors and Actuators B: Chemical. 2001; 72(3):233–8.

75. Lee SH, Rasaiah JC. *Proton transfer and the mobilities of the H+ and OH− ions from studies of a dissociating model for water.* The Journal of chemical physics. 2011; 135(12):124505.

76. Phillips R, Milo R. *A feeling for the numbers in biology.* Proceedings of the National Academy of Sciences of the United States of America. 2009 Dec; 106(51):21465–71.

77. Farmer IS, Jones CW. *The energetics of Escherichia coli during aerobic growth in continuous culture.* European Journal of Biochemistry. 1976 Aug; 67(1):115–22.

78. Hempfling WP, Mainzer SE. *Effects of varying the carbon source limiting growth on yield and maintenance characteristics of Escherichia coli in continuous culture.* Journal of Bacteriology. 1975 Sep; 123(3):1076–87.

79. Ramos Vega D, Mertens J, Calleja M, Tamayo de Miguel FJ. *Study of the origin of bending induced by bimetallic effect on microcantilevers.* Sensors. 2007 Sep; 7(9): 1757–1765.

80. Chiang Y-L, Lin C-H, Yen M-Y, Su Y-D, Chen S-J, Chen H-F. *Innovative antimicrobial susceptibility testing method using surface plasmon resonance.* Biosensors and Bioelectronics. 2009 Mar; 24(7):1905–10.

81. Petar Stupar. *Atomic Force Microscopy of biological systems: quantitative imaging and nanomotion detection.* PhD Thesis, EPFL, 2018.

82.   Kasas S, Longo G, Dietler G, Alonso S. *Nanoscale motion detector.* Patent application US2014287403 (A1), EP2766722 (A1), WO2013054311 (A1). 2013

83.   Anderson CH, Bergen JR, Burt PJ, Ogden JM. *Pyramid Methods in Image Processing.* RCA Engineer. 1984; 29 (6): 33--41.

84.   MacLean WJ, Tsotsos JK. *Fast pattern recognition using normalized grey-scale correlation in a pyramid image representation.* Machine Vision and Applications. 2008 May; 19(3):163–79.

85.   Alexander S, Hellemans L, Marti O, Schneir J, Elings V, Hansma PK, et al. *An atomic-resolution atomic-force microscope implemented using an optical lever.* Journal of Applied Physics. 1989 Jan; 65(1):164–7.

86.   Longo G, Rio LM, Roduit C, Trampuz A, Bizzini A, Dietler G, et al. *Force volume and stiffness tomography investigation on the dynamics of stiff material under bacterial membranes.* Journal of Molecular Recognition. 2012 May; 25(5):278–84.

87.   Longo G, Rio LM, Trampuz A, Dietler G, Bizzini A, Kasas S. *Antibiotic-induced modifications of the stiffness of bacterial membranes.* Journal of Microbiological Methods. 2013 May; 93(2):80–4.

88.   Ruggeri FS, Longo G, Faggiano S, Lipiec E, Pastore A, Dietler G. I*nfrared nanospectroscopy characterization of oligomeric and fibrillar aggregates during amyloid formation*. Nature Communication. 2015 Jul; 6:7831.

89.   Japaridze A, Muskhelishvili G, Benedetti F, Gavriilidou AFM, Zenobi R, De Los Rios P, et al. *Hyperplectonemes: A Higher Order Compact and Dynamic DNA Self-Organization.* Nano Letters. 2017 Mar; 17(3):1938–48.

90.   Roduit C, Longo G, Benmessaoud I, Volterra A, Saha B, Dietler G, et al. *Stiffness tomography exploration of living and fixed macrophages.* Journal of Molecular Recognition. 2012 May; 25(5):241–6.

91.   Kasas S, Longo G, Dietler G. *Mechanical properties of biological specimens explored by atomic force microscopy*. Journal of Physics D: Applied Physics. 2013 Feb; 46:133001.

92.   Arnal L, Longo G, Stupar P, Castez MF, Cattelan N, Salvarezza RC, et al. *Localization of adhesins on the surface of a pathogenic bacterial envelope through atomic force microscopy.* Nanoscale. 2015 Nov; 7(41):17563–72.

93.   Tamayo J, Kosaka PM, Ruz JJ, Paulo ÁS, Calleja M. *Biosensors based on nanomechanical systems.* Chemical Society Review. 2013 Jan; 42(3):1287–311.

94. Kosaka PM, Pini V, Ruz JJ, da Silva RA, González MU, Ramos D, et al. *Detection of cancer biomarkers in serum using a hybrid mechanical and optoplasmonic nanosensor.* Nature Nanotechnology. 2014 Dec; 9(12):1047–53.

95. Kosaka PM, Tamayo J, Ruz JJ, Puertas S, Polo E, Grazu V, et al. *Tackling reproducibility in microcantilever biosensors: a statistical approach for sensitive and specific end-point detection of immunoreactions.* The Analyst. 2013 Feb; 138(3):863–72.

96. Ndieyira JW, Kappeler N, Logan S, Cooper MA, Abell C, McKendry RA, et al. *Surface-stress sensors for rapid and ultrasensitive detection of active free drugs in human serum.* Nature Nanotechnology. 2014 Mar; 9(3):225–32.

97. Longo G. Cancer biomarkers: *Detected twice for good measure.* Nature Nanotechnology. 2014 Dec; 9(12):959–60.

98. Alonso-Sarduy L, Dietler G, Kasas S, Longo G, Pekkanen J. *Rapid Evaluation of Bacterial Antibiotic Resistance.* TechConnect Briefs. 2013 May; 3(2013):111–4.

99. Alonso-Sarduy L, De Los Rios P, Benedetti F, Vobornik D, Dietler G, Kasas S, et al. *Real-Time Monitoring of Protein Conformational Changes Using a Nano-Mechanical Sensor.* PLoS One. 2014; 9(7): e103674.

100. Kasas S, Stupar P, Longo G, Dietler G. *Detecting life thanks to the atomic force microscope.* Medicine Sciences. 2015 Apr; 31(4):369–71.

101. Kasas S, Radotic K, Longo G, Saha B, Alonso-Sarduy L, Dietler G, et al. *A universal fluid cell for the imaging of biological specimens in the atomic force microscope.* Microscopy Research and Technique. 2013 Apr; 76(4):357–63.

102. Wu S, Liu X, Zhou X, Liang XM, Gao D, Liu H, et al. *Quantification of cell viability and rapid screening anti-cancer drug utilizing nanomechanical fluctuation.* Biosensors and Bioelectronics. 2016 Mar; 77:164–73.

103. Nelson SL, Proctor DT, Ghasemloonia A, Lama S, Zareinia K, Ahn Y, et al. *Vibrational Profiling of Brain Tumors and Cells.* Theranostics. 2017 Jun; 7(9):2417–30.

104. Kasas S, Alonso L, Jacquet P, Adamcik J, Haeberli C, Dietler G. *Microcontroller-driven fluid-injection system for atomic force microscopy.* The Review of Scientific Instruments. 2010 Jan; 81(1):013704.

105. Kasas S, Ikai A. *A method for anchoring round shaped cells for atomic force microscope imaging.* Biophysical Journal. 1995 May; 68(5):1678–80.

106. Kalauzi A, Nikolic L, Savic D, Radotic K. *Cell death parameters as revealed by whole-cell patch-clamp and interval weighted spectra averaging: changes in membrane properties and current frequency of cultured mouse microglial cells induced by glutaraldehyde.* The Journal of Membrane Biology. 2015 Feb; 248(1):117–23.

107. Scholkmann F, Cifra M, Moraes TA, Gallep C de M. *Using multifractal analysis of ultra-weak photon emission from germinating wheat seedlings to differentiate between two grades of intoxication with potassium dichromate.* Journal of Physics: Conference Series. 2011; 329(1):012020.

108. Burnos S, Hilfiker P, Surucu O, Scholkmann F, Krayenbuhl N, Grunwald T, et al. *Human intracranial high frequency oscillations (HFOs) detected by automatic time-frequency analysis.* PLoS One. 2014; 9(4):e94381.

109. Holper L, Scholkmann F, Wolf M. *The relationship between sympathetic nervous activity and cerebral hemodynamics and oxygenation: a study using skin conductance measurement and functional near-infrared spectroscopy.* Behavioural Brain Research. 2014 Aug; 270:95–107.

110. Gao J, Hu J, Liu F, Cao Y. *Multiscale entropy analysis of biological signals: a fundamental bi-scaling law.* Frontiers in Computational Neuroscience. 2015; 9:64.

111. Clinical and Laboratory Standards Institute. *Performance Standards for Antimicrobial Susceptibility Testing: Twenty-Third Informational Supplement.* 2013.

112. EUCAST. *Antimicrobial susceptibility testing EUCAST disk diffusion method.* 2017.

113. Snyder JW, Munier GK, Johnson CL. *Direct comparison of the BD phoenix system with the MicroScan WalkAway system for identification and antimicrobial susceptibility testing of Enterobacteriaceae and nonfermentative gram-negative organisms.* Journal of Clinical Microbiology. 2008 Jul; 46(7):2327–33.

114. Theophel K, Schacht V, Schlüter M, Schnell S, Stingu C-S, Schaumann R, et al. *The Importance of Growth Kinetic Analysis in Determining Bacterial Susceptibility against Antibiotics and Silver Nanoparticles.* Frontiers in microbiology. 2014 Nov; 5:544.

115. Arnal L, Grunert T, Cattelan N, de Gouw D, Ines Villalba M, Serra D, et al. *Bordetella pertussis Isolates from Argentinean Whooping Cough Patients Display Enhanced Biofilm Formation Capacity Compared to Tohama I Reference Strain.* Frontiers in Microbiology. 2015 Dec; 6: 1352.

166

116. Serra D, Lücking G, Weiland F, Schulz S, Görg A, Yantorno O, et al. *Proteome approaches combined with Fourier transform infrared spectroscopy revealed a distinctive biofilm physiology in Bordetella pertussis.* Proteomics. 2008 Dec; 8:4995–5010.

117. Wang L, Fan D, Chen W, Terentjev E. *Bacterial growth, detachment and cell size control on polyethylene terephthalate surfaces.* Scientific Reports. 2015 Oct; 5:15159.

118. Altunaiji SM, Kukuruzovic RH, Curtis NC, Massie J. A*ntibiotics for whooping cough (pertussis).* Cochrane Database of Systematic Reviews. 2007; (3).

119. Pankey GA, Sabath LD. *Clinical relevance of bacteriostatic versus bactericidal mechanisms of action in the treatment of Gram-positive bacterial infections.* Clinical Infectious Diseases. 2004 Mar; 38(6):864–70.

120. Menozzi FD, Gantiez C, Locht C. *Identification and purification of transferrin- and lactoferrin-binding proteins of Bordetella pertussis and Bordetella bronchiseptica.* Infection and Immunity. 1991 Nov; 59(11):3982–8.

121. Nanduri B, Lawrence ML, Peddinti DS, Burgess SC. *Effects of subminimum inhibitory concentrations of antibiotics on the Pasteurella multocida proteome: a systems approach.* Comparative and Functional Genomics. 2008; 254836.

122. Yang D, Oyaizu Y, Oyaizu H, Olsen GJ, Woese CR. *Mitochondrial origins.* Proceedings of the National Academy of Sciences of the United States of America. 1985 Jul; 82(13):4443–7.

123. Schapira AHV. *Mitochondrial diseases.* Lancet. 2012 May; 379(9828):1825–34.

124. Meyer JN, Leung MCK, Rooney JP, Sendoel A, Hengartner MO, Kisby GE, et al. *Mitochondria as a target of environmental toxicants.* Toxicological Sciences. 2013 Jul; 134(1):1–17.

125. Lanza IR, Nair KS. *Functional assessment of isolated mitochondria in vitro.* Methods in Enzymology. 2009; 457:349–72.

126. Hong S, Pedersen PL. *ATP synthase and the actions of inhibitors utilized to study its roles in human health, disease, and other scientific areas.* Microbiology and molecular biology reviews. 2008 Dec; 72(4):590–641.

127. Li N, Ragheb K, Lawler G, Sturgis J, Rajwa B, Melendez JA, et al. *Mitochondrial complex I inhibitor rotenone induces apoptosis through enhancing mitochondrial reactive oxygen species production.* The Journal of Biological Chemistry. 2003 Mar; 278(10):8516–25.

128. Kristian T, Hopkins IB, McKenna MC, Fiskum G. *Isolation of mitochondria with high respiratory control from primary cultures of neurons and astrocytes using nitrogen cavitation.* Journal of Neuroscience Methods. 2006 Apr; 152(1–2):136–43.

129. Bowler MW, Montgomery MG, Leslie AGW, Walker JE. H*ow azide inhibits ATP hydrolysis by the F-ATPases.* Proceedings of the National Academy of Sciences of the United States of America. 2006 Jun; 103(23):8646–9.

130. Minkov IB, Strotmann H. *The effect of azide on regulation of the chloroplast H+-ATPase by ADP and phosphate.* Biochimica et Biophysica Acta (BBA) - Bioenergetics. 1989 Jan; 973(1):7–12.

131. Thalen M, van den IJssel J, Jiskoot W, Zomer B, Roholl P, de Gooijer C, et al. *Rational medium design for Bordetella pertussis: basic metabolism.* Journal of Biotechnology. 1999 Oct; 75(2–3):147–59.

Curriculum Vitae

Wojciech Chomicki

Personal info

Adress: Montelly 15, Lausanne, Switzerland
Phone: (0048) 537 229 326
E-mail: wojciech.chomicki@epfl.ch

Education

2014 – 2018	École Polytechnique Fédérale de Lausanne, Department of Basic Sciences, Institute of Physics, Laboratory of Living Matter, field of study: Physics, PhD
2013 – 2014	Poznan University of Technology, Faculty of Technical Physics, field of study: Technical Physics, M.Sc.
2009 – 2013	Poznan University of Technology, Faculty of Technical Physics, field of study: Technical Physics, B.Sc.

Research experience

2008 – 2014	Scientific Circle at Faculty of Technical Physics (2012 – 2014 chairman)
2010 – 2013	Organization, participation in Poznan's edition of Researchers' Night (physics)
2011	Internship at Department of Surface Physics and Tunneling Spectroscopy Ultra High Vacuum Laboratory at Institute of Molecular Physics at Polish Academy of Sciences in Poznan.
2011	Participation in a summer school on "Microsystem Technology" at Brandenburg University of Applied Sciences.

Other skills

- Software knowledge: Mathematica, MATLAB, Comsol Multiphysics, CST Studio Suite.
- LabVIEW, C/C++.
- Rapid prototyping, 3D modeling, 3D printing.
- Elementary knowledge in analog and digital electronics.

Languages

- English – fluent
- German – fair
- Polish – native language

Work experience

2011-2013	Poznan University of Technology, Chair of Optical Spectroscopy, positon: technician

Interests

- Astrophysics, cosmology.
- Cycling, alpinism.

Strengths

Logical, analytical, creative and ab initio thinking.